Eco-Driving planification profile for electric motorcycles.

Thèse de doctorat de l'Université Paris-Saclay et l'Université Pontificia Javeriana

École doctorale n° 575, electrical, optical, bio : physics and engineering (EOBE)
Spécialité de doctorat: Génie électrique
Unité de recherche: ESTACA.
Référent: : Cherif LAROUCI.

Thèse présentée et soutenue à ESTACA Lab., le 5 d'Octobre 2020, par

Cristhian Yesid BELLO CEFERINO

Composition du jury:

Giambattista GRUOSSO Professeur associé à temps plein, Politecnico Milano	Rapporteur
Rochdi TRIGUI Directeur de recherche, Université Gustave Eiffel /Campus de Lyon	Rapporteur
Andrés Emiro DIEZ Professeur associé à temps plein, Pontificia Universidad Bolivariana	Examinateur
Jean BIGEON Directeur de recherche CNRS, Laboratoire G-SCOP/Grenoble	Examinateur
Julián COLORADO Professeur associé à temps plein, Pontificia Universidad Javeriana	Examinateur
Cherif LAROUCI enseignant-chercheur HDR, ESTACA, UPS	Directeur
Diego PATIÑO Professeur associé à temps plein, Pontificia Universidad Javeriana	Codirecteur
Moussa BOUKHNIFER enseignant-chercheur, HDR, université de Lorraine	Coencadrant
Toufik AZIB Enseignant-Chercheur, ESTACA - Campus Paris Saclay	Coencadrant
Fredy RUIZ Professeur associé à temps plein, Politecnico Milano	Invité
Nassim RIZOUG enseignant-chercheur, ESTACA	Invité

Titre: Stratégies d'éco-conduite pour moto électrique.

Mots clés: éco-conduite, commande prédictive, optimisation, gestion d'énergie, véhicule électrique, moto électrique, optimisation de l'autonomie.

Résumé: Les stratégies d'éco-conduite sont des approches dédiées matérialisées par des algorithmes capables d'utiliser des informations liées à l'environnement du véhicule afin de faire des recommandations de conduite au conducteur ou de générer automatiquement un profil d'usage et une trajectoire optimisée dans le cas d'un véhicule autonome. Ce type de stratégie permet de réduire la consommation d'énergie, mais souvent n'intègre pas directement les performances requises par le conducteur et l'évolution de l'environnement en temps réel.

Ces travaux de thèse visent à développer une stratégie d'éco-conduite adaptée aux motos électriques. La stratégie développée utilise un contrôleur optimal basé sur une approche d'optimisation en temps réel afin de garantir que l'énergie disponible est suffisante pour effectuer un trajet donné, en adaptant le profil de vitesse suivant les conditions d'usage et les contraintes énergétiques.

Ces travaux ont été validés sur un banc de test expérimental à échelle réduite. Cette validation a montré que la stratégie d'éco-conduite développée permet d'augmenter l'autonomie de 20% avec une limitation maximale de 30% de la vitesse et l'accélération. En outre, cette stratégie est capable de garantir de terminer le trajet à 98% avec une erreur de distance inférieure à 1,5%.

Title: Eco-driving strategies for electric motorcycle.

Keywords: eco-driving, predictive control, optimization, energy management, electric vehicle, electric motorcycle, autonomy optimization.

Abstract: The eco-driving strategies are dedicated approaches based on algorithms capable to use vehicle data to create recommendations over the driver or to generate a complete reference to be followed in the case of an autonomous vehicle. They let to reduce the energy consummation, but currently, their usage is not directly related to the autonomy and the performance required by the driver in real time. In this context, this thesis work proposes an Eco-Driving strategy suitable for electric motorcycle. In fact, this strategy uses an optimal controller able to make an online optimization process. This controller is oriented to ensure that the energy available is enough to complete a demanded trip and to adapt the speed profile according to the usage requirements and the energetic constraints. The developed approach has been validated in with a reduced scale developed test bench. The validation shows that the algorithm can increase 20% the autonomy with a maximum limit of 30% of the speed and acceleration for the strict usage cases. In addition, the algorithm is capable to ensure completing the travel in the 98% of cases with a distance error lower than 1.5%.

Contents

List of Figures

7

List of Tables

Chapter 1

Introduction:

The electric vehicles buyers have been increasing along last 15 years. New technologies have allowed reducing the total cost of ownership of this kind of vehicles enough to make them a profitable product around the world. Even when China has the 57% of the customers, countries like Colombia has shown a growth of 88% in EV in comparison with 2015 sales (Electric vehicle) market [5] [6]. Electric vehicles have increased their presence in the Latin American market due to the behavior of oil price in comparison to energy price [7]. However, in countries like (EE.UU) where the oil price behavior is more stable, the electric vehicles have not enough strength to increase their presence, it can be seen with the short grown of EV from 2.5% in 2012 to 4.0% in 2017 [8]. Common sense says that in countries with this kind of oil behavior, the limitations of EV like lack of autonomy, lack of charge stations or the price are enough to make costumers ignore the ecological and even economic benefits of this technology but it is not completely true. Many scientific works have determined that electric vehicles already cover the 90% of trips made by an average user in one day, the conclusion of this scientific works is a Virtual Test-Drive [9] which let determine the real energy required to cover your common trips. As a conclusion, those limitations of EV are not the complete problem. Also, the user has uncertainty about his capability to cover a distance. Since there are many kinds of electric mobility means like cars, motorcycles or self-balanced wheels and it is important to notice that range limitation are inversely proportional to the size of the battery of the vehicle and the motor power used. In other words, the most sold electric vehicles (medium and small ones) are more affected by this phenomenon called "autonomy uncertainty". Also, the reduced prices of a small electric vehicle in comparison with an electric car makes that kind of vehicles (small electric vehicles) an attractive option on the electric vehicle market to cover small or even medium distance (from 1km to 8km). For this reason, the research work present in this report will be oriented to two wheels electric vehicles (TWEV) like motorcycles or bicycles due to their average size, high presence in the electric vehicle market, small energy consumption in comparison with electric cars, and small motor power.

The reduction of autonomy uncertainty can be a strong tool to push the presence of TWEV in vehicles market. For this reason, the topics covered will be:

- Modelization of the electric vehicle.

- External phenomena involved.

- Autonomy optimizers.

First, the power demand profiles will be covered to explain many useful terms and to highlight the range estimation problem. After that, driving the alerting system and speed

profile optimization will be explored as two research fields where autonomy uncertainties have an effect. Finally, since the objective of the Ph.D. research is to propose a speed profile optimizer and to model the power losses of different vehicle components. The power losses will be studied to be included ina an appropriated way inside the optimization algorithm.

1.1 Problem description

In order to help to increase the trust of consumers about autonomy offered by EV without aggravating the prices of this technology, the main proposal of this Ph.D. project is to develop a methodology and a tool able to determine automatically the torque and speed combination required in the electric motor to minimize the energy consumption against external conditions present in a travel with time and State of Charge (SoC) constraints. The tool will require information from 3 sources: the vehicle, an electronic device with GPS and Internet access, and the driver. The information sent by the vehicle is the brakes/throttle signal, constants like the front area or drag coefficient and electric characteristics (of motor, inverter and battery) like nominal power, nominal efficiency, torque range, work temperature, and current limitation. The electronic device lets to know the elevation, position changes, traffic and weather state along the travel. Finally, the driver is in charge of adding variable information like the total mass of the vehicle (taking into account load or a passenger), the place where he wants to go and an initial suggestion of minimal and maximal velocity desired.

Since the project requires a final prototype, the Ph.D. thesis has to be divided into two sections: Hardware and software.

As it can be noticed in Section 2, there are many aspects of the hardware which can improve the efficiency of an electric motorcycle but, in this project, the hardware will be bought, (it won't be designed) to fit the tool requirements in order to complete the diagram shown in Figure 1.1.
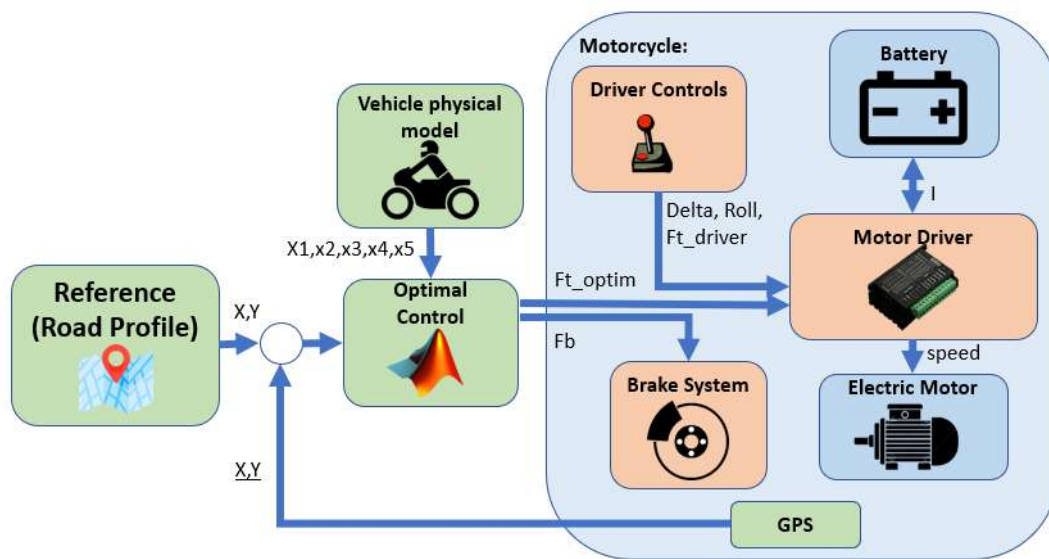
Figure 1.1: Main diagram.

It is important to notice the arguments to choose each component:

- Motor: A minimum power of 3KW to be suitable in city and highways.

- Inverter: It needs to fit with motor characteristics and it has to implement a communication protocol to update variables online.

- Battery: It needs to fit with motor and inverter characteristics.

- CPU: It needs to fit with software requirements.

- The total investment has to be comparable to other motorbike accessories.

1.2 Research problem

In electric two wheels vehicle (as a motorcycle) which uses an in-wheel (HUB) motor as the work specific case, there is an autonomy uncertainty caused by the lack of a sub-system to preserve the highest value of system efficiency against external vehicle parameters along a trip as driver behavior or weather/road conditions. In some settings, the efficiency decreases up to 62%. A mechanical and energetic model of an electric motorcycle will be studied in order to recreate the energetic behavior of an electric motorcycle. According to the model characteristics a controller has to be proposed to find the optimal torque/speed required in the motor to minimize the energy consumption along the travel with mechanical, time and State of Charge (SoC) constraints. In the future, it is expected to increase the autonomy of two wheels electric vehicles through an eco mode capable to adjust the motorcycle electric behavior to the most optimal energetic region. This region is a function of speed/torque, for this reason, the system will require to use future external conditions too. In consequence, it is expected to decrease the CO_2 footprint caused by urban transport by increasing the trust of the market in electric vehicles.

1.3 Objectives

The aim of our study is to reduce the energy uncertainties caused by external parameters present in a realistic environment like longitudinal acceleration profile and weather/road conditions through two elements; So we develop a model able to represent the energetic behavior of a motorcycle and a controller able to use present and future information about the weather and road to create constraints over the longitudinal acceleration profile. To obtain this objective, we need to:

- Build the dynamic model required to evaluate the energetic consumption in two wheels electric vehicles based on the current motorcycle dynamic models.

- Design control techniques based on dynamic model capabilities to reduce energy consumption.

- Build a range test for two wheels electric vehicles to reproduce the capabilities of current tests like (UDDS) or (FTP-75) [4] but taking into account external conditions.

1.4 Contribution

Nowadays, the control techniques are oriented to follow the speed profile proposed by the biker due to it lets to biker feels in control [10]. Unfortunately, the driver is not capable to use all information required to ensure the maximum efficiency point along the electric power chain with speed constraints. In consequence, when eco mode is required the constant constraint proposed by the eco-Driving algorithm just increases around a 2% the autonomy (it would be a 10% if it would be turned on from the trip beginning). The most scientific research around electric vehicles look for improving the efficiency of hardware or the controller (speed tracking) without takes into account the specific characteristics of travel that user wants to do.

The main contribution of this Ph.D. is an eco-mode able to propose a dynamic restriction over the torque and speed behavior of the motor to make a motor control-oriented to efficiency completely. To do that, three aspects have to be covered:

First, an analysis of energetic aspects involved in a mean trip: the electric vehicle model (the motor, weight, aerodynamics characteristics.. etc), the motorcycle model (longitudinal and lateral forces involved in the ride), the load (driver weight, baggage, or passenger weight) and the road (friction estimated, curve angle, wind direction, slope angle..etc). All those aspects have to be covered by a dynamic model able to predict the energetic behavior of the motorcycle along a trip.

Second, a controller able to use the dynamic model and all information available about the trip desired to keep the BLDC HUB motor in the highest value of efficiency through a torque/speed control.

Third, the controller needs to be implementable without increasing the price of the motorcycle significantly because the price of electric vehicles already is a disadvantage of this kind of vehicles.

In conclusion, the contribution of this Ph.D. is a complete methodology (modeling, design, and optimization) and an eco-mode algorithm capable to increase the trust of electric motorcycle drivers so that they will be able to complete the travel. In consequence, a product able to strengthen the presence of electric vehicles in the market will be obtained.

1.5 Methodology

The main task required by the eco-Driving algorithm is shown in Figure 1.2. The algorithm requires the mechanical and electrical characteristics of the motorcycle. Also internal and external input parameters of the vehicle are required too. The external input parameters are the place to go (with all parameters about road, weather or traffic) and the information about the driver, passenger and load. The internal parameters are information about the charge and health battery state. The algorithm of the software has to be able to use this information to anticipate the most efficient speed value in the function of the torque required along each section of the trip. Based on this optimization a speed profile is proposed.

In order to complete the goal mentioned before, there are two tasks that the software has to do:

- A prediction of the energy consumption.

- An optimization algorithm over the driving profile.

The first one ensures that the state of charge (SoC) present in the battery is enough
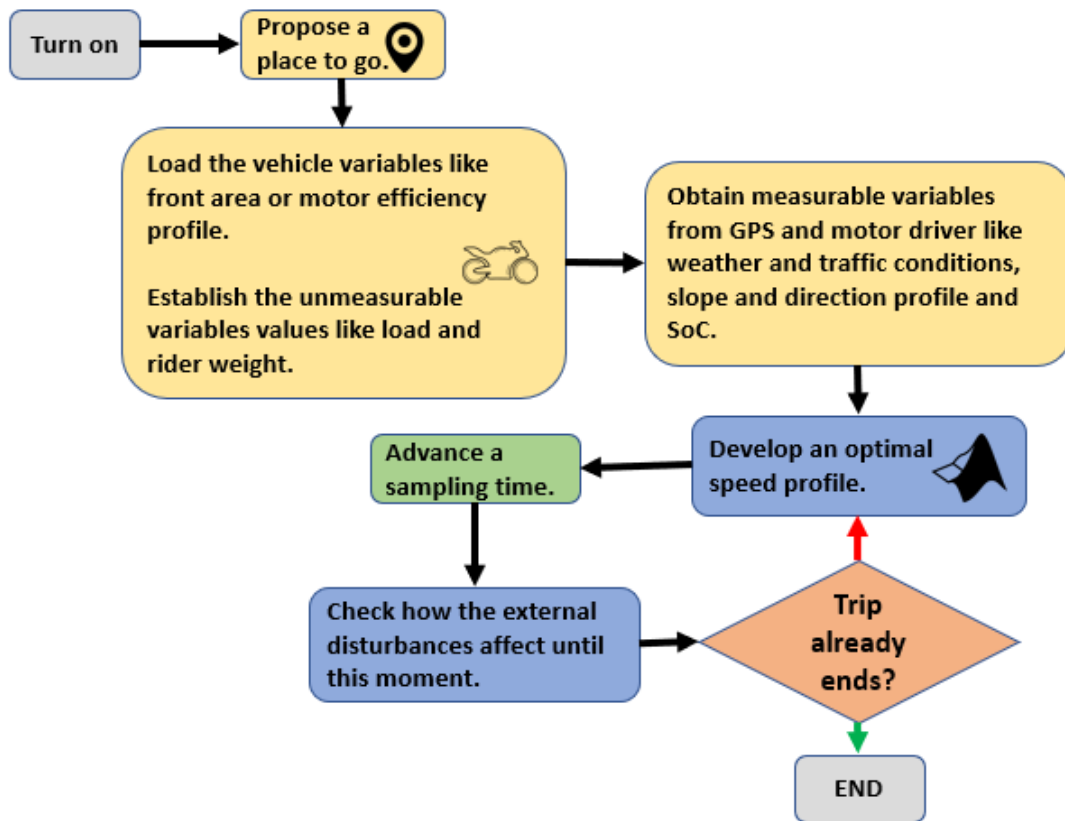
Figure 1.2: Software diagram.

to complete the required trajectory taking into account that the autonomy can vary depending on the trajectory conditions, driving profile and weather [11]. Indeed, there is a problem for the user, due to the uncertainty to complete the mission. To achieve this goal, the motor efficiency formulation from Section 2.3.1 and information about the effect of external parameters over autonomy from Section 2.5 will be used.

The second one aims to improve the way the user takes advantage of the regenerative braking, downhills and the inertia of the system. In an internal combustion vehicle, more than 80% of energy is lost in the mechanical system no matter the driving profile [12]. Then, a normal user is not aware of the driving profile required to obtain the maximum usability of the vehicle when (in the case of EVs) the lost energy can variate from 12% to 40% according to the driving profile [13], [14].

In order to accomplish the range prediction, the dynamic variables available in a motorcycle dynamic model need to be identified, study, and classify. To do that, technical information about how electric and hybrid cars autonomy is predicted from [15], [16], [17] will be used.

The chosen dynamics need to be validated to determine if they are enough to describe three behaviors: the position of the vehicle, the speed of the vehicle and the energetic behavior of the vehicle as a function of the two first aspects and external conditions. This validation will be made using a dynamic model software simulation tool because it already accomplishes with the vehicle market standards (resolution and accuracy) and it lets to change external road characteristics easily [18].

When all relevant dynamics for energetic behavior were identified and modeled, the controller needs to be proposed to reduce the impact of external conditions over the error

in maximum efficiency point of work proposed by the inverter. The controller needs to cover not just present and past information but also future information too in order to ensure the eco-driving profile proposed by the controller won't have strong changes. For this reason, an NMPC (Non-Linear Model predictive control) is proposed.

In order to clarify the NMPC components a first OPC (optimal problem controller) open loop is proposed. The optimization problem proposed considers three cases:

- Energy optimization.

- Time optimization.

- A combination of both, energy and time constraints.

In this research, the traffic is not modeled, it means that the speed controller has not any information about the traffic. In consequence, the variations over the speed tracking due to traffic conditions, driver maneuvers, driver comfort limitation established in the inverter or any other reason will be assumed as disturbances. Also, the acceleration signal is only affected by the torque variation optimization along the traject and not by the driver sensations.

The execution time of this controller can be high due to the NMPC repeats a non-linear optimization in each iteration. For this reason, implementation techniques need to be explored to achieve its usage. When implementation details will be completely covered, the controller has to be verified with a prototype. The prototype has to be enough to replicate not just a speed profile in flat and constant conditions as a conventional autonomy test. But also to be able to change the motor negative torque sensation in order to corroborate the effectiveness of the controller in face of a speed, slope and aerodynamic force profiles. All with traffic and curves emulation. In other words, the tester required by this range test has to be able to emulate over the motorcycle motor the negative torque which is the consequence of different slope angle, aerodynamic force, friction coefficient, etc... It has to be able to replicate a longitudinal motorcycle behavior.

1.6 Chapters contribution

Chapter 1: Introduction
All initial information about the project is presented in this chapter. The main initial information concerns to how the research problem is defined and it is turned in a set of objectives. Also, how the objectives were completed through a pre-established methodology to obtain a defined contribution. Finally, the scientific contributions referent to conference and journal papers are given.

Chapter 2: Literature Review
The state of the art is presented in the second chapter. It is divided into two main aspects: the main modeling knowledge required to make a correct representation of the motorcycle dynamic (Mechanical and electrical model) and the study of different techniques able to increase the autonomy of the vehicle using optimization as the main tool. Finally, the chapter exposes all the reasons why autonomy optimization has the priority as a research problem by analyzing the recent scientific works related to electric vehicles.

Chapter 3: Modeling
This chapter presents how the models given in Chapter 2 are adepted and used as well

as the contributions made in the modeling aspect. The electrical model of the motorcycle refers to the power losses model able to represent the amount of energy required to complete a trip. On the other hand, since the mechanical model was already discussed, the validation of the lateral and longitudinal mode is presented to choose what of both is required to represent the energetical environment of the motorcycle. Finally, how the power losses model is improved using a thermal model of the internal components behavior is presented.

Chapter 4: Control and Optimization
In this chapter, the way how the models were included in the control technique choose is presented. Also, two versions of the controller are developed: The open-loop version and the closed-loop one are presented to show how the disturbances affect the autonomy increment. Finally, the software elements required to integrate each controller version in a simulated environment are presented and analyzed.

Chapter 5: Experimental validation
In this chapter, a specific test bench is developed. An explanation of the hardware elements required to make a realistic representation of the controller capacities is exposed. Also, the implementation of each controller version is presented in order to explain the limitations and the conclusions of each carried-out physical experiment.

Chapter 6: Conclusions and Future work
Based on the validation made through simulation and experimentation, all the most important conclusions of the research and how it can be continued is discussed in this chapter.

1.7   Scientific contribution:

Accepted conference papers:

Y. Bello, T. Azib, Member, IEEE, C. Larouci, Senior Member, IEEE, , M. Boukhnifer, Senior Member, IEEE, N. Rizoug, Member, IEEE, D.A. Patino, Member, IEEE, F. Ruiz, Senior Member, IEEE. "Two wheels electric vehicle modelling : Parameters sensitivity analysis. ". 2019 6th International Conference on Control, Decision and Information Technologies (CoDIT'19), Paris. DOI: 10.1109/CoDIT.2019.8820319

Yesid Bello, Toufik Azib , Cherif Larouci , Moussa Boukhnifer , Nassim Rizoug , Diego Patino , FreddyRuiz. "Thermal Impact on Powertrain Efficiency Improvement for Two Wheels Electric Vehicle.". IEEE Industrial Electronics Society, (IECON'19), Lisboa. DOI: 10.1109/IECON.2019.8927381

Accepted journal papers:

Y. Bello, Toufik AZIB, Cherif Larouci, Moussa Boukhnifer, Nassim Rizoug, Diego Patino, and F. Ruiz. "Eco-driving Optimal controller for autonomy tracking of two wheels electric vehicles.". Hindawi Journal of Advanced Transportation. Volume 2020. DOI: https://doi.org/10.1155/2020/7893968

Summitted journal papers:

Y. Bello, Toufik AZIB, Cherif Larouci, Moussa Boukhnifer, Nassim Rizoug, Diego Patino, and F. Ruiz. "Motor Efficiency Modelling towards energy optimisation for Two Wheels Electric Vehicle.". Springer, Energy Efficiency.

Y. Bello, Toufik AZIB, Cherif Larouci, Moussa Boukhnifer, Nassim Rizoug, Diego Patino, and F. Ruiz. "Powertrain efficiency improvement through power losses analysis oriented to ECO-Driving profile optimization in Two Wheels Electric Vehicles.". IEEE Transactions on Energy Conversion.

Chapter 2

Literature Review:

2.1 Introduction.

This chapter exposes all knowledge required to understand out research problem and at the same time explores the different possibilities of improvement on each subject. The topics explored are:

- Classical speed control technique: This section shows how the speed and torque variables are currently controlled in electric vehicles. The analysis of this information lets to conclude the requirements of energy control.

- Electric vehicle modeling: Since the electric vehicle require an electrical and mechanical modelization which let to define the architecture will be work with. This modelization section highlight the physical limitation of the vehicle and also lets to determine the required control technique.

- External phenomenon: This section aims to choose the mechanical model based on the requirements present in the energetical representation and the mechanical models present in the literature. The mechanical model has to consider how the external agents like weather, road state, or driver characteristics affect vehicle energy consumption.

- Autonomy optimizers: Different techniques to improve the vehicle autonomy are presented and analyzed in this section.

- Electric vehicles challenges and scientific methodology to solve challenges: This section summarizes all information exposed in the previous sections in order to make a solid proposal of the research problem and how it can be solved according to the state of the art.

2.2 Classical speed control technique

2.2.1 Motor physical characterization

The information presented in this section is obtained from [1]. There exist many kinds of motors and each kind exhibits particular characteristics that make it useful of a particular industrial usage. For the electric vehicle industry, electric motors require attributes like low maintenance cost, simple design, high efficiency and relievable control techniques with the minimum additional electronic devices.

Between the synchronous motor and induction motor, the synchronous motor highlights due to its lack of speed variance face of load changes, and its high efficiency in low and medium speeds. Those characteristics caused the most used electric motors in the transportation industry are synchronous ones. In addition, they can be easily controlled in a profitable way. In a particular way, the BLDC (BrushLess Direct Current) motors are synchronous motor with permanent magnets used due to they improve the torque to weight ratio, reduce even more the maintenance cost and lets to increase even more the efficiency values in comparison to brushed motors [19].

The motors are composed by two main elements: the rotor and the stator. The stator is the static element composed by a number of windings which represent the number of electrical phases. In a three-phase motor, there are three windings able to represent the three phases with 120 grades of offset between them. The windings are activated following an order at a determined speed, This speed is called the electrical rotational speed and is the rotational speed of the magnetic field provoked inside the stator. The electrical speed and the mechanical speed of the rotor are related through the number of poles following this relationship:

$$\Omega = \frac{\omega}{p} \tag{2.1}$$

Where Ω, ω and p represents the mechanical speed [rad/s], the electrical speed [rad/s] and the number of poles.

The rotor is the element of the motor which can rotate. In the synchronous motor with permanent magnets, the rotors can be classified according to the way how the magnets are placed in the rotor. By one hand, the salient pole rotor presents the magnets as a final structure add to the metal structure, on another hand, in the smooth roll rotor, the magnets are added without any structural differentiation with the physical cylinder of the rotor, as a consequence, the air gap is smaller in the direct axis of the machine. This is the reason why in a salient pole machine, the direct inductance is higher than the inductance in the quadrature axis.

2.2.2 Mathematical model of the motor:

The mathematical model of the motor is required to implement most of the control techniques. The presented mathematical model takes into account the following hypothesis:

- A sinusoidal distribution of the F.E.M.

- The hysteresis and Foucault's currents are neglected.

- The magnetic circuit of the motor is not saturated.

- The airgap is uniformly distributed.

- The thermal effect over resistances is neglected.

From Figure 2.1 the following matrix equations are presented [1], [20]:
Stator voltage:

$$[v_s] = [R_s] * [i_s] + \frac{d}{dt}[\phi_s] \tag{2.2}$$

Stator flux:

$$[\phi_s] = [L_{ss}] * [i_s] + [\phi_{sf}] \tag{2.3}$$

where:

The stator voltage vector is:
$$[v_s] = [v_a v_b v_c]^T \tag{2.4}$$

The stator current vector is:
$$[i_s] = [i_a i_b i_c]^T \tag{2.5}$$

The stator flux vector is:
$$[\phi_s] = [\phi_a \phi_b \phi_c]^T \tag{2.6}$$

The stator resistance matrix is:
$$[R_s] = \begin{bmatrix} R_a & 0 & 0 \\ 0 & R_b & 0 \\ 0 & 0 & R_c \end{bmatrix} \tag{2.7}$$

The stator inductance matrix is:
$$[L_{ss}] = \begin{bmatrix} L_a & M_{ab} & M_{ac} \\ M_{ba} & L_b & M_{bc} \\ M_{ca} & M_{cb} & L_c \end{bmatrix} \tag{2.8}$$

The flux vector made by permanent magnets through stator windings is:
$$[\phi_{sf}] = [\phi_{af} \phi_{bf} \phi_{cf}]^T \tag{2.9}$$
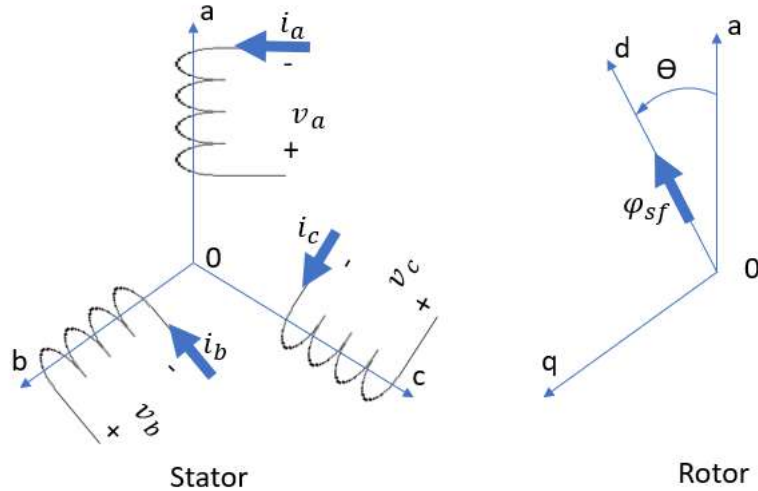
Figure 2.1: Representation of a synchronous motor with permanent magnets [1].

In order to simplify the mathematical model, Park transformation is used. The Park transformation is a coordinates changes able to turn a triphasic stationary system into a rotary coordinate system. The normalized expression of the Park matrix is given by [1], [20]:

$$[T] = \sqrt{\frac{2}{3}} \begin{bmatrix} cos(\theta) & cos(\theta - 2\pi/3) & cos(\theta - 4\pi/3) \\ -sin(\theta) & -sin(\theta - 2\pi/3) & -sin(\theta - 4\pi/3) \\ \frac{1}{\sqrt{2}} & \frac{1}{\sqrt{2}} & \frac{1}{\sqrt{2}} \end{bmatrix} \tag{2.10}$$

The resultant transformated vectors are:

$$[v_{dq0}] = [T][v_{abc}] \tag{2.11}$$

$$[I_{dq0}] = [T][i_{abc}] \tag{2.12}$$

$$[\phi_{dq0}] = [T][\phi_{abc}] \tag{2.13}$$

As a result of this transformation, the equivalent schematic of the motor shown in Figure 2.2 is obtained.
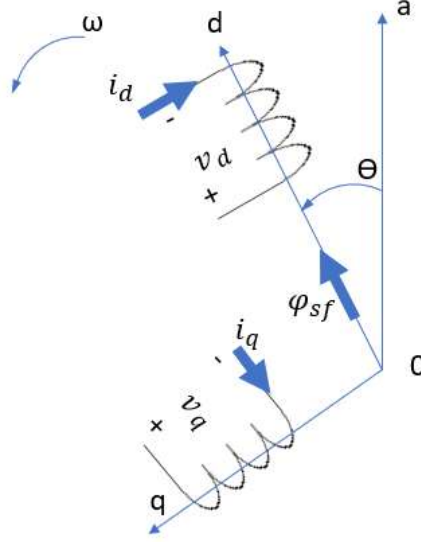
Figure 2.2: Equivalent representation of a synchronous motor with permanent magnets [1].

and the resultant voltage expresion are:

$$\begin{bmatrix} V_d \\ V_q \end{bmatrix} = \begin{bmatrix} R_s * I_d + \dot{\phi}_d - \omega * \phi_q \\ R_s * I_q + \dot{\phi}_q - \omega * \phi_d \end{bmatrix} \tag{2.14}$$

The resultant flux expresion are:

$$\begin{bmatrix} \phi_d \\ \phi_q \end{bmatrix} = \begin{bmatrix} L_d * I_d + \phi_{sf} \\ L_d * I_q \end{bmatrix} \tag{2.15}$$

where ϕ_{sf} is the total flux made by permanent magnets through stator windings.
The resultant electromagnetic torque is as follows:

$$C_e = p[(L_d - L_q) * I_d * I_q + \phi_q * I_q] \tag{2.16}$$

Finally, the mechanical equation is given by the following expresion:

$$J * \frac{d\Omega}{dt} + f * \Omega = C_e - C_r \tag{2.17}$$

Where J, f, Ω and C_r are the inertial moment $[kg * m^2]$, viscous friction coefficient $[\frac{Nm*s}{rad}]$, mechanical speed [rad/s] and load torque [Nm].
By adding equation 2.15 to equation 2.14 the following expresion is obtained:

$$\begin{bmatrix} V_d \\ V_q \end{bmatrix} = \begin{bmatrix} (R_s + p * L_d) * I_d - \omega * L_q * I_q \\ (R_s + p * L_q) * I_q - \omega * L_d * I_d + \omega * \phi_{sf} \end{bmatrix} \tag{2.18}$$

21

Finally, from equations 2.15 and 2.14, the state-space representation can be obtained too:

$$\frac{d}{dt}\begin{bmatrix} I_d \\ I_q \end{bmatrix} = \begin{bmatrix} \frac{-R_s}{L_d} & \frac{\omega * L_d}{L_q} \\ \frac{-\omega * L_d}{L_q} & \frac{-R_s}{L_q} \end{bmatrix} \begin{bmatrix} I_d \\ I_q \end{bmatrix} + \begin{bmatrix} \frac{V_s}{L_d} \\ \frac{V_q - \omega * \phi_{sf}}{L_q} \end{bmatrix} \tag{2.19}$$

In order to start to develop control techniques, only one step still being required. Since the direct axis and quadrature axis are coupled in equation 2.18 a decoupling has to be done. Figure 2.3 presents into a schematic way how both axes are coupled.
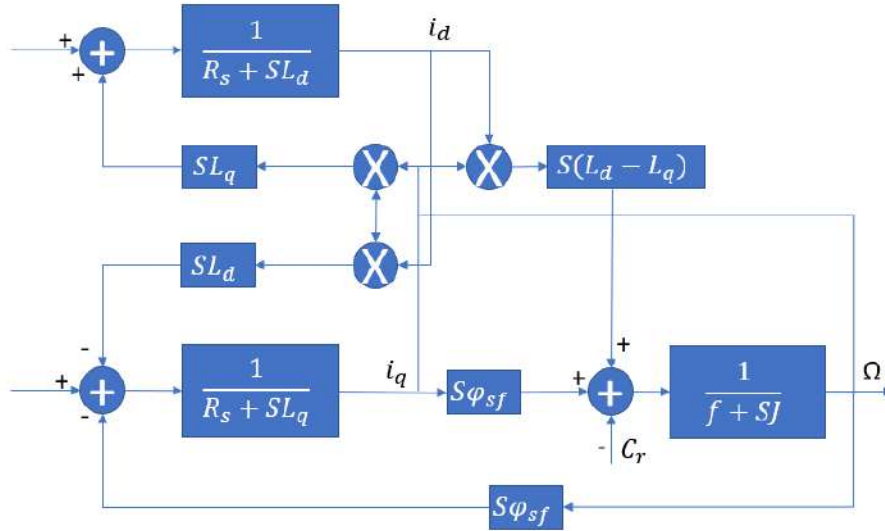
Figure 2.3: direct and quadrature axis coupling [1].

For each voltage shown in equation 2.18, only the values of the same axis are considered. The additional elements are considered perturbation corrected by compensation as it is shown in figure 2.4. The obtained voltage equations are:
In the direct axis:

$$V_d = V_d' + e_d \tag{2.20}$$

$$e_d = -\omega * L_q * I_q \tag{2.21}$$

In the quadrature axis:

$$V_q = V_q' + e_q \tag{2.22}$$

$$e_q = \omega * L_d * I_d + \omega * \phi_{sf} \tag{2.23}$$

Both transfer functions are:

$$\frac{I_d}{V_d'} = \frac{1}{R_s + S * L_d} \tag{2.24}$$

and

$$\frac{I_q}{V_q'} = \frac{1}{R_s + S * L_q} \tag{2.25}$$
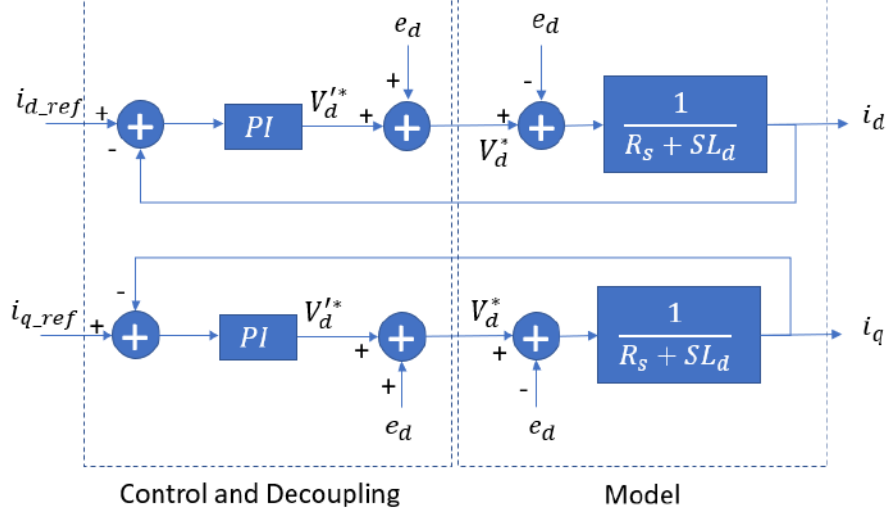
Figure 2.4: Direct and quadrature axis decoupling [1].

2.2.3 Current control

The most used control technique in the industrial environment to control the current in BLDC motors is the PI controller due to its easy implementation. The transfer function of the PI controller is:

$$F_{(PI)} = K_p + \frac{K_i}{S} \tag{2.26}$$

When both transfer functions are conected in open loop, the resultant equation is:

$$F_{ol} = (K_p + \frac{K_i}{S})(\frac{1}{R_s + S * L_d}) \tag{2.27}$$

The pole $\frac{-R_s}{L_d}$ is compensated with $\frac{-K_i}{K_p}$ in order to turn the open loop transfer function into:

$$F_{ol} = \frac{K_i}{S * R_s} \tag{2.28}$$

The compensation means a condition where:

$$\frac{R_s}{L_d} = \frac{K_i}{K_p} \tag{2.29}$$

In closed loop, the transfer function is:

$$F_{cl} = \frac{1}{\frac{R_s}{K_i} * S + 1} \tag{2.30}$$

Then the time constant τ_{cl} is $\frac{R_s}{K_i}$. Finally, the integral gain of the controller is obtained as:

$$K_i = \frac{R_s}{\tau_{cl}} \tag{2.31}$$

If we chose the response time as $t_{rep} = 3\tau_{cl}$ and takking into account the equation 2.29 and 2.35, then:

$$\begin{aligned} K_p &= \frac{3L_d}{t_{rep}} \\ K_i &= \frac{3R_s}{t_{rep}} \end{aligned} \tag{2.32}$$

The process is the same in the quadrature axis.

2.2.4 Speed control

The design of the speed control is similar to the continue current motor.The obtained scheme is shown in Figure 2.5.
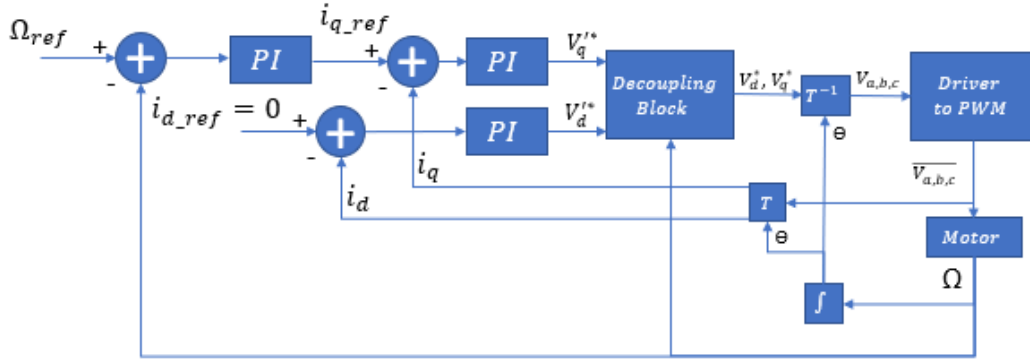
Figure 2.5: Final schematic of speed and current control.

The equations which represent the behavior scheme before are:

$$\Omega(S) = \frac{1}{J * S + f}(C_e(S) - C_r(S)) \tag{2.33}$$

and

$$C_e(S) = p * \phi_{sf} * I_{qref} = K_t * I_{qref} \tag{2.34}$$

If the load torque is considered as a disturbance, the closed-loop transfer function can be presented in a classical way:

$$F_{cl}(S) = \frac{\omega_o^2}{S^2 + 2 * \eta * \omega_o * S + \omega_o^2} \tag{2.35}$$

Where:

$$\begin{aligned} \omega_o^2 &= \sqrt{\frac{K_p * K_t * K_i}{J}} \\ 2 * \eta * \omega_o &= \frac{f}{J} + \frac{K_{p*K_t}}{J} \end{aligned} \tag{2.36}$$

Finally, the controller elements are assined by chossing an optimal damping factor equal to 0.7 and the pulsation of the non-damped oscillations from the desired dynamic.

2.3 Electric vehicle modelling

The modelization is the most important aspect to be considered in order to propose an optimization around the torque and speed profile. The modelization has to cover two topics: the electrical and the mechanical behaviors. According to the electrical devices used in the vehicle (the number of motors, the battery technology used... etc), the mechanical modeling can vary. For this reason, in the next section, the electrical devices contemplated in the research will be explained and different scientific works about how this particular device affect the energy efficiency of the complete system and how to improve it will be presented.

2.3.1   Electrical modelling

The most important aspects related to the energy optimization are the losses in each component of the power train system: Motor, inverter, and DC power source. The electrical diagram who descrives the interaction between those devices is shown in Figure 2.6, where $Vx_r, Idq_r, Vdq, Udc, Cr, Iabc, Idq, C, \Omega$ are the longitudinal reference speed, direct and quadrature reference currents, direct and quadrature reference voltages, DC voltage, the load torque, the motor phases currents, the direct and cuadrature currents measured on the motor, torque measured on the motor and the angular speed measured on the motor.
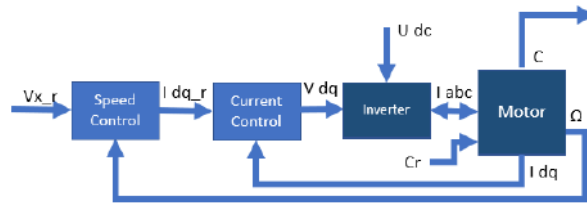
Figure 2.6: General control diagram of a BLDC motor.

The mechanical aspect makes reference to the movement possibilities available in the vehicle according to its DOF (degrees of freedom) and they causes constraints over the longitudinal speed dynamic.

A. Motor losses:

As indicated before, the BLDC(BrushLess Direct Current) motors are used due to they improve the torque to weight ratio, reduce even more the maintenance cost and lets to increase even more the efficiency values in comparison to brushed motors [19].
BLDC motors can be classified as: Hub and Mid-Drive (One example of each type can be seen in Figure 2.7. Although the Mid-Drive motor offers more energy efficiency in comparison to the Hub motor (because the torque losses are less in a mid-drive motor than in a hub motor), the mid-Drive motor change the balance sensation in the TWEV (Two Wheel Electric Vehicle), it produces more noise and its average cost is more than 400% of the Hub motor average cost of the same power. For this reason, the HUB BLDC motors of power between 500W and 8000W are highly extended in the market and then, that kind of motors will be covered in this work [21].
 The BLDC motor efficiency behavior can determine the optimal operation point of the
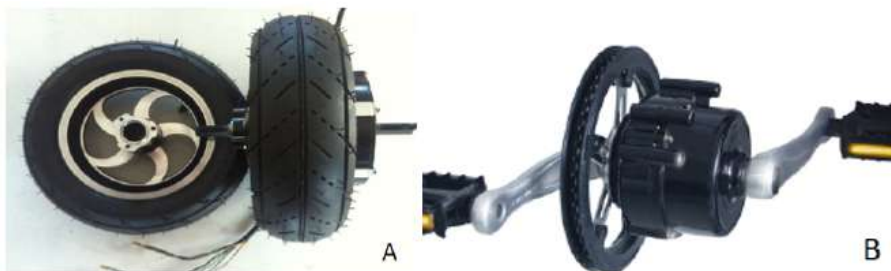
Figure 2.7: Hub Motor (A) and Mid-Drive Motor (B).

electric vehicle. In order to analyze the efficiency function by its optimal and suboptimal

regions, a theoretical analysis of the steady-state efficiency is presented.In a BLDC motor, the efficiency in steady-state can be defined as:

$$\eta = \frac{P_{out}}{P_{in}} = \frac{T_e \Omega_s}{T_e W_s + P_{lcu} + P_{lfe} + P_{lmag}} \tag{2.37}$$

Where, η is the efficiency definded as the relationship of the output power (P_{out}) over the input power (P_{in}) of the system. The output power is described by the mechanical power obtained by the motor. In other words, the product between the electromagnetical torque (T_e) and the angular speed of the motor (Ω_s). The input power is described as the output power plus the losses of the motor. In the motor the losses will be P_{lcu}, P_{lfe} and P_{lmag}. They are the Joule losses (also called iron losses), the core losses and the magnetic losses in rotor magnets.

AI. Magnetic Losses: The magnetic losses caused by Eddy-current in the permanent magnets of brushless machines are usually neglected [22]. Since the fundamental air-gap field usually rotates in synchronism with the rotor, and time harmonics in the current waveform in the winding distribution are generally small. For this reason, $P_{lmag} \approx 0$.

AII. Joule losses: The Joule losses are the losses caused by the resistivity of the cooper in winding. When a current cross a conductor material, the resistivity of the material opposes to this current movement. As a result, heat is produced and part of the electrical power is dissipated.
They can be expresed as [23], [24]:

$$P_{lcu} = \frac{\frac{\rho_{cu}}{K_{fill}}(L + L_{ew})(K_{sp}\pi D_o)}{\frac{\pi}{4}(D_o^2 - (D_i + \frac{B_g \pi D_o}{B_j 2pK_{fe}})^2) - \frac{B_g \pi D_o}{B_t}(\frac{D_o - D_i}{2} - \frac{B_g \pi D_o}{4B_j pK_{fe}})} \tag{2.38}$$

Where ρ_{cu}, D_o, D_i, B_g, B_t, B_j, K_{fill}, K_{fe}, p, L, L_{ew}, K_w and K_{sp} are the copper resistivity [Ohm.m], the stator outer diameter [m], the stator inner diameter [m], the air gap flux density [T], the flux density in stator tooth [T], the flux density in stator yoke [T], the slot filling factor, the lamination factor, the number of pole pairs, the stator lamination length [m], the length of end-winding [m], the fundamental winding factor, and the fundamental current density [A/m], which can be expresed in term of load torque "T_l" as follows, [23]:

$$K_{sp} = \frac{T_l}{B_g D_o^2 L sin(p\alpha_{pm})} \tag{2.39}$$

where α_{pm} is the half of mechanical magnet angle.

AIII. Core Losses: Core losses appear in a magnetic core due to alternating magnetization as a consequence of the not perfect synchronization between electrical and magnetic fields. They are the sum of the hysteresis losses (due to the difference between magnetization rate and demagnetization rate) and the eddy current losses (due to Farady's law effect over lamination motor structure caused by magnetic fields). The core losses are defined as [25]:

$$P_{lfe} = P_{LEy} + P_{l_t} + P_{l_t t} \tag{2.40}$$

Where, P_{LEy}, P_{l_t} and P_{l_tt} are the losses in rotor yoke due to eddy current and losses in tooth body and tooth tip caused by hysteresis and eddy current. Those expresions are given by:

$$P_{LEy} = n_y(\frac{f}{p})^{1.5}R_{Ym}^2 A_{ry}\sqrt{\frac{\pi^2}{i\rho_{Fe}\mu_{Fe}}\sum_{i=1}^{\inf}\frac{B_i}{\sqrt{i}}} \tag{2.41}$$

$$P_{l_t} = K_h f^\alpha B_t^\beta + \frac{4}{\pi}K_e\frac{f^2 B_t^2}{\alpha_t} \tag{2.42}$$

$$P_{l_tt}K_h f^\alpha B_{tt}^\beta + \frac{4}{\pi}K_e\frac{f^2 B_{tt}^2}{\alpha_{tt}} \tag{2.43}$$

Where n_y, f, p, R_{Ym}, A_{ry} are the number of rotor yokes, frequency, number of poles pairs, mean radius of the rotor yoke, the area of the rotor yoke face.

Also, ρ_{Fe}, μ_{Fe}, B_i, B_{tott} and α_{tott} are resistivity and the mean permeability of the rotor yoke material, the magnitude of ith harmonic of the armature flux density wave, the peak value of flux density at the tooth or the tooth tip and the mean pole transition angle in electrical radians. Finally K_h, α, β and K_e are constants obtained from the curve fitting of core loss data measured with sinusoidal excitation. This representation requires three lookup tables, the magnetic flux density as a function of stator current measured in the stator yoke, the rotor yoke, and the air gap.

Even when the BLDC electric motor highlight by its efficiency in comparison with other machines available in the transport field. Its energy losses sources are considerable and they vary strongly with the Speed/Torque value. Many scientific works have been made around the modelling and minimization of the power losses of the electric motors for increasing the autonomy of electric vehicles.

The most evident power loss source is the power dissipation (Joule Losses).In [26] it is explored in order to ensure an improvement over the efficiency estimation.In this paper, the efficiency of the inverter and the motor are calculated together to compare the theoretical developments with measures made in different work points. Even when this approach is able to reproduce the efficiency behavior with less than a 10% of error (this value grow up linearly with the speed value), it has a disadvantage, it is blind in face of other energy losses sources, it can be noticed due to the non constant behavior of the error.

The scientific research presented in [27] proposes an equivalent circuit capable to use the no-load and full-load test to reproduce four kind of losses: Cooper losses, Core losses due to Hysteresis and Eddy current, viscous friction losses and Joule losses present in stator and inverter. The accuracy of this approach is comparable to the 10% described in [26] but, its error does not grow up with the speed and torque. In other words, even when the accuracy of the method has to be improved, it is capable to represent most of the power losses sources.

The scientific research exposed before mixed the inverter and motor losses.It makes difficult to make optimizations directly over the motor structure or the motor energy requirements. Then, another approach is explored in [22], [24] and [25]. The Joule, core and copper losses caused inside the motor are analyzed through making an electromagnetic analysis. In [25], Steinmetz and Bertotti equations are compared to determine that Bertotti equation is capable to make a better representation of the stator core losses in flux weakening region due to it takes into account the dynamic of the magnetic flux density. The magnetic flux density is variable difficult to represent in time, then, the effect of its harmonics is studied theoretically (as it is shown in [28]) and after it can be compared with two software applications or direct measures over the motor. The first software application is a representation of the magnetic flux density as a function of the

current present in the stator (as it is shown in [29]). This representation requires three lookup tables, the magnetic flux density as a function of stator current measured in the stator yoke, the rotor yoke, and the air gap. In [25], the representation of the magnetic flux density of the stator is separated in the magnetic flux density present in the body of the tooth and the tooth tip. This differentiation lets to reduce the average error of the algorithm. Some examples of software used to represent the magnetic flux density are ANSYS/Maxwell, Altair/Flux2D and COMSOL. The second software appication is a direct representation of the efficiency map made by a logical programming working with an ensemble of magnetic simulation software, this option is available just in few softwares like ANSYS/Maxwell. In conclusion, in the EV market, the HUB BLDC motors have been the most used for these reasons:

- Their build is cheaper than other motor technologies.

- Better speed-torque characteristics in comparison to other types of engines.

- This kind of motors improves the energy efficiency in long time periods.

- Long operating life due to a lack of electrical and friction losses.

- Noiseless operation.

- Higher speed ranges.

Also, the power sources from the motor have to be studied separately to the inverter or battery power losses sources and the phenomenon represented will be:

- Cooper losses, they are called Joule losses too and it makes reference to the power dissipation due to the current trajectory along the copper wires in the stator.

- Core losses, they represent the power losses in stator and rotor due to Eddy currents and Hysteresis effect.

Finally, the power losses calculation will be made under the following assumptions:

- The input current is assumed to be ideal sinusoidal.

- The effect of the inverter and power source losses is well ignored through simulation.

- The temperature effect over each operation point (speed/Torque) can be neglected.

- Mechanical friction loss effect can be ignored.

- The effect of the magnetic flux density dynamic is minimum due to the size of the air gap and the stator/rotor materials properties.

B. Inverter losses:

The inverter controls the power input of the motor in order to develop the speed required by the driver. In a three-phase BLDC motor there exists three groups of stationary coils in the stator in charge to generate the magnet field in charge of interact (attraction and repel) with the magnet field of the rotor magnets. This interaction between both magnet fields have to be synchronous to drag the rotor and let it turns. The process to inject current into the coils in a synchronous way to activate them is called commutation due to the inverter has to commute transistors to turn on the motor stator coils. This process

has energy losses.

The typical commutation arrangement is called "six-step commutation" (Figure 2.8) and it keeps two phases activated to make a smoothy commutation. However, the commutation process can be modified to vary some characteristics of the motor movement. The speed
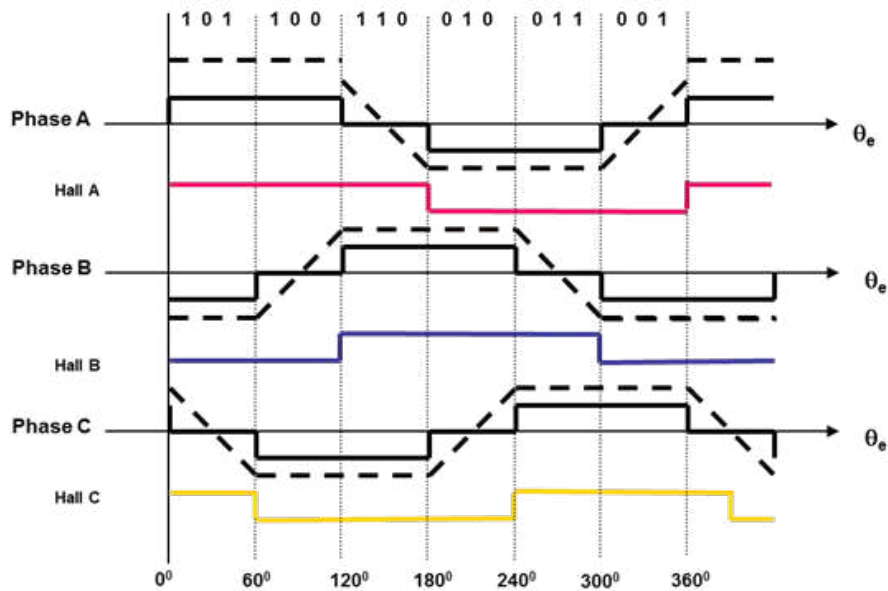
Figure 2.8: Six steps conmutation. [2].

control is made controlling the commutation frequency. In order to close the speed control loop, two techniques to estimate the speed from the rotor position can be used [2]:

- BEMF estimation: This technique requires a voltage measurement of the different motor phases to detect the effect of the permanent magnets of the rotor over the stator coils or, the back electromotive force (BEMF) over the coils.

- Hall sensor measurement: Hall effect sensors are solid-state, magnetic field sensors capable to measure the magnetic field from permanent magnets in the rotor.

A typical control diagram is shown in Figure 2.9, the typical control is composed by the speed loop and the current loop. Based on the present value of both variables the correct commutation step and frequency are chosen. Due to semiconductor resistances and
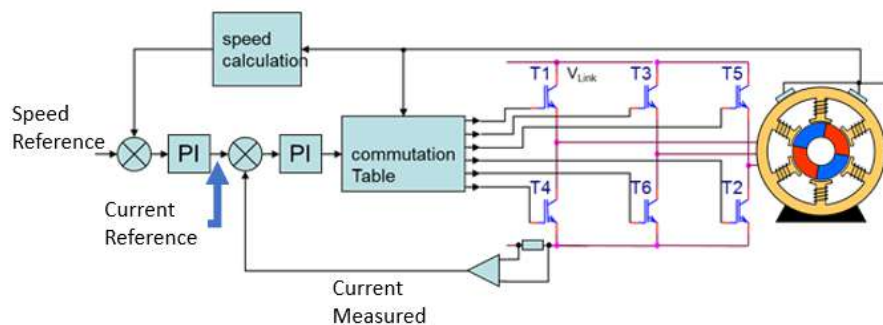
Figure 2.9: BLDC motor control diagram [2].

capacitances associated with the different work regions, there is an important quantity of losses associated with the inverter. One of the first approaches to estimate these energy

losses was to build data-based models. Two possible sources of data are the parameters from semiconductor materials and connections architectures from manufacturers manuals and the experimental verification of the same data. In [30] a comparison of three IGBT generations and a lookup table proposed are used in order to determine the behavior or the power losses. The four-dimensional lookup table has a dependence of the semiconductor temperature, the motor RMS phase current, the mechanical speed of the motor and the DC voltage of batteries. The analysis of this paper lets to determine a polynomial of second order capable to describe the losses of the inverter based on different IGBT generation parameters and the behavior observed in the four-dimensional lookup table. This representation is able to reproduce the energy losses behavior by periods of 1100 seconds with less than 2% of error in comparison with measured data. However, the acceleration present in real speed profile increases the error.

In order to improve the power losses analysis, in [31] the same author proposed a new look-up table structure. The resistivity losses and the switching losses are divided to be analyzed separately. In this paper, the author used the analysis made in the first paper to propose an inverter optimized which ensures high efficiency at low and medium loads. This change and the usage of third generation IGBT helps to improve the efficiency of the inverter around 25%. This paper showed the impact of transport load analysis under efficiency optimization.

The characterization of power losses effect is deeply analyzed in [32]. The power losses model cover three kind of losses: the conduction losses of the mosfet, the IGBT and the diode, the switching losses of the IGBT, and the magnetic elements losses divided into core and copper losses. This study was made with a co-simulation workspace created between PSIM and Matlab/Simulink. An efficiency analysis at different output voltage was made in order to verify the data obtained with the model and the data measured, also, this comparison lets to determine maximum efficiency zones and how the different output voltages can change move the most efficient zone according to the main operation power region. Even when the results of the paper are oriented to the low error efficiency simulation obtained, this paper aims to obtain an additional analysis of how the different power losses sources affect the efficiency estimation result. As a conclusion, the most significant losses source into the inverter are the conduction losses and the switching losses but their relevance can vary according to the final inverter architecture, also the effect of the temperature have to be explored. This conclusion is suported also with [33]. Finally, in [34] the efficiency of the inverter is analyzed through a thermal model and the effect of the control frequency. The presented thermal model is a fourth order exponential term foster network model. This model lets to take intto account the effect of the thermal behavior of the material on the diode, the copper substract, the diode copper substract and the heat skin-ambient. The results of this papers lets to conclude that even when the electrical losses reported before are the most relevant power losses source, the thermal effect have to be include into the inverter model in order to obtain efficiency calculus error under the 5% when a real speed profile is applied into a realistic ambient characterization. As the conclusion of this section, the most relevant inverter losses are the electrical losses due to switching and conduction from the MOSFET and the diode. Those losses have to be analyzed to ensure the correct current signal components are classified to describe the behavior of the semiconductor between conduction, reverse and switching regimen. Besides, due to the period of work of the device is medium or long, the thermal effect has to be includes and controlled in order to estimate and improve the electric vehicle range.

C. Battery losses:

The electric vehicle is a technology which is entering the market in the last years, for this reason, the power system of this kind of devices have not been standardized but two battery technologies have been positioned on the top of chemical technologies used: Lithium-ion and Lead-acid. Lithium-ion technology is the most common rechargeable battery type for its energy density. Besides its high capacity, its advantages cover maintenance-free, low self-discharge rate, long cycle life, it does not develop a memory effect, lightweight, it can be made in small size, its safety and it counts with the possibility to do fast charging to full capacity. By the other hand, the lead-acid batteries are cheaper than the lithium-ion batteries, this is the main reason why the lead-acid batteries continue being used in the EV market nowadays although they are heavier, bigger and less efficient than the lithium-ion batteries.

The battery needs to be carefully charged and discharged taking into account its chemical characteristics. For this reason, before to present the battery power losses, the scientific works around the state of charge estimation will be presented.

Although the charger is which control the charge curve, there is a device in charge of ensuring the battery safety. The BMS is an electronic circuit responsible for:

- Disconnect the load when a voltage of one of the cells is under its critic value (2.5 [V] for Lithium).

- Stop the charging process when a voltage of one of the cells is over its maximum value (4.2 [V] for Lithium).

- Disconnect the load when the temperature of one of the cells is over its critical value (50 °C for Lithium). The BMS ensures that the temperature of the battery is not just safe to avoid accidents but, it has to be highly efficient also because the output resistance of the battery increase with high temperatures the energy losses increase too.

As it was mentioned before, the battery is a set of electrochemical cells with external connections, for this reason, the electronic scientific works related with this area are related with the BMS.

Since the BMS is in charge to care the battery cells, many works improve the accuracy of the information source to improve the behavior of the BMS. For example in [35], expanded Kalman filter is used to makes the SoC error converge to zero. This improvement is tested on a BMS circuit to corroborate the effect over the BMS capabilities. The BMS has more than one usability, it has to sample current, voltage and temperature of each cell of the battery and in some cases, it has to estimate the SoC. In high-density batteries with hundreds of cells, it is difficult to measur the voltage. For this reason, works like [36] propose and compare methodologies to calculate the integral value of the current to estimate the voltage current. In this specific work, the processes are software integration method and the other one is Single-Phase Multifunction Metering IC. Both processes can calculate the current integration but the second one is cost-saving. Also, the BMS is able to work with external devices like chargers or inverters to increase safely the charge and discharge current range [37] [38]. As the BMS has to switch between two modes: battery cell balance and temperature control. The current range expansion is possible with the correct switching of those two modes.

In conclusion of this first step, the Battery requires a BMS to ensure the most efficient and to secure output and input powers. The correct usability of the information available

in BMS lets to make fast charge process and high-temporal discharges. For this reason, is important to reduce the uncertainty of sensor measurement or variables estimations. Also, the usage of models able to use external information with low uncertainty improves the energy output uncertainty.

Since the charge and discharge process have to be done carefully, the SoC (State of Charge) is a variable highly followed along extended periods of usage. For this reason, the SoC estimation is one of the most-studied topics, to determine the characteristics which are relevant for an EV performance.

In order to discuss the energy losses inside the battery, it is important to present the model required to make the SoC estimator. Even when there are more detailed dynamic models, the circuit presented in Figure 3.4 is able to describe the battery behavior provoked by frequencies present in electric vehicle mean usage (less than a 100Hz) [3].
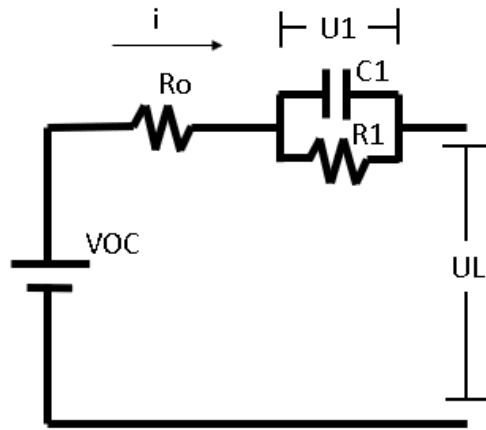
Figure 2.10: Equivalent circuit model of a lithium-ion battery [3].

The energy losses will be presented in the power dissipation made by the resistances Ro and R1. According to [39], those losses represent from a 2% to a 10% according to the internal resistance behavior. Its behavior is a function of the SoC, the temperature and the material of the battery. For this reason, it is required to make SoC and temperature estimations to describe the evolution of energy losses.

The SoC estimator is an algorithm able to recreate the behavior of the battery to estimate how it will evolve in the future. Kalman filter is commonly used for this purpose. Since the internal parameter of the model can vary according to the temperature. In [40], the Kalman filter is used to predict the effect of the temperature over the discharge rate estimation. It is important to notice that the effect of the temperature requires a look-up table able to recreate the resistance value in different temperatures or a thermal model of the battery. And, a thermal model accuracy can be a field of study by its self like [41] presents. Another option is to include the model parameters value inside the prediction model in order to make the estimations of the state and the parameter estimation all inside the same algorithm like in [42]. This approach makes the estimation more robust. Finally, it is important to note that even when the parameters identification process can be done with a pack (a set of battery cells in series and parallel) too, the possibility to makes a parameter identification only with one cell is cheaper and quicker. Then, in [43], the pack behavior is recreated based on the information of one cell. This paper introduces

a new battery pack modeling which lets to reduce the error caused by ideal assumptions of series and parallel and at the same time lets to make cheaper and quicker parameter identification only with one cell.

2.3.2   Mechanical modelling

Although motorcycles are composed of a variety of mechanical parts, from a kinematic point of view, a motorcycle can be defined as simply a multi-body platform composed of four rigid bodies:

- The rear assembly.

- The front assembly.

- The front wheel.

- The rear wheel.

This motorcycle definition is valid under the following assumptions [4]:

- The suspension is enough rigid, in consequence, the θ dynamic along the Y-axis (Figure 2.11) caused by load exchange between the front and rear assembly can be ignored.

- A perfect coupling between driver and motorcycle bodies. The momentum caused by the driver body is not considered.

- An homogenous pressure distribution of pneumatic. This assumption lets to conclude that the longitudinal and lateral forces are distributed homogeneously along the pneumatic too.

The four rigid bodies are connected by 3 revoluted joints, as each revoluted joint remove 5 degrees of freedom (DOF), 3 revolute joints inhibit 15 DOF of the spatial freedom of the platform. Taking into account the three kinds of wheel motions: roll, spin and forward, each wheel point of contact remove 3 DOF. Since each body has 6 DOF, from the 24 DOF of the 4 main bodies, 21 DOF are removed by the movement restrictions (15+(2*3)). It is a total of 3 spatial DOF [4]. Those are forward, roll and steering motion of the motorcycle. This hypothesis is valid if slippage is ignored. In real conditions, longitudinal and lateral slippage cause the combination of DOF mentioned before becomes in the 6 DOF shown in Figures 2.11 and 2.12. Those DOF are [4]:

- Forward motion: It is caused when there is slippage on front and rear wheel by braking events or by acceleration events in the traction wheels. This dynamic will be referenced as longitudinal dynamic and it is parallel to X wheels axis.

- Lateral motion: This dynamic will be referenced as Lateral dynamic and it is parallel to Y wheels axis.

- Roll motion: It is the moment generated around X axis formed by the two points of contact of both wheels. This is an unstable dynamic relevant for trajectory tracking. As the model is oriented to energetic behavior this dynamic is ignored but the roll angle is used as a parametric input.

- Steering motion: It is the moment generated around the vertical axis of the handlebar. This dynamic won´t be considered due to the energetic model orientations. Instead, the steering angle effect will be considered as a parametric input too.

- Yaw motion: It is the moment generated around the Z vehicle axis. Even when the dynamic model is energetic control oriented, this dynamic is useful to make security constraints over the longitudinal feasible profile in future works. For this reason, it will be contemplated.

- Theta motion: It is the dynamic caused by the load exchange between rear and front assembly. This dynamic is ignored.
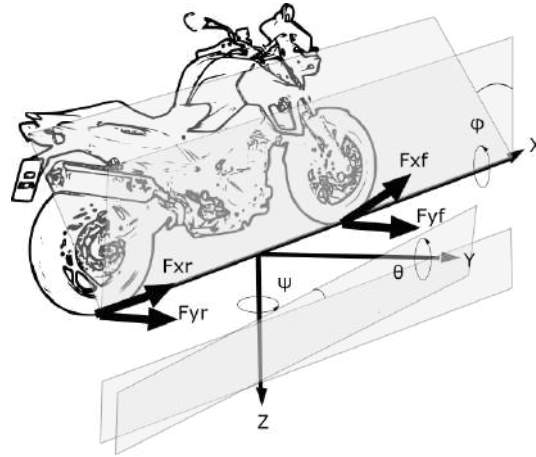
Figure 2.11: Degrees of freedom of motorcycle.
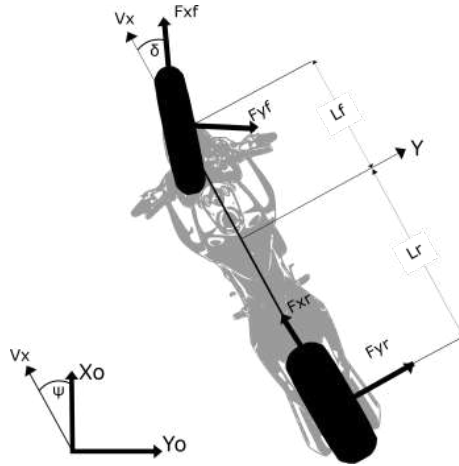
Figure 2.12: Top view of degrees of freedom of motorcycle.

In conclusion, the dynamic model required is composed by following states, inputs, and parametric inputs [4], [18]:

$$x = [\dot{x} \quad \dot{y} \quad \psi]$$
$$u = [T_r \quad T_f] \qquad (2.44)$$
$$u_p = [\phi \quad \delta]$$

Where $\dot{x}$, $\dot{y}$, ψ, T_r, T_f are longitudinal/lateral speeds, the angle between local X axis and global X axis, and rear/front wheel torques.

A. Longitudinal Model:

This research considers an urban speed profile, for this reason, slippage over a longitudinal axis can be omitted [44]. As a result of this hypothesis, the angular speed of each wheel can be omitted as a new state and the longitudinal movement won´t depend on the relationship of longitudinal speed and its equivalent angular speed [16]. It will be the result of the summation of forces along the X-axis.
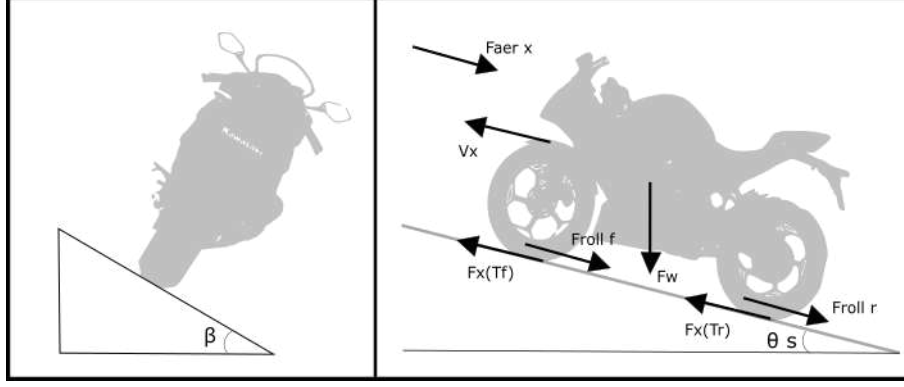
Figure 2.13: Forces involved in longitudinal dynamics.

In Figure 2.13, the road considerations and the forces involved are reported. Applying Newton's second law for motion along the X axis and contemplating two components involved in total longitudinal acceleration (longitudinal acceleration due to motion along the X-axis $\ddot{x}$ and the centripetal acceleration $\dot{y}\dot{\psi}$), the Longitudinal dynamic is described as [45], [16], [44]:

$$M(\ddot{x} - \dot{y}\dot{\psi}) = \frac{T_f}{R_{wf}} + F_{roll} + F_{aer_x} + F_w sin(\theta_s)sin(\beta) \tag{2.45}$$

Where $R_{wf}, F_{roll}, F_{aer_x}, F_{w,s}, \beta$ are the effective radius of rear wheel, roll resistance, aerodynamic force associated to X-axis, weight, slope angle and bank angle. The negative forces related to energy losses will be discussed deeply in section 2.4.

B. Lateral Model:-

Applying Newton's second law for motion along the Y-axis and contemplating the two components involved in total lateral acceleration (lateral acceleration due to motion along the Y-axis $\ddot{y}$ and the centripetal acceleration $\dot{x}\dot{\psi}$), the Lateral dynamic is described as [45], [44]:

$$M(\ddot{y} + \dot{x}\dot{\psi}) = F_{y_f} + F_{y_r} + F_{aer_y} - F_w cos(\theta_s)sin(\beta) \tag{2.46}$$

$$I_{zz}\ddot{\psi} = M_z = L_f F_{y_f} - L_r F_{y_r} \tag{2.47}$$

Where, F_{y_f}, F_{y_r}, F_{aer_y}, F_w, M_z, I_{zz} are the rear and front lateral force, aerodynamic force asociated to Y axis, lateral effect of weight, momentum along Z axis and inertial moment around Z axis. The behavior of lateral forces will be discussed in next sub-section.

BI. Lateral Forces: The lateral forces are known as slip forces because its behavior is strongly related with slip angle. The slip angle is the angle between the vehicle gravity center speed and the X-axis of the vehicle. The expression of slip angle is [46]:

$$\alpha_f = -arctan^{-1}(\frac{\dot{y} + L_f\dot{\psi}}{\dot{x}}) + \delta cos(\epsilon) \tag{2.48}$$

$$\alpha_r = -arctan^{-1}(\frac{\dot{y} - L_r\dot{\psi}}{\dot{x}}) \tag{2.49}$$

Lateral forces in motorcycle are considerably affected by the camber angle too. The camber angle is the angle between the ground surface and the XY plane of each wheel- Its mathematical expression is:

$$\gamma_f = sin(\epsilon)cos(\phi)sin(\delta) + sin(\phi)cos(\delta) \tag{2.50}$$

$$\gamma_r = \phi \tag{2.51}$$

Lateral forces are:

$$F_{y_f} = C_{f1}\alpha_f + C_{f2}\gamma_f \tag{2.52}$$

$$F_{y_r} = C_{r1}\alpha_r + C_{r2}\gamma_r \tag{2.53}$$

If the equations 2.48 and 2.49 are used to make lateral forces calculus with small angle approximation, equations 2.52 and 2.53 becomes in:

$$F_{y_f} = C_{f1}(\frac{-\dot{y} - L_f\dot{\psi}}{\dot{x}} + \delta cos(\epsilon)) + C_{f2}\gamma_f \tag{2.54}$$

$$F_{y_r} = C_{r1}(-\frac{\dot{y} + L_r\dot{\psi}}{\dot{x}}) + C_{r2}\gamma_r \tag{2.55}$$

The relevant equations for lateral dynamics $"F_{y_f} + F_{y_r}"$ and $"L_fF_{y_f} + L_rF_{y_r}"$ can be reorganized to separate the effect of ψ rate, lateral and longitudinal speed ratio and steering angle [45], [44], [47].

$$
\begin{aligned}
F_{y_f} + F_{y_r} =& (-\frac{L_fC_{f1}}{\dot{x}} + \frac{L_rC_{r1}}{\dot{x}})\dot{\psi} - (C_{f1} + C_{r1})\frac{\dot{y}}{\dot{x}} \\
&+ C_{r1}\delta cos(\epsilon) + (C_{f2}\gamma_f + C_{r2}\gamma_r) \\
L_fF_{y_f} - L_rF_{y_r} =& (-\frac{L_f^2C_{f1}}{\dot{x}} - \frac{L_r^2C_{r1}}{\dot{x}})\dot{\psi} - (L_fC_{f1} \\
&- L_rC_{r1})\frac{\dot{y}}{\dot{x}} + L_rC_{r1}\delta cos(\epsilon) + (L_fC_{f2}\gamma_f + L_rC_{r2}\gamma_r)
\end{aligned}
\tag{2.56}
$$

In a short way, we to write it by following equations:

$$F_{y_f} + F_{y_r} = C_r\dot{\psi} + C_\beta\frac{\dot{y}}{\dot{x}} + C_\delta\delta cos(\epsilon) + (C_{f2}\gamma_f + C_{r2}\gamma_r) \tag{2.57}$$

$$L_fF_{y_f} + L_rF_{y_r} = D_r\dot{\psi} + D_\beta\frac{\dot{y}}{\dot{x}} + D_\delta\delta cos(\epsilon) + (D_{gf}\gamma_f + D_{gr}\gamma_r) \tag{2.58}$$

Finally, lateral dynamics are:

$$
\begin{aligned}
M(\ddot{y} - \dot{x}\dot{\psi}) =& C_r\dot{\psi} + C_\beta\frac{\dot{y}}{\dot{x}} + C_\delta\delta cos(\epsilon) \\
&+ (C_{f2}\gamma_f + C_{r2}\gamma_r) + F_{aer_y} - F_wcos(\theta_s)sin(\beta)
\end{aligned}
\tag{2.59}
$$

$$I_{zz}\ddot{\psi} = D_r\dot{\psi} + D_\beta\frac{\dot{y}}{\dot{x}} + D_\delta\delta cos(\epsilon) + (D_{gf}\gamma_f + D_{gr}\gamma_r) \tag{2.60}$$

Even when most of the speed optimization algorithms presented in 2.5 and 2.5 use the longitudinal speed dynamic of the vehicle as main representation of the vehicle speed behavior. In a motorcycle, the lateral movement is highly important due to the natural

unstable lateral dynamic. This instability causes constraints over the longitudinal dynamic which are completely different to the constraints caused by lateral dynamics over a car's longitudinal dynamic.

The lateral forces are known as slip forces because its behavior is strongly related to the slip angle. The slip angle is the angle between the vehicle gravity center speed and the X-axis of the vehicle 2.11. The security of the driver can be represented by a limitation of the relationship between both vectors or in other words, a slip angle control. The slip control lets to introduce the speed limit for two wheels vehicles like bicycles or motorcycles. One of the first approaches was the speed limitation in a corner situation. In [48], the lateral physics of the vehicle movement is studied to proposed a speed limitation in function of the road curvature, the friction coefficient of the road and additional information from the vehicle. For urban and professional drivers, the corner situation presents a challenge to reduce the speed variation without sacrifice the safety. In [49], an optimization is proposed to solve this problem. The optimization takes into account the lateral and longitudinal dynamics of a bicycle, also the damping dynamics are included too. In this paper, two cost function were compared: The minimum time and maximum exit speed. The results of the optimization are sensitive to the curvature of the segment and the initial conditions of the vehicle. Besides, even when in simulations the lap time is reduced, in a real environment the results will depend on the GUI between optimizer and driver.

Besides the scientific works related to lateral dynamics, the commercial systems which require the lateral dynamics are studied to find inspiration. According to the National Highway Transportation Safety Administration (NHTSA) of the United States of North America, the main reason for fatal crash accidents or rollover accidents in that country is related to lane changing [4]. This is the reason why the Yaw angle is taken into account by the dynamic model. There are three kinds of lateral systems [17]: Lane departure warning, lane keeping system and yaw stability control system. The first one alerts the driver to lane departures. Good examples of this system are AutoVue, AssistWare or SafeTrac. The second one is able to detect undesired lane departure and control the steering angle of the vehicle to keep the line. It is a steering control in parallel to the driver steering control. Examples of these technologies are lane-keeping-system (LKS) by Nissan or lane-departure-avoidance (LDA) by the same company [4][16]. The last system is in charge to prevent spinning and drifting events. The system is able to estimate road/weather conditions to find a minimum risk curvature possible for speed and friction available. In this case, the system is able to change the steering and speed reference value in order to improve the safety of the driver.

In conclusion, to take into account the lateral forces lets to increase the security of driver through the steer angle control based on external variables like distance to other objects, vehicles... etc or internal parameters like slip angle, roll angle... etc. However, it does not add important information to reduce the error of speed profile estimation and in consequence, just the longitudinal speed model is enough to make reliable of energy estimators.

2.4 External Phenomenon involved

The autonomy can be strongly affected by the external parameters due to they make the motor works in different torque/speed regions. This difference between the torque/speed region expected and the real one creates not expected energy wastes by the motor, and the inverter; also, it causes non-regenerative regions that affect the ability of RBS (Re-

generative Braking Systems) to harvest energy. For this reason, this section will cover the most important external parameters. Those are the conditions of road and weather and the driver behavior.

A. Road and Weather Conditions.

According to [17] and [50], the most relevant opposite forces to the longitudinal movement in a vehicle are:

- Aerodynamic force.

- Rolling resistance force.

- Slope of road.

AI. Aerodynamic force: It can be expressed as:

$$F_{aereo} = \frac{-1}{2}\rho C_d A_f (V_{wind} * cos(\alpha_{air}))^2 \qquad (2.61)$$

Where $\rho, C_d, A_f, \dot{x}, V_{wind}, \alpha_{air}$ are the air density, drag coefficient, front area, vehicle speed, wind speed and the angle between air and vehicle direction. In average conditions, the aerodynamic force can cause between 20% and 40% of energy expenses in a motorcycle depending on the motorcycle chassis, the speed of air and the angle between vehicle speed and airspeed [4]. The aerodynamic force has to be separated by its influence on X-axis and Y-axis. Those magnitudes will depend on the angle between wind direction and vehicle speed vector direction.

AII. Rolling Resistance Force: It can be expressed as:

$$F_{roll} = -(\mu_0 + \mu_1 \dot{x}^2)F_z cos(\theta_s) \qquad (2.62)$$

Where μ_0, μ_1 are two friction coefficients of the road, F_z is the normal force of the vehicle and θ_s is the slope of the road. The friction coefficients of the road depend on the state of the road. For example, a new asphalt is [0.01, 0.008] and the frozen asphalt is [0.001, 0.00082]. This variation of the coefficient can cause an error of 15% of the autonomy estimation [4]. The motorcycle is a multi-body platform then, there is a load exchange between the front frame and rear frame caused by acceleration and brakes profile. However, a peak normal force is considered to calculate the rolling resistance force due to the frequencies of the normal force transference is faster than energetic dynamics.

AIII. Slope of the road: When the road presents a slope by a medium or long distance, the load exchange cannot be ignored. In this case, the load exchange has not a dynamic but it creates a weight component in X and Y axis which affects the forward and lateral movement dynamic. The equation which describes this effect is given by:

$$F_w = mg \qquad (2.63)$$

Where m, g the mass and gravity.
In [51], the authors have modeled the impact of the external parameters to reduce the energy uncertainty. With this model, an electric vehicle assistant able to improve the usability of an electric vehicle was developed. Even when the electric vehicle assistant

(EVA) is able to reduce the energy uncertainty about a 34%, those results do not use mechanical limitations of motor, inverter, and battery. For this reason, it is expected to improve those results using those data.

In conclusion, the external parameters cause an autonomy uncertainty able to be considered a research problem. The last sections have developed most of the tools to deal with it, this information is used to makes the motor works in the most effective energy region.

B. driver.

The driver is the person who is in charge of controlling the speed of the vehicle and guide the direction of the motorcycle movement. For this reason, A big quantity of options to increase or decrease the energy waste will depend on him because the variance of the weight, posture, and acceleration profile creates an uncertainty in the model which affects the effectiveness of any controller. It is possible to affirm that even an expert driver continues to spend unnecessary energy in most of the cases for three reasons:

- Unknown future parameters like the specific curvature and slope of the road, weather, traffic or road state.

- Undertanding of electromechanical aspects of the EV like SoC dynamic, battery health or motor efficiency behavior.

- Biological reasons like driver posture, driver's fatigue, or simply by driver's impossibility of keeping the same posture for long periods of time.

The posture is the unique disturbance caused completely by the driver (user). There are so many ways to take into account the driver posture for canceling its effect over the energy consumption. Most methods can be agruped into two sets [45], [4]:

- Understand the posture as a disturbance of the control loop.

- Improve the model to use the user body in the gravity center calculus.

The first one, the posture observed as a disturbance of the model output, is the most basic try to make robust the model in front of posture changes. This option builds a model of the vehicle which separates the vectorial components of each force involved in the movement. When the motorcycle is in middle of a curve, longitudinal and lateral forces appear. Those forces are depending on the slip. In the case of longitudinal forces, they depend on the slip ratio which is the longitudinal slip over the longitudinal speed during braking and over equivalent rotational speed during acceleration. The longitudinal slip is the difference of both values mentioned before along the X axle. In the case of lateral forces, they are depending on the lateral slip which is the ratio between the longitudinal speed of the center of gravity and the longitudinal speed along X axel. Those forces are shown in Figure 2.14, since both forces, can be characterized, the slip angle presents in the movement of the vehicle can be controlled. This force needs to be controlled because the peaks of the slip force could cause an accident. For example in [52], the multibody model is used to be controlled by a robust Hinf controller and achieve acceptable stabilization times and it is able to reject the disturbances caused by the posture. The natural structure for controlling the steering angle in an TWEV is the handlebar then, the easiest way to control the direction of the vehicle is this one. The model of an electric vehicle
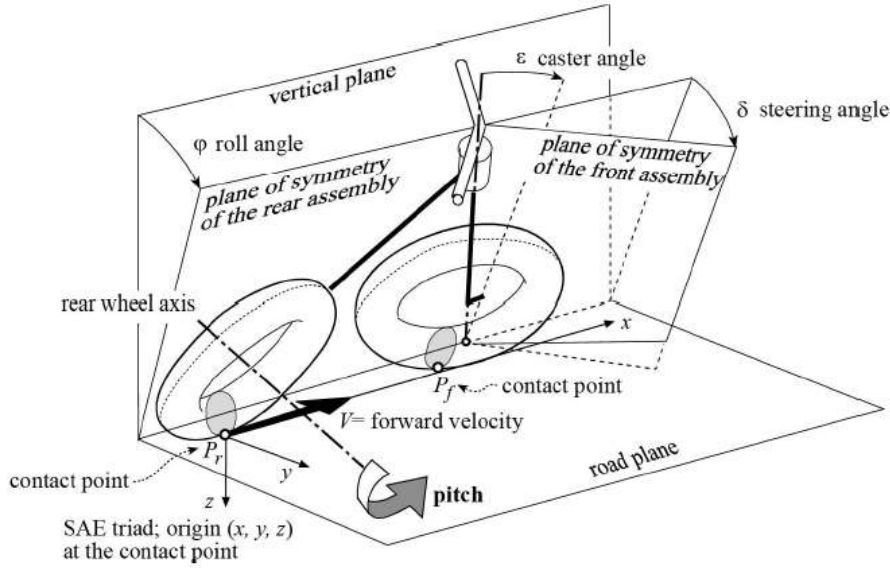
Figure 2.14: Slip force present in a motorcycle [4].

needs the steering angle as an operational point because is a nonlinear parameter. It is possible to transform the original model into an equivalent model that can be controlled with linear techniques because a linear controller generally requires less CPU than a nonlinear controller [53]. Works like [54] [55] develope a linear version of motorcycle dynamics to determine the movement limitations. Even when these controllers are not relevant to energetic behavior, they let to determine the range of speed, load, and acceleration where a linear model can be used.

The second one, an improvement of the modellets to contemplate the user interaction with the vehicle model capabilities. The mass center depends on the user and his posture. For this reason, a multi-body model is studied to determine how the force caused by user posture variation affects the vehicle mass center. To improve the mathematical model parameters like weight, position, and height are required. In [56], more information about the driver to develop a virtual driver and an augmented vehicle model (vehicle and driver dynamics), it lets to improve the controller capabilities and it makes easier to find an equilibrium point. The virtual driver and the nonlinear control developed in this paper was able to reduce the tracking error lower than 2%. The virtual driver is responsible for proposing to take into account the upper and lower driver body as different bodies which interact with each other. However, this concept is more useful in tracking problem than the energetic efficiency problem.

As a conclusion, even when the motorcycle dynamic model is widely used to tracking task; the usage of spatial degrees of freedom is relevant to determine the energy consumption. Since the longitudinal dynamics describes the longitudinal acceleration behavior and this behavior affects the motor energy consumption, the dynamic have to be used as a constraint to proposed a valid electric vehicle assistant.

40

2.5 Autonomy Optimizers

A. Power demand profiles.

Power demand profiles are strongly related to the considered drive-cycles. A drive cycle is a set of speed data that tries to represent a common speed profile for an average vehicle under certain characteristics. It is currently used to compare the pollution emission between different vehicles. Taking into account that, the power demand will be the translation of the drive cycle to the amount of energy required by the electric vehicle to follow that reference. It is important to note that the different properties of the electric vehicle like the weight, the front area or the power devices capabilities will be required to do the translation between the speed reference (drive cycle) and the power demand profile.
There are two kinds of drive cycles [4], [44]:

- The modal cycles, they are composed of straight accelerations and constant speed references. The most used modal cycles are the European standard NEDC or Japanese 10-15 Mode.

- The transient cycles are a better representation of an average speed dynamic. The most representatives transient cycles are the FTP-75 or Artemis cycle.

Those drive cycles have a different version for describing the behavior of a vehicle in different environments. For example, Artemis cycle has four versions: Urban, Rural, Motorway 150 and Motorway 130. Since the propose of the research is to represent an urban environment, four power demand profiles were chossen;

- NREL class 3: low size vehicles with speed profile between 0 and 70 kmh.

- NREL class 6: Meddium size vehicles with speed profile between 0 and 80 kmh.

- WLTC class 1: low size vehicles with speed profile between 0 and 70 kmh.

- WLTC class 2: Meddium size vehicles with speed profile between 0 and 90 kmh.

In all cases, the external conditions like wind speed and slope profile are the same to keep comparable the results. In the case of slope profile, realistic data obtained from GoogleMaps in a traject from Paris to Brussels are used.

B. Driving alerting systems.

The driving alerting system is algorithm able to considerate external variables for updating the autonomy estimated value. This kind of algorithm requires a set of data and one model: longitudinal vehicle data and battery model. The algorithm uses internal vehicle states (speed and acceleration) to related them with the external parameters of each travel. According to the external current data about weather, road, traffic... etc. The estimated acceleration profile is based on the historical data set of acceleration profiles in the same conditions. The acceleration profile is translated to power demand and it is sent to the SoC estimator. The SoC estimator uses the power demand profile and the battery dynamic model to determine if there are or not enough energy to complete the travel. External information required by the driving alerting system are:

- Terrain parameters.

- Weather conditions.

- Driving profile.

- Traffic conditions.

- Speed limits.

Those parameters let to determine the capability of the driver to follow a speed reference. In [57], [58], all this information is obtained from different sources like GoogleMaps, Wunderground.com.. etc, to make a historical data based range estimation. This is one of the most simple algorithms proposed to evaluate the current travel configuration to make a realistic autonomy estimation. The data-based estimator proposed in [57] does not use traffic behavior and it is not able to distinguish the travel time and travel speed for different users. In other words, it is not able to use the drive profile historical data information. Even when the algorithm has those limitations, it is able to reduce the expected autonomy in function of weather/road conditions. This capability is shown a reduction from 12% to 64% of the autonomy estimated in comparison to contemporaneous algorithms. Those results depend on the conditions of each travel. The data-based proposed in [58] can increase the number of variables used in order to contemplate the drive profile and the traffic conditions but due to the number of possible combinations between all the external variables used, there is a computational time limit which makes impossible to continue reducing the autonomy uncertainty.

The data-based estimations accuracy depends on the amount of obtained data and the classification capacity to determine the useful and not useful information. For this reason, the authors in [59] propose an algorithm able to become to each person into an information source. This kind of proposals brings to software developments like "Waze".

Another algorithm able to be used in the driving alerting system is the speed/range estimator. This kind of algorithm does not use a database to predict the autonomy available in the electric vehicle, it requires two models: longitudinal vehicle model and battery model. The algorithm uses current external information to estimate the forces which are involved in the longitudinal movement of the vehicle. According to the current acceleration profile the power demand is calculated and the rest of the process is the same. The main difference between speed/range estimator and data-based range estimator is the quantity of data required because even when speed/range estimators require external variables of weather and road, those variables are not related directly with the speed value estimated. Those variables are the inputs of the longitudinal dynamic model of the vehicle to be compared with the occupancy and acceleration rate sensor data to determine the power demand along each travel segment. Avoid to makes this relationship between the road/weather conditions and the speed profile lets to reduce the sample time required by data of the mobile data network variables and it reduces the error caused by the speed profile freedom of the user.

In [11], other specific variables are taken into account. The power demand for heating/cooling, wipers, lights, and traffic are considered as power losses into the resultant power demand profile estimated. Also, when the variables of road/weather conditions and the speed profile are not related, it lets to introduce a new concept: the historic efficiency. This term refers to the motor, inverter and battery efficiency. The efficiency of electrical power transfer devices is considered constant in many longitudinal dynamic models but, the results of this paper demonstrate that this hypothesis (constant efficiency) causes a significant error due to the range of torque and speed contemplates into an average journey.

This kind of algorithm is open-loop systems but in papers like [60], the interaction between a GUI (graphic user interface) able to show the power demand along each road segment and the user lets to the user infers the efficiency behavior. In other words, the user is in charge to close the loop. The mentioned research in the last paper uses this interaction to increase the capability of the driver to comes to a charge station when it is required. Also, the algorithm is used to calculate the minimum quantity of energy required to complete the travel to the destination or the next charge station, it is called the optimal charging profile. A similar approach is [51] where the quantity of energy required by each segment of travel is evaluated to determine not just the range estimation, the optimal road between two places too. This estimation is a function of external temperature and initial electric vehicle conditions.

The variability of the power devices efficiency along different travels makes important to contemplate the losses. The losses in all induction motors are mainly due to stator and rotor copper losses, and friction losses. In [61] only copper and core losses are modeled for the calculation of efficiency of induction motors due to they are considered the main electrical losses in the induction motors. In this paper, the SoC uncertainty achieves to decrease around 10% in comparison with range estimators which consider constant efficiency values. Those results can vary depending on external parameters. In order to integrate this information into the Ph.D. research, the inverter losses considered have not changed but the losses in BLDC motor have to be reconsidered due to the motor architecture differences. Two kinds of losses will be considered like [25]: Core losses and Eddy Current Losses. The core losses refer to the losses in stator tooth and stator yoke due to hysteresis and eddy current losses. A detailed description of losses model considered will be discussed in subsection 2.3.1.

In conclusion, besides that the speed model used by the range estimator improves its accuracy in comparison to the data based estimations, it lets to detect the efficiency behavior along a trajectory according to the speed reference proposed by the driver. This is a tool useful to reduce the energy demand through two techniques: to avoid higher power demand trajectories and to let the user becomes a controller about the speed-power demand profile through a GUI. Both techniques contribute to the autonomy increase. The efficiency control imposes restrictions over the route or the speed profile to contemplate the torque profile described by the external variables. Then, new energetically optimal speed or position profiles are obtained.

C. Speed profile optimization

As it was mentioned before, the possibility to estimate the range opens the possibility to quantify the efficiency of the road and the driver's actions. In consequence, the "eco-driving profiles" appear. An eco-driving methodology consists in finding the optimal way to reduce the overall energy consumption. Besides, the "eco mode" is a mode of driving where limitations imposed by eco-driving are active for increasing the range of the vehicle. In [62] the potential of "eco-driving profiles" is evaluated. This paper concludes that even when internal combustion and electric vehicles are sensitive to speed optimizations, electric vehicles show a higher potential with an improvement of 18% of the total range in front of the average range improvement in internal combustion vehicles (around the 7%). It is due to the proportion of the losses for heat and friction in internal combustion engines that are not comparable with the electric vehicle losses due to the same phenomenon. In other words, the power chain is more efficient in electric vehicles than in internal combustion vehicles, then the efficiency of electric vehicles is more sensitive to losses due to

external factors.

Due to this potential, in parallel to the estimators, the speed profile optimizers appear. In [63] a macroscopic representation of the energetic behavior is used to synthesize a fuzzy controller. The objective of this controller is to evaluate the external parameters of the travel and battery state of charge to determine when it is required to extend the range. The controller manipulates the speed/acceleration limitations through the drive mode options: dynamic (sport), economic or eco-dynamic (eco-mode). As a result, even when power chain losses and gear losses are not considered, the "Adaptative operation mode" proposed by the Fuzzy controller increased the range around 10%.

Fuzzy controllers are sensitive to rules description. For this reason, a controller which uses the non-linear model of the mechanical and electrical behavior of an electric vehicle can improve the resolution of the control signal based on the model information. For example, in [64] an optimal control is formulated and five models were consider: The model of longitudinal dynamics of the vehicle, the motor/inverter model based on efficiency maps obtained by FEA (finite element analysis), the model of auxiliary power consumption sources, the hydraulic brakes model and the battery model. The dynamic programming algorithm cost function proposed has three components: the power of the battery, the complete travel time and the smoothy of speed profile. Besides, there are two constant values which have to be proposed by the user to achieve a balance between the complete travel time and smoothy of speed profile. The algorithm was able to save a 14.8/% of the SoC in a trip of 19km with a combination of urban and highway speed profiles. This algorithm is an offline approach, then a higher quantity of SoC can be saved if a closed-loop controller is proposed due to the controller would be able to react to external disturbances in real-time. Dynamic programming requires segmentation of the complete problem to divide the optimal problem into subproblems easy to solve. The number of subproblems (n) and the number of possible states (N) in each subproblem will describe the complexity of the solution O(n, N). Then, two options can be explored to deal with the dynamic problem complexity. By one hand, the number of subproblems (n) required to bring resolutions to the algorithm can be optimized. For example, in [65] the quantity of energy saved is compared to the number of traject segmentations (n) to find the optimal value of segmentation required. On another hand, the number of possible states in each subproblem (N) is reduced to keep an acceptable balance between complexity and resolution. For example in [66], the same energy management problem is boarded but a simplification of the battery model is proposed to avoid the relationship between the internal resistance and the open-circuit voltage with the state of charge. As a consequence, the dynamic of the state of charge can be ignored in each subproblem using average values of internal resistance and open-circuit voltage. This approximation achieves to reduce between an 80% to 95% the compilation time without affecting more than a 1% the quantity of energy spend along the trip when the algorithm is applied.

The potential of the eco-driving made with offline optimization like the one presented before is reduced by the inconvenience of offline optimization, the open-loop optimization does not take into account the disturbances that could appear along the traject like traffic, lights, etc.... For this reason, a closed-loop technique is presented in [65] is explored. In this paper, an hybrid vehicle's energy management is optimized along with two types of speed profiles: the new European driving cycle (NEDC) and the urban dynamometer driving schedule (UDDS). A bi-level MPC is proposed in order to reduce computational time and to simplify the hybrid optimal problem. In the external loop, a Krylov subspace method is introduced to optimize the velocity trajectory and to improve computational efficiency at the same time. In the internal loop, an explicit solution of the optimal

torque split ratio and gear shift schedule is used by Pontryagin's minimum principle and numerical methods combination. Even when the energetical results are not comparable between this paper and the latest papers presented to the hybrid vehicle, this paper lets to determine the feasibility of online techniques. Besides, the comparison made in the paper between offline techniques and the proposed online techniques lets to determine that the proposed closed-loop method is able to save the same quantity of energy than an open-loop technique and it is also able to take into account the disturbances.

Finally, the onboard implementation is proposed in [67]. This paper proposes a multi-objective offline optimization between energy and travel time optimization. Both values are organized hierarchically to be optimized based on the values predefined by the driver. Besides, the optimization covers the two faces of energy optimization: speed and torque. The first stage of the paper is to make a speed profile optimization and the second stage is to add the torque limitations based on speed profile proposed and efficiency map established. The proposed method used an hybrid strength Pareto evolutionary algorithm differential evolution (SPEA-DE) based on SPEA2 and improving the inaccuracy of its solutions by differential evolution (DE) to make the method simple and robust. As a result of the technique proposed, the vehicle was able to highlight in the European Eco-Marathon energy efficiency competition in transportation by its 23% of energy saved.

The presented research works let to conclude four ideas: The first one, Even when the current devices can be replaced with the newest ones with efficiency improvements, the optimization of usage of the current devices is a field of research that helps to expand the possibilities of the electric vehicles. In the second one, the presented papers show the importance of the different parameters (Quantity of states, number of steps) in order to make the controller available to be implemented. The third one, the segmentation of the road is not only a tool to reduce the complexity of the optimal problems, but it is also a tool to explore parallel algorithms and segmentation techniques based on elevation, traffic or other variables apart from the length. Finally, one of the most important stages of the optimal controller developing will be the modelization of the vehicle in its electrical and its mechanical performances to determine the power losses of the power chain and the dynamic behavior of the vehicle.

D. MPC Optimiser:

Since there are many noise sources, optimizers have to face the challenge to close the control loop and make real-time optimizations. One option to face this task is an MPC (Model Predictive Controller), this advanced control technique is able to find an optimal control signal which considers constant constraints like physical or mechanical limitations of the plant and dynamic constraints which represent the dynamic description of a system. This ability lets to predict the behavior of a platform based on past events and face future state values in a smooth way.

The dynamic platform evolution of the system is considered along a period called the prediction horizon (via the solution of Euler–Lagrange equations). After a vector of an input signal is found by minimizing a cost function (via a numerical minimization algorithm) and considering all constraints, the first element of the control vector is usually used. The MPC algorithm is described in Algorithm 1.

The MPC is able to face non-linear restrictions when the MPC covers non-linear restriction it is called a non-linear MPC (NMPC). The limitations of an MPC are caused by the dynamic system representation. This control technique depends on a model representation, it means variation between the real model and the model representation will cause a bad designed feasible space. Also, the complexity of the restrictions increase the

Algorithm 1 NMPC Controller.

1: BEGIN
2: Introduce optimization constraints and cost function.
3: Introduce the optimization dynamic constraints (dynamic model of the system).
4: Choose the initial states of the dynamic system.
5: Make initial measures to complete constraints information.
6: Minimize the cost function inside the feasible space designed by the constraints.
7: Apply the first component of optimal reference for a period of time equal to the sample time.
8: Evaluate the final state satisfaction.

- If the error between states and references has to be reduced, then use final states as new initial states and go to 5.

- If the error between states and references is enough small, then the control process has ended.

---

compilation time and it has to be less than the sample time in order to make usable the control technique.

Some variations of the MPC controller can handle the limitations described before. For example, explicit MPC is based on the parametric programming technique and it lets to compute offline optimizations to reduce the compilation time [68], [69]. Another example of MPC variations is the robust MPC. This variation is able to consider the disturbance evolution to guarantee the control signal feasibility. There are three main approaches to robust MPC:

- Multi-stage MPC: It is able to make modifications in the cost function and the constraints based on an uncertainty space approximation through a scenario-tree formulation.

- Constraint Tightening MPC: It pre-consider the effect of the disturbances in the feasible space designed by constraints in order to ensure the feasibility of the control signal proposed even in face of disturbances.

- Min-max MPC: In this case, many optimization are made to cover all possible disturbances values.

Like those examples, there are many other MPC variations to make implementable the MPC technique.

In the vehicle environment, the MPC has been started to cover different aspects of the driver task due to the augmentation of compilation power and the embedded of more sophisticated and feasibility variations of MPCs. For example in [70], the trajectory of a set of UAVs (Unmanned aerial vehicles) is controlled to avoid obstacles while they go from point A to point B. In this example, the numerical minimization algorithm is implemented with a sequential quadratic programming method with the Gaus-Newton approximation of the Hessian. Also, the code is a combination of ACADO code and C++/ROS to minimize the compilation time. As a result, the NMPC is suitable for an AR. Drone 2.0 quadrotor. It was able to keep a compilation time under 2mS with two UAVs and a minimum safety distance of 50 centimeters between any other UAV and another obstacle. Those results are made with "Dell Latitue E5440 (CPU: i5-4300U with 11:29GFLOPS=s)".

In hybrid vehicles (Internal combustion engine and electric motor), the MPC has been

started to conquer energy efficiency optimizations. In [65] energy optimization is proposed to increase the amount of energy harmed in each brake event. The optimization problem is separated into two steps in order to reduce the dynamic model complexity and in consequence the compilation time too. This kind of MPC is called a Bi-level MPC because there are two control loops. One of them controls the speed optimization and the other one is in charge of the torque split. On one hand, the speed optimization uses a Krylov subspace method to solve a nonlinear time-varying optimal problem with high computational efficiency. On the other hand, an explicit solution of torque split ratio and gear shift schedule is proposed as a combination of numerical methods in the framework of MPC and Pontryagin's minimum principle. As can be seen, the reduction of the complexity is able to reduce the compilation time a 98.4% in comparison with a sequential quadratic programming (SQP) MPC and a 99.6% in comparison with dynamic programming depending of the initial model complexity. This compilation time reduction makes suitable the NMPC technique.

More specifically speaking in pure electric vehicles with a hybrid power source (supercapacitors and Lithium battery), the MPC has been started to conquer energy efficiency optimizations too. In [71] an NMPC is used to take into account the trip information to accomplish with two objectives: track a state of charge reference for supercapacitors and minimize the battery current. This objective increases the cycles of life of the battery and lets to increase the usability of supercapacitors energy. In consequence, the complete system increases the durability and autonomy of the vehicle. The NMPC has been solved using a self-coded SQP solver in MATLAB, which permits to generate C code for HiL (Hardware in the loop) purposes. The compilation time is not optimized due to the dynamic behavior of the state of charge (SoC) of battery is enough slow to work with compilation times between 22.62s and 14.59s.

Finally, in [72], the eco-driving optimal problem adds stochastic information using a Markov chain. With this way, the optimal control is able not only to predict the dynamic of the vehicle but also to take into account the human interaction to increase the autonomy of the vehicle. In this paper, a stochastic model predictive control (SMPC) strategy lets to calculate the optimal required speed value to enhance the amount of energy recovered when the vehicle stops into an intersection but, taking into account the human driving error caused by the interaction between the driver and the controller. The SMPC achieves to save 12% more energy in comparison to classical MPC techniques. In average, the compilation time is close to 1s if the horizon time is less than thirteen seconds.

In conclusion, the MPC technique is highly used to take into account the dynamic model and disturbances characteristics into the control signal. As a result, the control signal is stable and smoothy. The limitation of the MPC technique can be solved in different ways and it lets to use this technique for making energy optimization for an electric vehicle with high-performance results in comparison to other open loop or standard techniques.

2.6 Electric vehicles challenges and scientific methodology to solve challenges.

The previous literature review allowed us to find the EV's limitation where scientific works have possibilities. This kind of vehicle is challenging many problems as can be seen in Table 2.1, but there is an issue that is present in most of them, the energetic efficiency. Currently ECO driving mode is a function of electric vehicles which is in charge to reduce the throttle, torque and speed capabilities of the vehicle to increase around a

20% autonomy. The capacities of ECO mode driving can be improved using external information and vehicle dynamics. For this reason, the goal of this Ph.D. research will be to propose a way to incorporate the external parameters in control techniques in order to find an optimal balance between energy efficiency and driver control and to complete a trip. Section 2.3.1 concludes that the freedom of the user to choose the speed reference of the motor without taking into account the required torque along each section of the road is the main cause of uncertainty in longitudinal motorcycle dynamics. So, the required torque along each section of the road and the required models to achieve it are studied in Section 2.4. Constraints and degrees of freedom of the balance optimization are presented in Sections 2.3.2 and 2.4. The result of this research has to be an algorithm able to keep the motor work in the most efficient work region along a trip using road, driver and weather information. The algorithm is based on speed optimizers described in Section 2.5. Also, it has to cover the implementation methodologies proposed in section 2.5 according to MPC limitation and nonlinear problem characteristics.

Subsystem	Problem	Bibliography	Solution
Motor	Energetic efficiency	[73] [74]	Strategies to improve the input signal treatment.
		[75] [10] [76]	To design motors for specifics work ranges (speed or torque).
	Regional Laws	[77] [75] [78] [79]	Make laws to classify the electric vehicles based on their speed and power in order to propose the correct place to use them (speed and power limiters are designed to accomplish with these laws).
Battery	Efficiency		Choose most efficient battery based on advantages or disadvantages of each material currently used.
		[80] [81]	Improve DC-DC efficiency through new BMS (Battery manager System) topologies or new materials to reduce switching energy losses an increase Regenerative braking.
		[36] [35] [11] [16]	Use the SoC estimation to optimize the power management.
	Charge/Discharge process	[37] [38] [81]	Cells equalization process with a multilevel DC-DC is proposed.
Driver controls	Speed dead point	[82] [83] [84]	The optimal energy harvest region is studied to propose control over the brakes system or a hybrid brakes system (Electric and ABS brakes).
	Maximum energy harvestable	[85] [86] [87] [88] [14] [89] [90] [91] [53] [92] [93] [94]	Add new electric motor to increase the optimal speed/torque region in brakes scenario. Control techniques by PWM, optimal control, Fuzzy or Hinf proposed. Manage model uncertainties to keep the motor in its most efficient energy harvest region.

Inverter	Switching response	[95] [96] [97]	An ultra-capacitor system between the inverter and the battery pack would allow higher current flux in strong accelerations and decelerations events. Control the charging process to replace the DC-DC bidirectional converter with a PWM three phase signal or buck converter.
	Power management	[98] [99] [50] [100]	Study the different factors involved in the energy control process in order to build tools to predict the optimal control signal. In consequence, the controller usage is improved. An example is the DSP technique. Improve the BMS/Inverter mathematical model and in consequence, the energy management control too.
Driver	Security parameters	[54] [101] [52] [56] [102]	Improve the mathematical model to obtain a model where the center of mass variation takes into account the driver posture. The slip angle is a non-linear system state which can be controlled. The dynamic model of the lateral behavior of two wheels electric vehicle is improved by adding more information to determine risk probabilities. Fuzzy and Hinf controllers are proposed to reduce the impact of uncertainties on the system.
	Lateral stability	[4] [18] [45] [55]	Improve the mathematical model and take into account the posture as a disturbance of a roll control loop (Handel-bar or CMG). The stability of the driving profile is studied to ensure the vehicle will be able to track different reference trajectories. In order to reduce the error magnitude, longitudinal aspects are taken into account.
	Energetic consumption profile	[103] [50] [100] [103] [11] [12] [51] [65] [104]	An analysis of the different energy consumption reasons is made to develop a consumption estimator based on internal and external information of the vehicle. Since future states are estimated, optimal control are proposed to use this characteristic.

Table 2.1: EV technology challenges and its possibilities at the moment.

It is suitable to conclude that the previous section (2.5) and the Table 2.1 allows us to compare different optimization algorithms and relate them with the EVs limitations then,

this comparison justifies the choisse about the optimization algorithm for our research problem.

2.7 Conclusion.

The electric vehicles have become a transport possibility thanks to the efficiency increasing on each of their components, but cost and energy loss management still being the main challenges of this technology. Even when faster charge methodologies or hybrid power sources are proposed in order to reduce the charge time and autonomy variability, the amount of energy available inside the vehicle will always be finite. Therefore, the capability of the inverter to manage the energy consumption will determine the capacity of the electric vehicles to position themselves as the most ecological, secured and comfortable transport option. Since the torque and the speed will determine the energy consumption, the dynamic model able to represent the correct information for the inverter or another kind of energy controller is highly imperative. Finally, The speed profiles optimizers are a strong technique to use the information available not only inside the vehicle (the dynamic model of the vehicle) but also the external information to the vehicle as trip requirements, driver weight, driving habitudes, slope characteristics or traffic alerts to create an accurate estimation of the energy consumption and lets the driver to take decision with this information. Since the speed optimizers represent an open-loop methodology, the presence of disturbances caused by parameter variance or traffic has to be considered in a closed-loop methodology. For this reason, the MPC is presented as a required methodology in this thesis. Even when the MPC has some implement ability limitations, many MPC variations are presented to show that according to the optimization problem characteristics, there are some MPC variations able to increase the implement capacity of the MPC technique.

In the next chapter, the electrical, mechanical and thermal models required to make an online optimization algorithm with high accuracy are proposed based on the information presented in this section.

Chapter 3

Modeling

3.1 Introduction

This chapter takes the state of art presented in previous chapter to highlight the mathematical model requirements to make an energetical dynamic representation. Based on those models and their requirements, the adaptations made to theoretical models in order to adapt them to our research problem requirements are explained. The relationship between models is presented in Figure 3.1. Where the $P_e(\tau, \omega)$ is the estimated power based on the torque and the speed calculated by the longitudinal model, the $P_l(\tau, \omega, °C), P_r(\tau, \omega, °C)$ are the power losses and the required power demand based on the torque and the speed calculated by the longitudinal model but also on the temperature, $R_i(°C)$ is the value of the resistive element of each device based on temperature and $C_b(°C)$ is the battery capacity based on temperature.
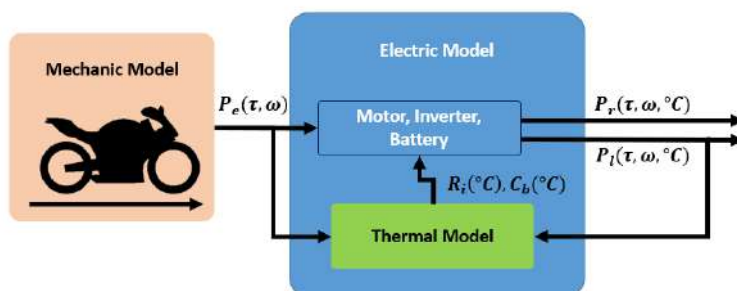
Figure 3.1: Diagram model.

The specific explored topics are:

- Electrical Model: The electrical model of the components is presented as the main information required to obtain a model of the electric vehicle. Since the objective of our research problem is related to autonomy optimization, the electric model is oriented to represent the energy losses dynamics along the power chain, how to prevent them and how to be simulated in real-time applications.

- Thermal Model: The electrical model requires a characterization based on the temperature inside and outside of the electrical components. For this reason, a thermal model is required to make the adjustment automatically without decreasing the real-time capabilities and resitive elements of the electric model.

- Mechanical Model: The mechanical distribution of the electrical elements and the longitudinal or lateral mechanical considerations of the motorcycle movement determine how the energetical behavior is calculated. Then, this section presents the mechanical considerations related to energy estimation and how it affects the electric model.

3.2 Electrical Model: Power losses

The used electrical model describes the power losses of an electric vehicle. They can be represented by the three main elements (see Figure 3.2): The battery (battery source), the inverter (the power electric converter) and the electric machine (mainly used as motor). The driver proposes a speed reference translated to a torque reference and sent to the inverter, the inverter uses the DC voltage from the battery to recreate an AC triphasic voltage signal proportional to the speed required. Even when there exists other electrical devices in the power chain which can present losses, these three elements represent the main losses with the major efficiency variation due to torque/speed operation point of the motor or another external phenomenon.
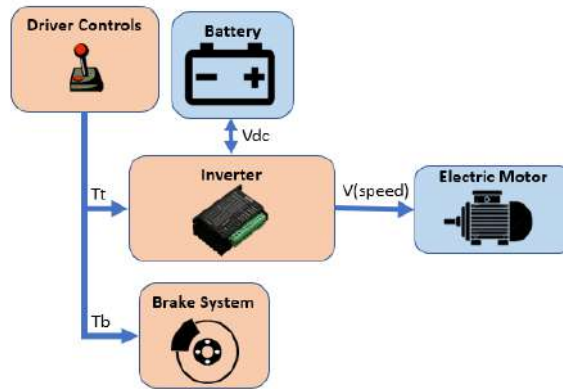
Figure 3.2: Pure electric general component diagram.

3.2.1 Motor power losses

In our case, the BLDC (BrushLess Direct Current) motor is considered due to their presence in the transportation market caused by their torque to weight ratio, the low maintenance cost, and the high-efficiency values.

In a BLDC (BrushLess Direct Current) motor, the efficiency in stady state can be defined as:

$$\eta = \frac{P_{out}}{P_{in}} = \frac{T_e W_s}{T_e W_s + P_{lcu} + P_{lfe} + P_{lmag}} \tag{3.1}$$

Where, η is the efficiency definded as the relationship between the output power (P_{out}) over the input power (P_{in}) of the system. The output power is described by the mechanical power obtained by the motor. In other words, the product between the electromagnetical torque (T_e) and the angular speed of the motor (W_s). The input power is described as the output power plus the motor losses. In the motor, the considered losses are P_{lcu}, P_{lfe} and P_{lmag}, they are respectivily the Joule losses (also called copper losses), the core losses (iron losses) and the magnetic losses in rotor magnets.

The magnetic losses are caused by eddy-current loss in the permanent magnets of Brush-Less machines are usually neglected [22]. Since the fundamental air-gap field usually rotates in synchronism with the rotor, and time harmonics in the current waveform in the winding distribution are generally small, P_{lmag} can be neglected.

The Joule losses are caused by the resistivity of the cooper in winding. When a current cross a conductor material, the resistivity of the material opposes to this current movement. As a result, part of the electrical power is dissipated and heat is produced. They can be expresed as in [23], [24].

$$P_{lcu} = \rho_{cu} * Vol_{cu} * J^2 \tag{3.2}$$

And with the copper volume and rms value of the surface current density remplacement:

$$P_{lcu} = \frac{\frac{\rho_{cu}}{K_{fill}}(L + L_{ew})(K_{sp}\pi D_o)}{\frac{\pi}{4}(D_o^2 - (D_i + \frac{B_g\pi D_o}{B_j 2pK_{fe}})^2) - \frac{B_g\pi D_o}{B_t}(\frac{D_o - D_i}{2} - \frac{B_g\pi D_o}{4B_j pK_{fe}})} \tag{3.3}$$

Where ρ_{cu}, Vol_{cu}, J, D_o, D_i, B_g, B_t, B_j, K_{fill}, K_{fe}, p, L, L_{ew}, K_w and K_{sp} are the copper resistivity [Ohm.m], the volume of copper[m^3], the rms value of the surface current density [A/m^2], the stator outer diameter [m], the stator inner diameter [m], the air gap flux density [T], the flux density in stator tooth [T], the flux density in stator yoke [T], the slot filling factor, the lamination factor, the number of pole pairs, the stator lamination length [m], the length of end-winding [m], the fundamental winding factor, and the fundamental current density [A/m^2], which can be expresed in terms of load torque "T_l".

$$K_{sp} = \frac{T_l}{B_g D_o^2 L sin(p\alpha_{pm})} \tag{3.4}$$

where α_{pm} is the half of mechanical magnet angle.

Core losses appear in a magnetic core due to alternating magnetization as a consequence of the not perfect synchronization between electrical and magnetic fields. They are the sum of the hysteresis losses (due to the difference between magnetization rate and demagnetization rate) and the eddy current losses (due to Farady's law effect over lamination motor structure caused by magnetic fields). The core losses are defined as in [25].

$$P_{lfe} = P_{LEy} + P_{l_t} + P_{l_t t} \tag{3.5}$$

Where, P_{LEy}, P_{l_t} and $P_{l_t t}$ are the losses in rotor yoke due to eddy current and losses in tooth body and tooth tip caused by hysteresis and eddy current. Those expresions are:

$$P_{LEy} = n_y(\frac{f}{p})^{1.5} R_{Ym}^2 A_{ry} \sqrt{\frac{\pi^2}{i\rho_{Fe}\mu_{Fe}} \sum_{i=1}^{\inf} \frac{B_i}{\sqrt{i}}} \tag{3.6}$$

$$P_{l_t} = K_h f^\alpha B_t^\beta + \frac{4}{\pi} K_e \frac{f^2 B_t^2}{\alpha_t} \tag{3.7}$$

$$P_{l_t t} = K_h f^\alpha B_{tt}^\beta + \frac{4}{\pi} K_e \frac{f^2 B_{tt}^2}{\alpha_{tt}} \tag{3.8}$$

Where: n_y, f, p, R_{Ym}, A_{ry} are the number of rotor yokes, frequency, number of poles pairs, mean radius of the rotor yoke, the area of the rotor yoke face. ρ_{Fe}, μ_{Fe}, B_i, B_{tott} and α_{tott} are resistivity and the mean permeability of the rotor yoke material, the magnitude

of ith harmonic of the armature flux density wave, the peak value of flux density at the tooth or the tooth tip and the mean pole transition angle in electrical radians. Finally K_h, α, β and K_e are constants obtained from the curve fitting of core loss data measured with sinusoidal excitation. This representation requires three lookup tables, the magnetic flux density as a function of stator current measured in the stator yoke, the rotor yoke, and the air gap.

3.2.2 Inverter power losses

Losses caused by the semiconductors inside the inverter appear on one of each current flux case [33]:

- Conduction, when the current is going from drain to source along the drain-source resistance.

- Blocking, when a minimum part of the conduction current is able to cross along the blocking diode.

- Switching, when the gate starts or stops to be excited.

Since the current which is able to cross the blocking diode is minimum, this power loss is neglected (Figure 3.3).
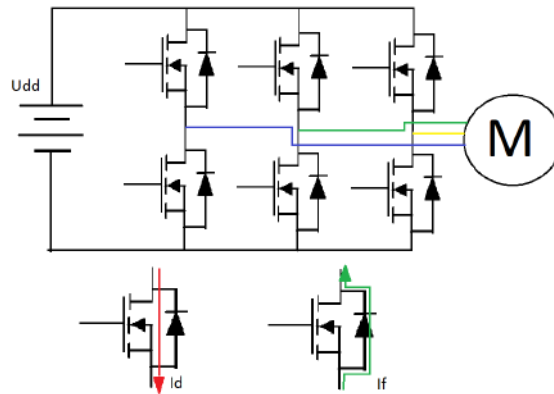
Figure 3.3: Inverter circuit

Those losses can be classified in two cases: Forward and reverse current (Figure 3.3) [33]. The first one, when the current goes from power source to motor (I_d). In this case, the losses per semiconductor are expressed as:

$$P_{LCm} = R_{ds_{on}} I_d(t)^2$$
$$P_{LSm} = \tfrac{1}{3}(W_{SMon} + W_{SMoff}) f_{sw}$$

(3.9)

Where, $R_{ds_{on}}$, I_d, W_{SMon}, W_{SMoff}), f_{sw} the drain-source on resistance, the drain RMS current, the energies which are dissipated along the rise and fall time caused by internal capacitances and the switching frequency.

The second case, when the current goes from motor to power source (I_f). In this case, the losses per semiconductor are expressed as:

$$P_{LCd} = U_{D_o} I_f(t) + R_D(t) I_f(t)^2$$
$$P_{LSd} = \tfrac{1}{3}(W_{SDon}) f_{sw}$$

(3.10)

The conduction losses along the diode are described by the power consumed by the voltage drop (U_{D_o}) across the diode during the saturation regime and the diode resistance (R_D) due to the reverse current through the diode (I_f).

3.2.3 Battery power losses

A battery model enough capable to represent the state of charge (SoC) dynamic is shown in Figure 3.4 [35].

Where: VOC, R_o, C_1, R_1 are the open-circuit voltage (a function of SoC), the series resistance, and the RC components which describe the frequency response. Finally, the FCC value represents the total capacity of the battery. The states of this model are the voltage U_1 and the SoC. The input is the current and the output is the voltage U_L.

$$C_1 \frac{\delta U_1}{\delta t} + \frac{U_1}{R_1} = i \tag{3.11}$$

$$SoC(t) = \frac{1}{FCC} \int_0^t i(\tau)\delta\tau + SoC(0) \atop \frac{\delta SoC}{\delta t} = \frac{i}{FCC} \tag{3.12}$$

$$U_L = VOC(SoC) + U_1 + R_o i \tag{3.13}$$
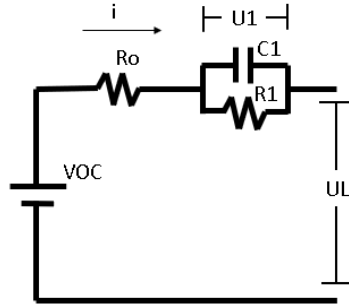
Figure 3.4: Equivalent circuit model of a Lithium-Ion battery
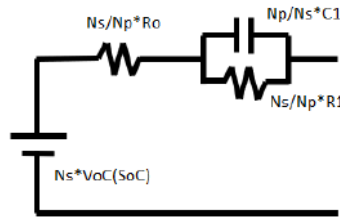
Figure 3.5: Equivalent circuit model of a Lithium-Ion Pack battery

In order to obtain realistic data, parameters obtained from LIR18650 2600mAh lithium battery cell [105] are used and ideal serial/parallel relationship from [43] is used to obtain the model parameters of a 45Ah 72v battery.

Finally, the lithium battery pack model is shown in Figure 3.5.

Where Ns, Np are the number of series and parallels required to complete the pack.

The losses in the battery will be caused by the power dissipated by the resultant serial resistance and the voltage on the resultant RC circuit.

$$P_{loss_{bat}} = R_o I^2 + \frac{U_1^2}{R_1} \tag{3.14}$$

3.2.4 Electrical model verification

In Figure 3.6, an experiment is proposed to verify the behavior of the presented electrical models. The NREL Class 3 Speed/Torque profile presented in Section 2.5 is used to recreate the output mechanical power. In order to evaluate the losses of the system, two hypotheses are required:

- The voltage variation of the battery can be underestimated along all the trip.

- The air flux is enough to avoid strong temperature changes on electronic devices. Then, the model variations caused by temperature are not considered.

Once the mechanical power is calculated, the motor power losses are estimated using the efficiency map. Finally, the mechanical motor power and motor losses are summed to become the inverter output power. The inverter output power ignores the voltage variations to obtain a current profile. This current profile has to be divided into positive and negative values to use the conduction and reverse conduction semiconductor losses model. When the losses in inverter are calculated, they are added to inverter input power to obtain the battery output power. Finally, the current profile is used to obtain the battery losses and the complete amount of energy required by the vehicle is obtained.

The amount of energy required along all the trip is compared to the amount of energy available in the battery final range to determine the theoretical range of the vehicle. Also the estimated is compared in Table 3.1 with the theoretical range of a similar vehicle (w100 km) [106].

Brand	Battery Capacity	Battery Material	Motor power	Autonomy
Motorcycle Modeled	40 [Ah]	Li-ion	3000 [W]	82 [Km] (No EB) 106 [Km] (EB)
Maker (EnergyMotion)	40 [Ah]	Li-ion	3000 [W]	90 [Km] (EB)
Amovible (TopMove)	40 [Ah]	Li-ion	3000 [W]	120 [Km] (EB)
EM001 (XTM)	40 [Ah]	Li-ion	3000 [W]	<110 [Km] (EB)

Table 3.1: Electric motorcycles performance comparison. (*EB = with Electric Brakes function)
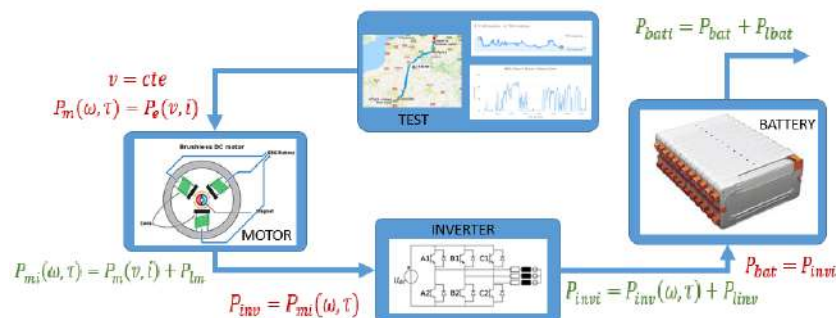
Figure 3.6: Experiment diagram to check the electric model behavior.

Along the trip proposed by the experiment, the used speed profile was the NREL Class 3 and the torque parameter was obtained from the external characterization of a real trip

between Paris and Brussels. As a result of the traject proposed, the BLDC motor power shows predominant high losses. Its peak value is 61% and its mean value is 7%. This is the most important waste of power and its variance is caused by the nonoptimized speed variation along the torque variation required by the road. The battery losses represented a mean of 3.7% of the losses with a 27% as a peak value. Finally, the inverter was the smallest source of losses with a mean of 2% and a peak value of 9%. This research lets to determine the hierarchy required by a losses optimization to make the highest impact over the electric vehicle range.

A. Motor Power

As it can be seen in Section 3.2.1, the theoretical model of motor losses is the most complex in comparison with other models required (Inverter and battery losses). For this reason, it is required to decrease its complexity. A first tool commonly used to achieve this is to use an efficiency map [107], [108], [65]. Then, this section uses this tool to obtain the losses hierarchy required.

A virtual representation of the BLDC motor model by magnetic simulation software using logical programming (ANSYS and Python) is used to consider the theoretical model presented in Subsection 3.2.1 without making the parameter estimation one by one required by the theoretical representation and without making a customized coding of the theoretical equations. The efficiency map can be determined as Figure 4.1.

In Figure 3.7, the positive limitations can be noticed around 3000 Watts but in the efficiency map, the motor is not able to give the torque required to achieve the maximum power when the speed is high due to its physical limitations and the motor losses. In other words, the limitation of the power in the efficiency map is due to the constant power limitation of the motor added to the losses predicted by the magnetic simulation software.

Figure 3.7 also shows the negative power under the -4000W. It is caused by the not modeled heat power dissipation in the inverter model. In a real environment, this negative value is reduced by the inverter and battery input power limitation and the usage of mechanical brakes to improve the efficiency of the BLDC motor as a generator. The parameters of the considered BLDC machine are shown in Table 4.1.

Parameter	Value
The rated voltage	72 v
The rated power output	3000 w
The rated torque	185.6 Nm
The rated speed	91.3 RPM
No Load maximum speed	157.6 RPM
Maximum efficiency speed	773 RPM
Maximum efficiency torque	73.2 RPM
Maximum efficiency	96.4 %
Pole pairs	16
Outer diameter of the motor	253.3 mm
Magnet Height	50 mm
Number of turns per coil	30
Phase resistance	0.03 Ω
Phase inductance	0.04 mH

Table 3.2: BLDC motor characteristics.
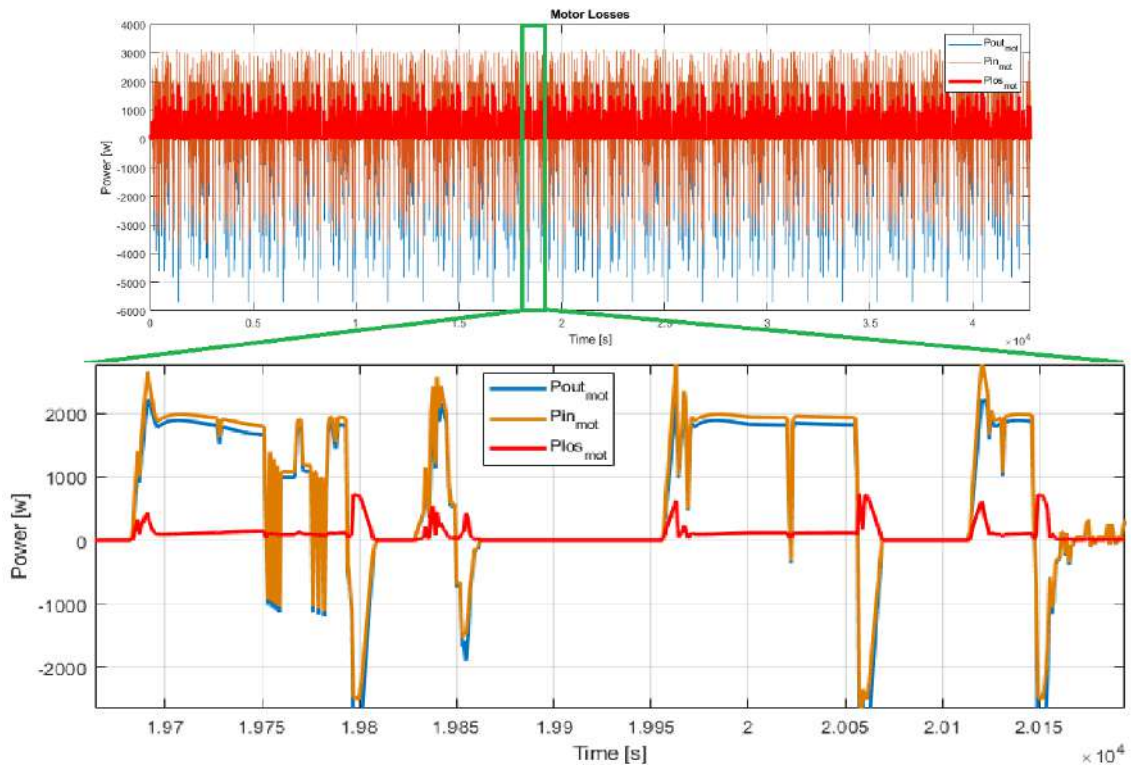
Figure 3.7: input/output motor power profile.

The controller of the BLDC machine aims to preserve high efficiency values of the motor even under different torque/speed requirements. In this case, the maximum efficiency of the motor is 96.4% and the mean losses in motor represent 7% of the total power required along the travel. However, the variations of the speed reference create over-damped disturbances in the power losses due to variations of the efficiency. It means an optimal mission profile would require smooth speed profile in order to reduce those undesired waste of energy. The only way to make smoothy speed profiles is to analyze

enough information about the traffic and the vehicle environment.

B. Inverter

In the case of the inverter, the data required to implement the theoretical model was obtained from STP75NF75 datasheet [109]. This semiconductor lets to drive a BLDC motor with the characteristics previously presented.

As in Figure 3.8, the overdamped behavior is minimum in the inverter losses in comparison with the motor losses. In this case, the theoretical model presented in Subsection 3.2.2 lets to determine a correspondence between the power and inverter losses. For this reason, the correlation between the losses and the components of mechanical power was studied.
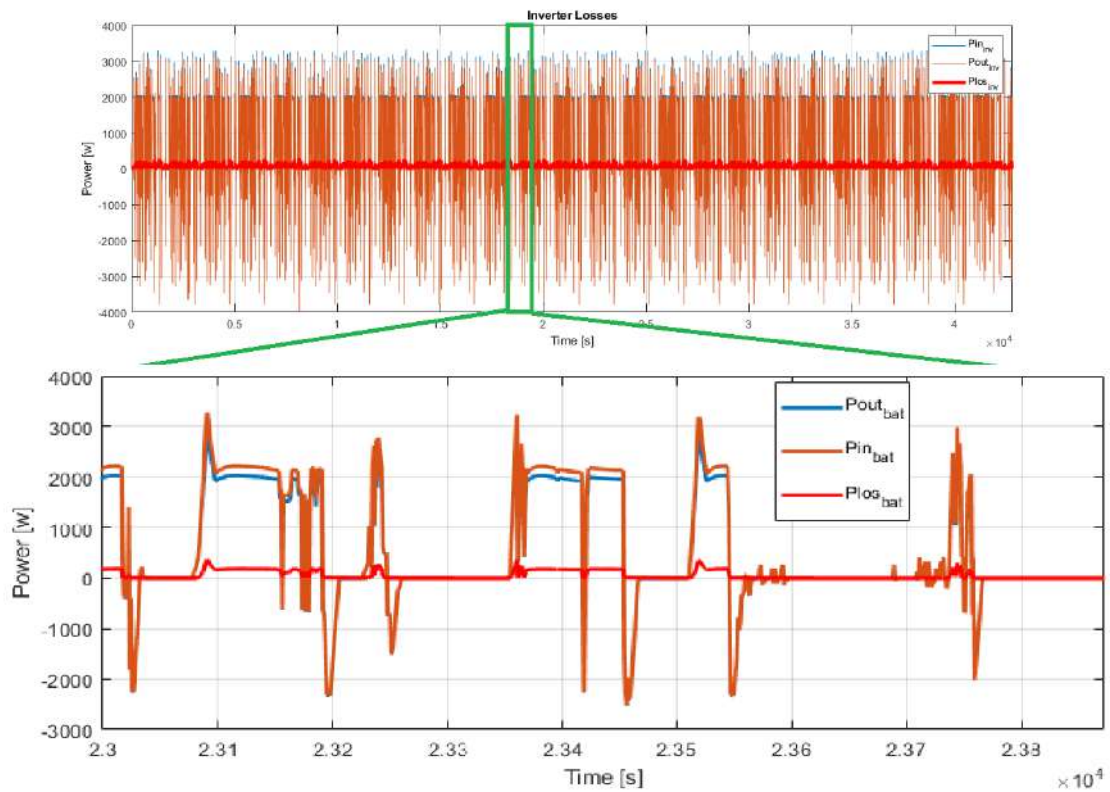
Figure 3.8: input/output inverter power profile.

This study shows that the speed has a stronger effect over the inverter losses than the torque. This is due to the longer range of the speed in comparison with the torque range. In Figure 3.9, the speed and the inverter losses are presented. As can be seen, the inverter losses are proportional to the speed and their value increase by an instant when the speed is reduced abruptly. These results enforce the theory of a smoothy speed profile as a way to make a power optimization. Also, the optimized speed profile has to keep in mind the maximum speed value available to reduce not just the total power required, but the inverter losses too. However, the inverter losses represent in average 2% of the total power required to follow the speed profile then, the inverter does not represent an important degree of freedom or limitation to make power optimization without additional circuits or new semiconductor materials.
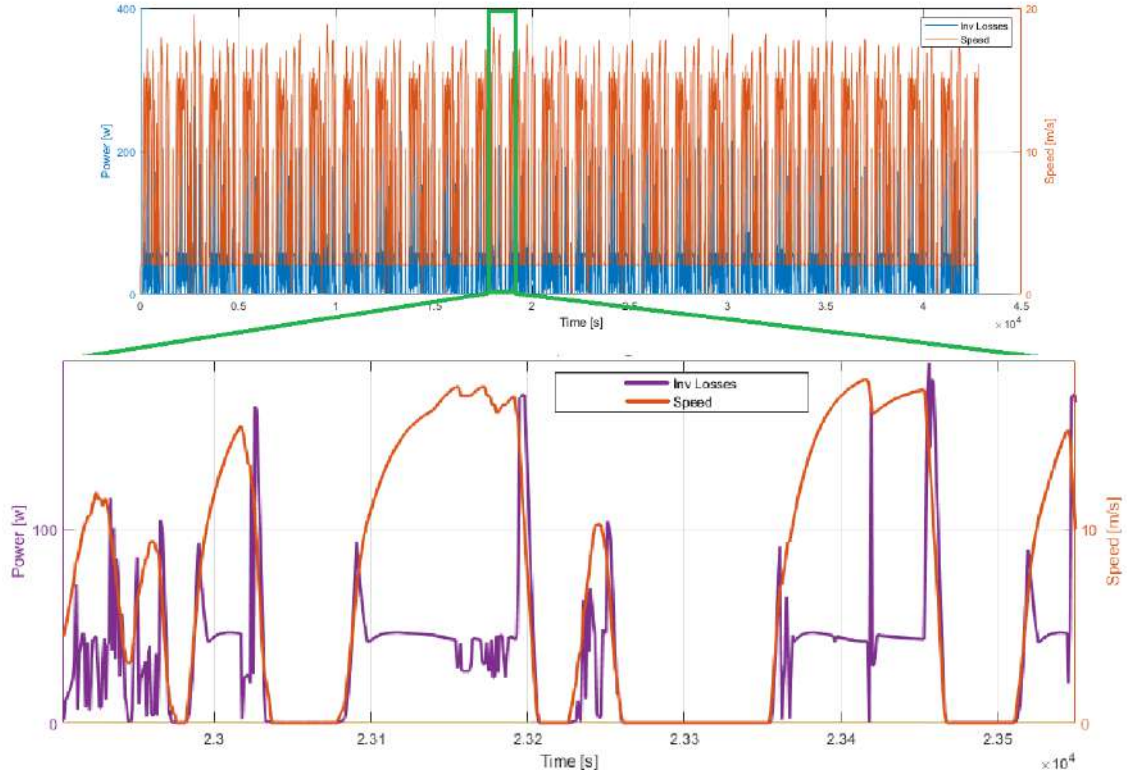
Figure 3.9: Speed and inverter losses.

C. Battery

According to the model presented in Subsection 3.2.3, the battery losses are caused by resistivity properties of the connection ports and the RC response. The $P_{out_{bat}}$ and $P_{in_{bat}}$ refer to the power delivered by the battery to the inverter and the power initially stored inside the battery respectively. The losses are proportional to the amplitude of the power signal due to the resistivity component of the battery losses model. Also, the RC circuit has a barely perceptible sub damping effect over the losses (see Figure 3.10). As a conclusion, the linear resistivity component of the losses is the most important component to consider into a lithium battery as power source.
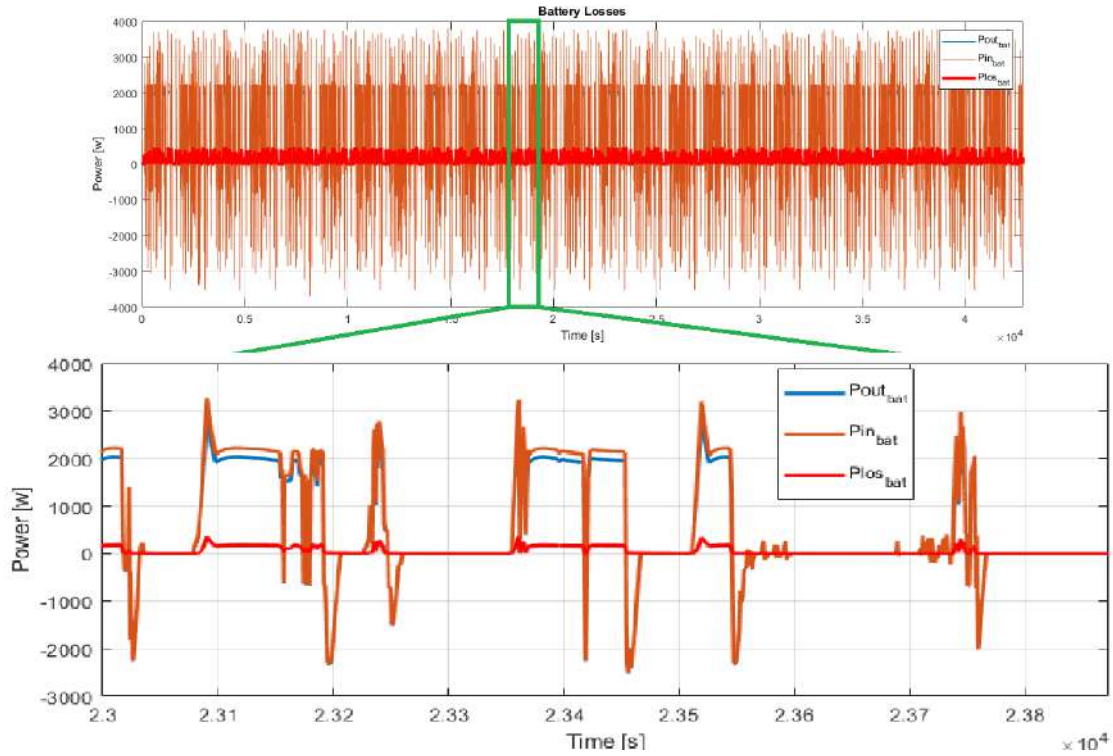
Figure 3.10: Battery power losses behavior.

The Lithium battery presents additional constraints imposed by its charging process limitations, those constraints are present on the battery management system (BMS). The BMS is in charge to ensure a safety charge/discharge current based on additional data like battery temperature and state of charge (SoC) of the battery. This is why the efficiency of the regenerative brakes is strongly affected. To model, those constraints additional dynamic modeling are required to represent the power constraints due to the process to make a suitable current profile from the BLDC motor to the battery. Since these constraints reduce significantly the amount of energy recovered by the regenerative brakes and also it requires an additional dynamic model to represent the phenomenon (increasing the compilation time), this is why those constraints were not modeled in this work. Even when the additional range by brakes energy recovery is about 29%, the limitation of electric brakes capacity to recover energy (the interaction with the BMS) will reduce this value to a smaller one. According to [110], the additional range obtained by the regenerative brakes are from 8% to 25% but it will be strongly affected by the temperature and SoC condition, they propose the supercapacitors as a tool to overcome some limitations imposed by the BMS (as a filter) ensuring a smooth charge current profile.

The mean of the battery losses is 3.7% of the total energy required along the trip. It means that even when the battery losses have similar behavior in comparison with the inverter losses due to its resistivity power dissipation, the effect of the battery has higher priority to be solved because it represents almost the double of the energy waste. This result explains why the supercapacitors are an option even when the economic cost of them are high. Therefore, a more global optimization approach considering the cost constraints could be interesting in future works.

As a conclusion, the motor losses represent around 55% of total losses that can be described by the electric model. Also, its behavior presents two degrees of freedom: the speed and the torque value. Those characteristics of the motor losses make it the most important element to be considered in the Eco-Driving Controller. Finally, the battery

and inverter losses are proportional to the speed value then, they can be limited through speed constraints.

3.3 Thermal Model

3.2 The electrical losses presented in the last section can vary according to the thermal

behavior of the electrical components used. For this reason, this section presents a method to consider this variance and reduce the error between the power losses estimated and measured.

In order to consider the thermal behavior, the Forster network is used to reproduce temperature exchanges. For each Foster representation (battery, inverter and electricmachine), the resulting circuit is composed by four kinds of elements:

- Current source: the current is the representation of power. For this reason, in each Foster representation, there is a current source which represents the losses (dissipated power) responsible of the temperature augmentation.

- Voltage source: the voltage is the representation of the temperature. If the element is in contact of the outside, there is a voltage source at the end of the circuit which represents the ambient temperature.

- Resistance: it represents the capability of a surface to dissipate or absorve temperature. It will be affected by the area and material characteristics.

- Capacitor: the capacitor represents the capability of a body to change its temperature, this capability will be affected by the mass of the body and the material characteristics (specific heats).

In general words, the Foster network will be described by the following equation [111]:

$$C_i \dot{T}_i = P_{in} - \frac{\Delta T_{ij}}{R_i} \tag{3.15}$$

Where i represents each node of the circuit, C_i the capacitor, P_{in} the thermal input power (the dissipated power), ΔT_{ij} is the temperature difference between two surfaces and R means the resistance of the surface.

The capacitor and the resistance have the following expression:

$$C_i = m * C_b \tag{3.16}$$

$$R_i = \frac{1}{h * A} or R_i = \frac{1}{K * A} \tag{3.17}$$

Where: $m, C_b, h, K, and A$ are the mass, the specific heat, the convection and conduction parameters, and the area.

The expression of the resistance can vary according to the temperature exchange process present (conduction, convection or radiation). The material coefficients considered are shown in Table 3.3.

Material	$C_b[J/Kg*C]$	$K[C/w]$	$h[C/w]$
Litium	3.56	301.2	-
Aluminium	0.92	209.3	-
Air	0.001	-	0.026

Table 3.3: Considered material characteristics.

3.3.1 Battery Foster network

The battery Foster network is based on [36] [41] [112] and it is shown in Figure 3.11. The representation lets to notice three main bodies. The battery which is in contact with the aluminum case in the 82% of the surface and with locked air in the 15% of the surface. 3% of the contact with other kinds of materials is not considered. Also, it is important to notice that there is another power source from outside since the battery is one of the biggest bodies in a two wheels vehicle (like a motorcycle), the surface of the aluminum case will be in contact with solar radiation.
The input power of this Foster network is the resistive power dissipated in the electrical battery model.
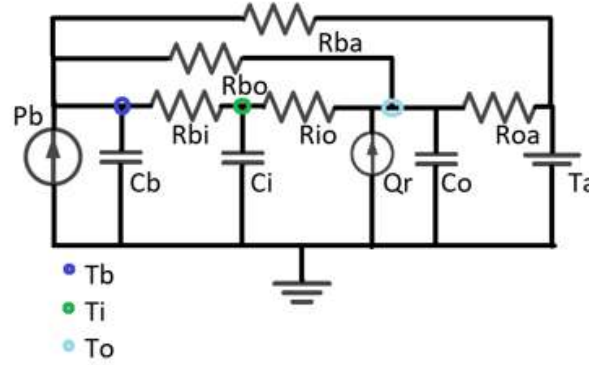
Figure 3.11: Equivalent thermal circuit model of a Lithium-Ion battery

Where $P_b, T_b, T_i, T_o, T_a, Q_r, C$ and R are the battery losses, the battery temperature node, the node of the inside air temperature, battery case temperature node, ambient temperature, dissipated power added by radiation, thermal capacitance representation of each element, and the resistance which represents the temperature exchange dynamic between two nodes.

3.3.2 Inverter Foster network

In Figure 3.12, the Foster network representation of the inverter can be seen [113], [114]. There are four main elements represented in the network: The Mosfet drain, the heatsink, the locked air, and the aluminum case. Even when the inverter outside surface can be in contact with locked air from the motorcycle structure, the variation from external air and locked air between motorcycle structure and inverter is not considered.
The input power of this Foster network represents the inverter losses.
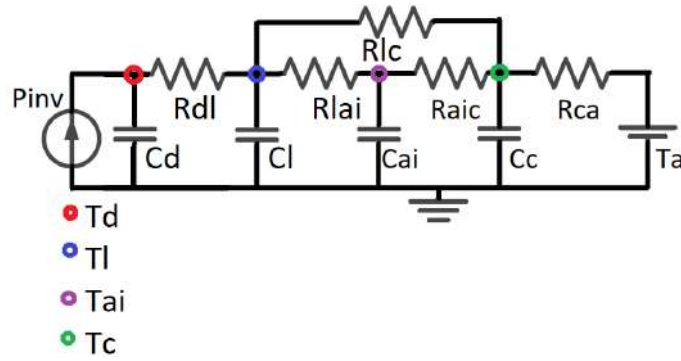
Figure 3.12: Equivalent thermal circuit model of an inverter.

Where: P_{inv}, T_d, T_l, T_{ai}, T_c, T_a, C and R are the inverter losses, the diode temperature node, the heatsink temperature node, the node of the inside air temperature, inverter case temperature node, ambient temperature, thermal capacitance representation of each element, and the resistance which represents the temperature exchange dynamic between two nodes.

3.3.3 Electric machine Foster network

The thermal analysis of a BLDC motor can be a challenge due to the number of involved structures. Currently, FEA [115] (Finite Elements Analysis) is used to resolve the thermal circuit with a node number higher than 20 in many cases [116]. But in this case, a stationary analysis based in [111] lets to summarize the analysis.

In Figure 3.13 the Foster network representation of the outer BLDC motor is shown. In this model, five main bodies are represented: The winding, the stator, the air gap, the core, and the external case. Due to a hub motor, the solar radiation present close to the wheel will affect the case temperature.

The heat affects the motor in more than one way. By one hand, the resistive losses increase according to iron temperature response [117]. Taking into account that the resistive losses (Joule losses) are less than one-fifth of the total losses [24], the effect of iron response in face of temperature augmentation is reduced considerably. By the other hand, the magnets suffer a demagnetization at the same time [25]. It reduces the magnetic losses but at the same time the capacity of the motor to achieve high torque values. In this work, the demagnetization is not considered.

The power input of this Foster network is the resistive power present in the electrical BLDC motor model (Joule losses).
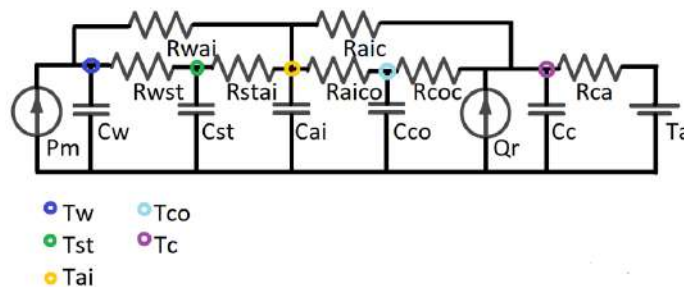
Figure 3.13: Equivalent thermal circuit model of a BLDC outer motor.

Where: $P_m, T_w, T_{st}, T_{ai}, T_{co}, T_c, T_a, Q_r, C$ and R are the Joule motor losses, the winding temperature node, the stator temperature node, the node of the inside air temperature, the core temperature node, motor case temperature node, ambient temperature, dissipated power added by radiation, thermal capacitance representation of each element, and the resistance which represents the temperature exchange dynamic between two nodes.

3.3.4 Thermal Model validation

In this test, the flux of heat is evaluated in order to determine if the thermal exchange show a logical direction.

Also, in order to validate the behavior of each thermal model, a test is proposed. Since all simulations are based in real devices properties, the test is to run the simulation using the maximum constant power admissible by the device according to the datasheet and to compare with the maximum working temperature. Using this test, the thermal limitations of real devices and simulated devices can be compared.
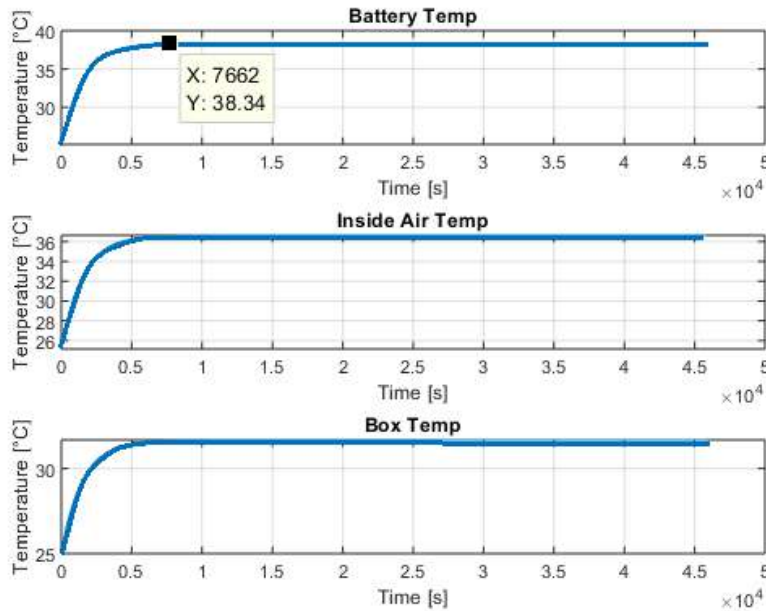
Figure 3.14: Battery foster network validation

The considered battery is a pack build with LIR18650 2600mAh Lithium cells. Those cells consider an ideal serial/parallel relationship between them to build a 45Ah 72v battery pack. No external battery cases are considered between the battery and the motorcycle. Also, the thermal coupling between all individual cells is considered perfect. The maximum output current is 1C (C= 45Ah) and voltage variation of the discharge process and unbalanced cells are not considered. Initial temperature states are 25°C for all elements and the external temperature is 25°C too.

The thermal response of the battery is slow due to the specific heat of Lithium (see Figure 3.14). Also, the maximum temperature of the battery has an error of (4%) in comparison with the maximum value of the battery datasheet (40°C). Finally, the distribution of the temperature is consistent with user experience. Even when, the model has a strong

considerations it is able to reproduce the lithium thermal behavior in order to consider these characteristics in energy consuming.
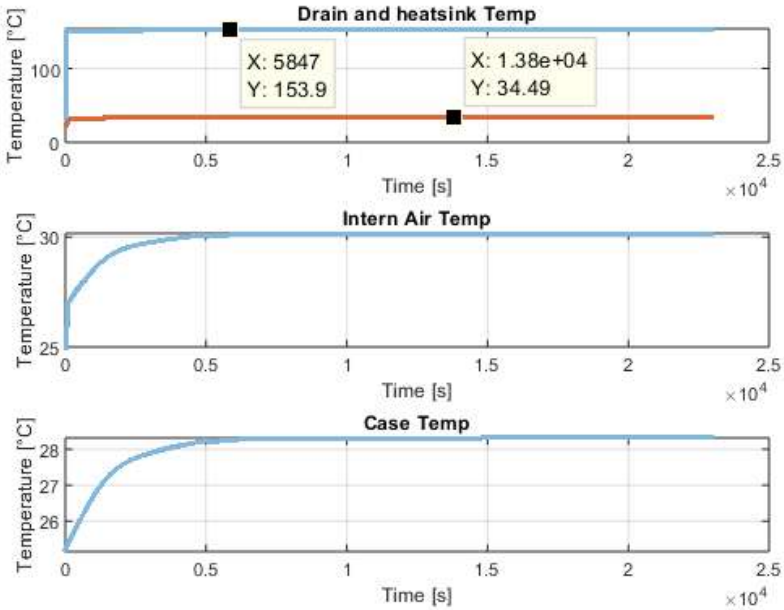
Figure 3.15: Inverter foster network validation

The inverter considers the usage of STP75NF75 transistors and the dimensions of Sabvoton Controller, model 72200. The transistor drain temperature increases three times faster than the heatsink temperature and twenty times faster than the other structures. This behavior is caused by the value of the temperature exchange coefficient of the materials considered in transistor, its heatsink and its dimensions. Also, the thermal coupling considered between each drain with the heatskin reduces the error in stabilized time. The heat flux is consistent with the literature and the losses caused by the maximum output current (80A) causes an error of 2% over the maximum temperature reported by transistor datasheet (see Figure 3.15).
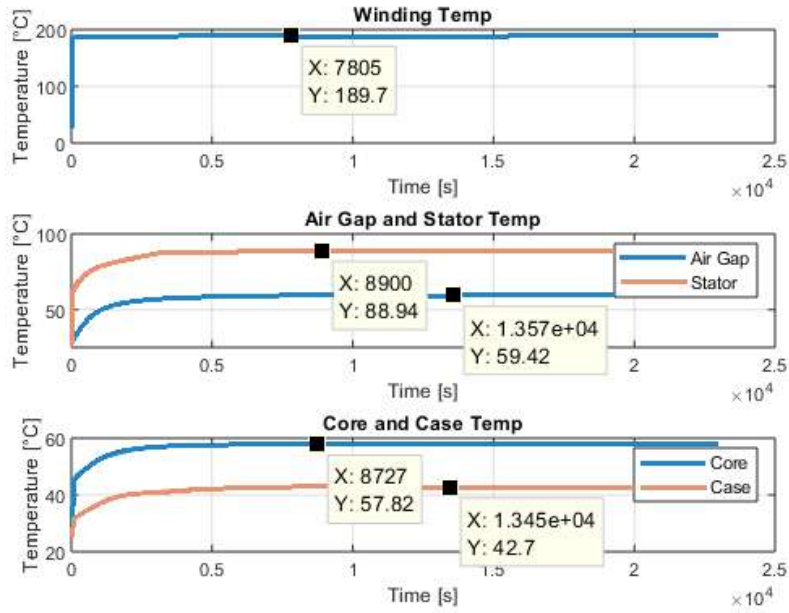
Figure 3.16: BLDC Motor foster network validation

The motor thermal network has the biggest error in the winding structure (11.5%) in comparison with maximum temperature value reported by the datasheet. This error is caused by the number of simplifications made by the proposed Foster network (see Figure 3.16). When thermal analysis wants to be done over a BLDC motor, a FEA analysis is commonly used with a matrix version of Foster network in order to increase significantly the amount of considered thermal nodes. Also, as just the Joule losses are considered as thermal heating source, the effect over the losses variations is minimum and it is proportional to the amount of current. In consequence, high-speed values can increase the thermal error due to the presence of high magnetic looses.

For those reasons, even when the heat flux of the proposed Foster network is consistent with user experience and the error can be improved increasing the number of nodes, the thermal behavior of the motor with just Joule losses won't be considered in future autonomy estimations due to its reduced effect over the motor energy losses. To compensate the lack of thermal modelization of the motor, the efficiency of the motor will have the heaviest participation in optimization objective. With this way, the motor losses will be prioritized and their thermal effect will be reduced too.

3.3.5 Thermal effect over the autonomy

Once the thermal dynamic is modeled, it is possible to know the ambient temperature affects the autonomy. In an electric vehicle design process, the ambient temperature is considered to estimate the optimal heatsink required, the weight of this element is representative in comparison to the vehicle weight. For this reason, there are works related with heatsink dimensional optimization [118]. However, in this work, the Foster network is used to divide each electric component into different thermal nodes to make a dynamic representation of the temperature at each element. It lets to obtain the resistivity characteristics required by the electric model but taking into account its augmentation estimated by the thermal behavior and technical data. The lookup table required to make

the link between the thermal model and the electric model is presented in Table 3.4.

Temperature [°C]	Inverter diode resistance [%]	Battery Resistance [%]	Battery Capacity [%]
-15	80 (8 [mΩ])	733 (2.27 [Ω])	71 (681.6 [F])
-10	82 (8.2 [mΩ])	497 (1.54 [Ω])	75 (720 [F])
-5	85 (8.5 [mΩ])	358 (1.19 [Ω])	78 (748.8 [F])
0	87 (8.7 [mΩ])	269 (0.83 [Ω])	82 (787.2 [F])
5	90 (9 [mΩ])	207 (0.64 [Ω])	86 (825.6 [F])
10	92 (9.2 [mΩ])	163 (0.50 [Ω])	89 (854.4 [F])
15	95 (9.5 [mΩ])	130 (0.40 [[Ω])	93 (892.8 [F])
20	97 ([mΩ])	114 (0.31 [Ω])	97 (931.2 [F])
25	100 (10 [mΩ])	100 (0.35 [Ω])	100 (960 [F])
30	105 (10.5 [mΩ])	91 (0.28 [Ω])	104 (998.4 [F])
35	110 (11 [mΩ])	84 (0.26 [Ω])	107 (1027.2 [F])
40	115 (11.5 [mΩ])	77 (0.23 [Ω])	109 (1046.4 [F])
45	120 (12 [mΩ])	-	-
50	122 (12.2 [mΩ])	-	-
55	125 (12.5 [mΩ])	-	-
60	127 (12.7 [mΩ])	-	-
65	130 (13 [mΩ])	-	-
70	135 (13.5 [mΩ])	-	-
75	140 (14 [mΩ])	-	-
80	145 (14.5 [mΩ])	-	-
85	150 (15 [mΩ])	-	-
90	155 (15.5 [mΩ])	-	-
95	160 ([mΩ])	-	-
100	165 ([mΩ])	-	-

Table 3.4: Electric parameters based in thermal characteristics.

In Table 3.5 and Table 3.6, the autonomy and the losses obtained in different ambient temperatures are compared in four cases: The low, medium and high temperature and an additional case where the thermal and efficiency dynamic are not considered, the energy is calculated by constant efficiency values on each electrical component. On one hand, the 100% of the autonomy reported when the temperature is 25°C is the same one presented in Table 3.1 and the autonomy reported in other temperature cases is compared with this value. On another hand, the percentage reported in power losses is the percentage of lost energy in comparison with the total energy required to complete the trip in each temperature case.

As can be seen, the variation of the motor losses is minimum because the demagnetization is not considered and the Joule losses are small in comparison with magnet losses. The battery losses are reduced with high temperatures because the capacity of the battery increase and the internal resistance of the battery decrease in this case. By the opposite side, low temperatures increase the internal resistance and decrease the battery capacity [40]. Unfortunately, high temperatures have a negative effect over the battery health. The inverter losses increase almost linearly with the temperature because all losses are related to the resistive characteristic of the Mosfet.

Besides, the constant efficiency is considered to compare the classic representation of autonomy estimators like [60]. This comparison lets to see that even when motor and battery losses are comparable with variable efficiency and thermal considerations, the constant efficiency is not enough to represent the inverter efficiency behavior. In consequence, it causes a 5% of additional inverter losses which increase the autonomy estimation error. Finally, the autonomies of the three cases are compared. The autonomy is considerably reduced in low temperatures and it has a small increased in high temperatures. This is the behavior expected according to [40].

Parameter	T= 0°C	T= 25°C	T= 40°C	Eff=cte
Autonomy	83.1%	100%	108.5%	77.3%
	(77.3 [km])	(93.02 [km])	(101.01 [km])	(71.96 [km])

Table 3.5: Temperature effect over autonomy.

Parameters	T= 0°C	T= 25°C	T= 40°C	Eff=cte
Total energy required	(2.10 [kWh])	(2.38 [kWh])	(2.57 [kWh])	(1.90 [kWh])
Inverter energy losses	3.8% (80.19 [Wh])	4.3% (103.6 [Wh])	4.6% (119.12 [Wh])	9% (171.81 [Wh])
Battery energy losses	13% (275.74 [Wh])	9.5% (228.60 [Wh])	9.3% (240.60 [Wh])	10% (190.92 [Wh])
Motor energy losses	14.3% (300.3 [Wh])	14.8% (352.2 [Wh])	15.6% (400.9 [Wh])	16.4% (309.7 [Wh])

Table 3.6: Temperature effect over power losses.

3.4 Mechanical Model

A speed estimation is required to calculate the energy intended to complete a trip. For this reason, it is important to determine the requirements of the speed dynamic model according to the algorithm application. As it was exposed in the section 2.3.2, it is possible to work just with the longitudinal speed value or to improve the speed dynamic representation using the lateral speed value. In this section, the capability of the lateral speed model to be used in the optimization of autonomy is evaluated. The test presented uses the results obtained by a vehicle dynamic simulation tool oriented to industrial ADAS products as a tool to compare the precision of the lateral dynamic model results under different cases.

3.4.1 Lateral dynamic model verification.

The considered lateral and longitudinal model are deeply explained in Sections 2.3.2 and 2.3.2. The resultant dynamic model is [4]:

$$M(\ddot{x} - \dot{y}\dot{\psi}) = \frac{T_f}{R_{wf}} + F_{roll} + F_{aer_x} + F_w sin(\theta_s) sin(\beta) \tag{3.18}$$

$$M(\ddot{y} - \dot{x}\dot{\psi}) = C_r\dot{\psi} + C_\beta\frac{\dot{y}}{\dot{x}} + C_\delta\delta cos(\epsilon)$$
$$+ (C_{f2}\gamma_f + C_{r2}\gamma_r) + F_{aer_y} - F_w cos(\theta_s)sin(\beta) \tag{3.19}$$

$$I_{zz}\ddot{\psi} = D_r\dot{\psi} + D_\beta\frac{\dot{y}}{\dot{x}} + D_\delta\delta cos(\epsilon) + (D_{gf}\gamma_f + D_{gr}\gamma_r) \tag{3.20}$$

In order to verify the behavior of this model, a virtual test scenario is built in a vehicle dynamic simulation tool. The designed road (see Figure 3.17) has two curves of radius 50m, a bank angle of 30% and an intersection with an elevation of 2m and slope angle of 5°. Two kinds of tests are made: constant speed values from 5 to 20 [m/s] to notice yaw response at different speed values and variable speed in the same range to see the dynamic response of error. The constants values required by the model are obtained by simulation and they are shown in Table 3.8.

Figure 3.17: The designed road.

M	234.36 [Kg]
I_{zz}	14 [Kg/m^2]
g	9.81 [m/s^2]
Rwr	0.29 [m]
ϵ	27.72 [°]
Lf	0.56 [m]
Lr	0.81 [m]
C_d	0.52
ρ	1.167 [Kg/m^3]
A_f	0.6 [m^2]
μ_0	0.008
μ_1	7e-6

Table 3.7: Constant values of the mechanical model.

According to [47], the motorcycle can use pneumatics with the friction parameters reported in Table 3.8.

C_{f1}	14900
C_{r1}	27296
C_{f2}	927
C_{r2}	1527

Table 3.8: Friction coefficients a priori estimation.

These parameters are useful to make an initial approximation of the motorcycle behavior. However, it is an a priori estimation. For this reason, those friction coefficients and the effect of dynamics approximation have to be verified in order to determine friction coefficients which cause the minimum error and the limitations of the developed model.

A. Constant speed test: This test is made to verify the behavior of each component of the longitudinal equation and to detect model mistakes.
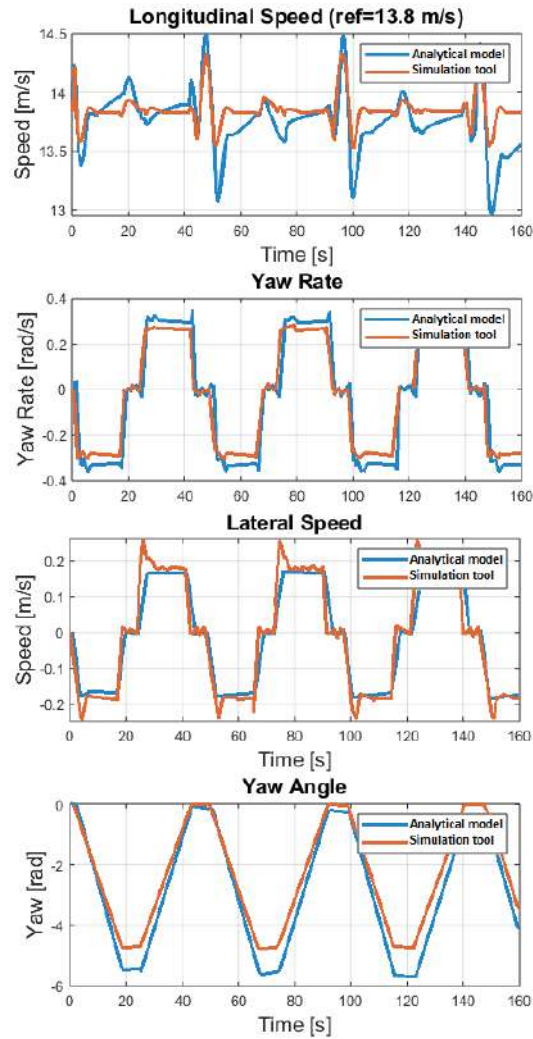
Figure 3.18: Static speed results.
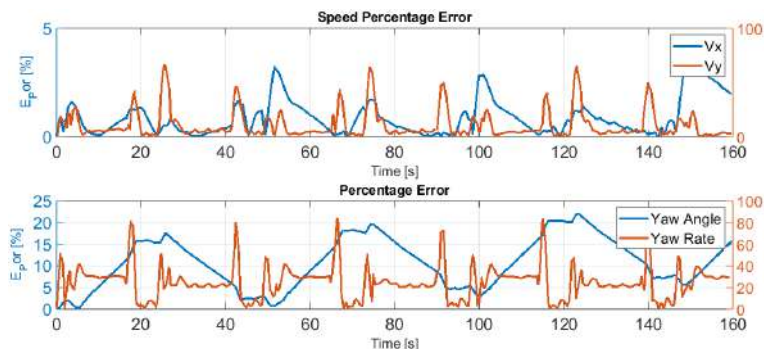
Figure 3.19: Static speed profile results (error percentage).

As it can be seen in Figure 3.18 and 3.19, even when the error percentage of the longitudinal and lateral speed is lower enough (under 5%) to be considered as an acceptable estimation, the error of angle yaw increases fastly with the linear pneumatic friction model. As a consequence, it makes impossible to use yaw information as a constraint of a speed profile optimizer.

B. Dynamic speed test: It is expected that the error increases in face of dynamic speed references. For this reason, an estimation with a prediction horizon under 10 seconds is considered acceptable when the mean error is under 10% in dynamic speed conditions (see Figure 3.20). Figure 3.21 lets to determine the prediction horizon for the current accuracy of the model. From the results obtained (see Figure 3.21), the chosen prediction horizon is 8 seconds to consider a longitudinal speed error and a yaw angle error under 10%.
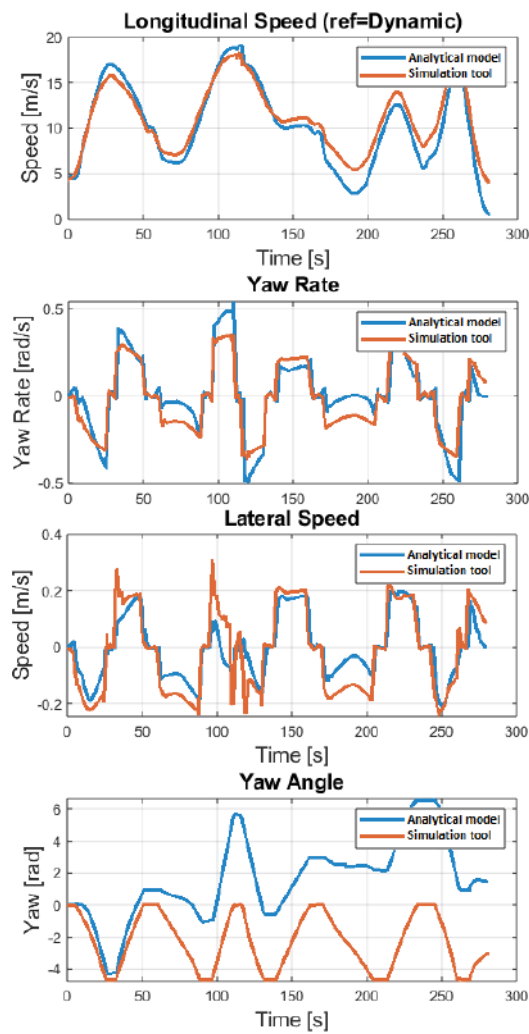
Figure 3.20: Dynamic speed results.
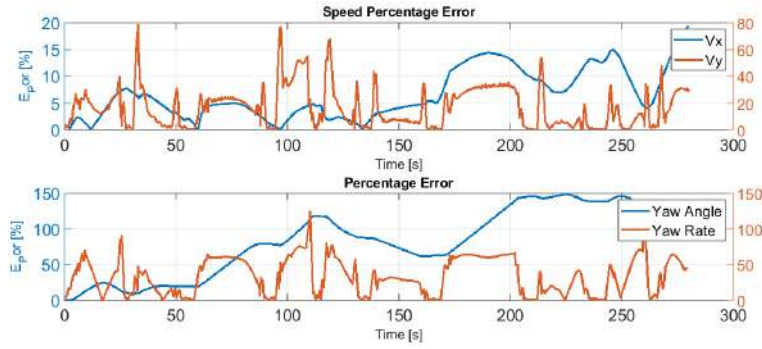
Figure 3.21: Dynamic speed profile results (error percentage).

Taking into account the current results, it is important to make a sensitivity test to determine the behavior of percentage error as a function of the friction coefficients. Since the friction coefficients are assumed constant by the analytical proposed model, but they have a non-linear behavior described by Pacejka equation in the simulation tool (see Figure 3.22 [44]), better results are expected with a better estimation of these parameters in an urban drive profile where the speed is from 0 to 60km/h.
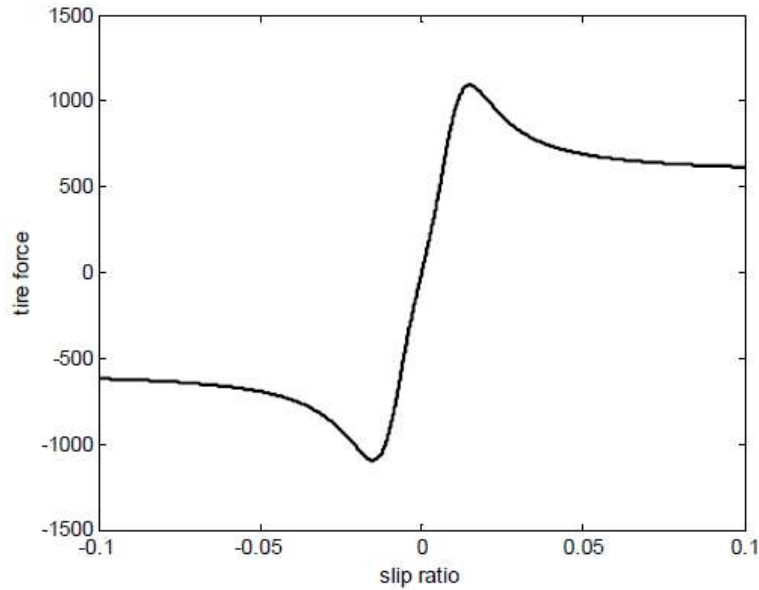
Figure 3.22: Magic Formula tire force curve (Pacejka equation).

C: Sesitivity Test:

The sensitivity test consists in the study of how each friction coefficient variation affects the mean percentage error between the analytical model and the simulated one. It is important to note that only one parameter is varied along each test, the other 3 parameters are considered constant along the test with an a priori estimation value. For example in test 1, only C_{f1} varies, C_{r1}, C_{r2} and C_{f2} are considered constants. The minimum and maximum values used in the test were chosen based in the physical restriction of the pneumatic dynamics and the friction coefficients found in the pneumatic industry. The delta values were chosen with the objective of causing a minimum variation of 0.5% in one or more model states between iterations.

	Minimum	Maximum	Delta
C_{f1}	5000	90000	100
C_{r1}	5000	90000	100
C_{f2}	0	10000	50
C_{r2}	0	10000	50

Table 3.9: Sensitivity test parameters.
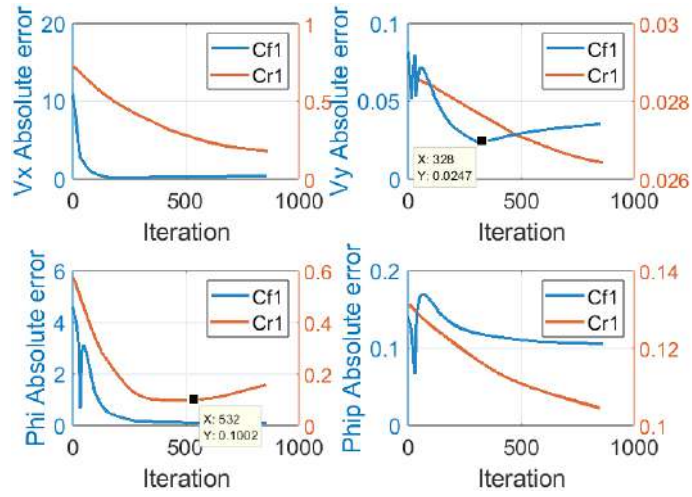
Figure 3.23: Sensitivity test Cf1 & Cr1.
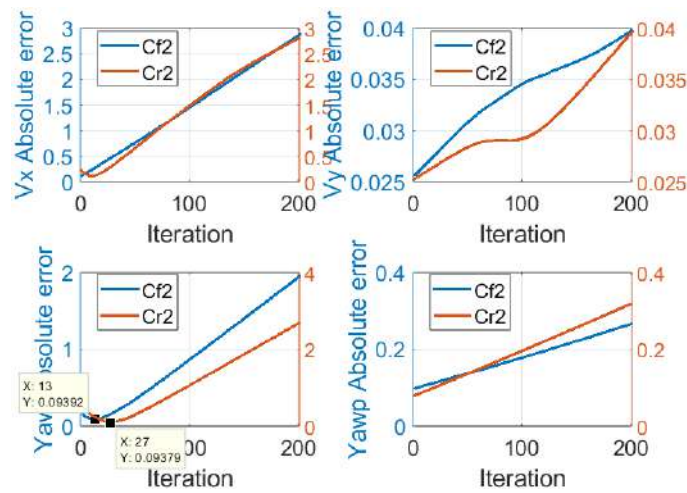
Figure 3.24: Sensitivity test Cf2 & Cr2

The results of sensitivity test are shown in Figures 3.23 and 3.24. The coefficients obtained by the error minimization along sensitivity test are summerized in Table 3.10.

$Coeff$	Iteration	Value
C_{f1}	328	37700
C_{r1}	532	58100
C_{f2}	13	600
C_{r2}	27	1300

Table 3.10: Friction coefficients estimation based on speed profile data.

Simulation results after sensivity test

A. Static speed value   After the utilization of new friction coefficients estimated by the sensitivity test, the results show a decreasing of 73% in yaw mean error percentage. The static speed test result's Figure (3.26 and 3.25) report a mean error percentage of 1.15% for longitudinal speed and 3.4% for yaw angle.
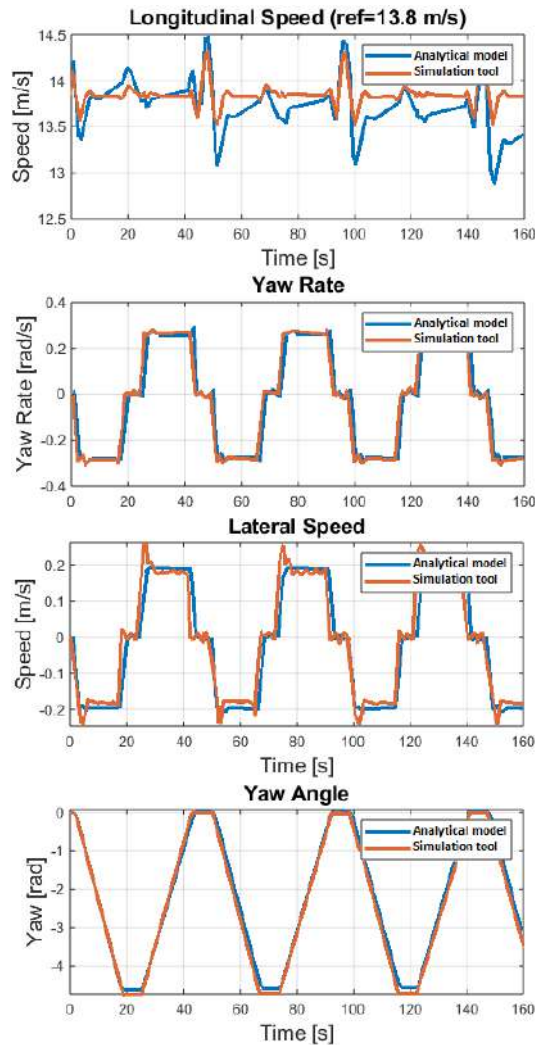
Figure 3.25: Static speed results after sensitivity test.
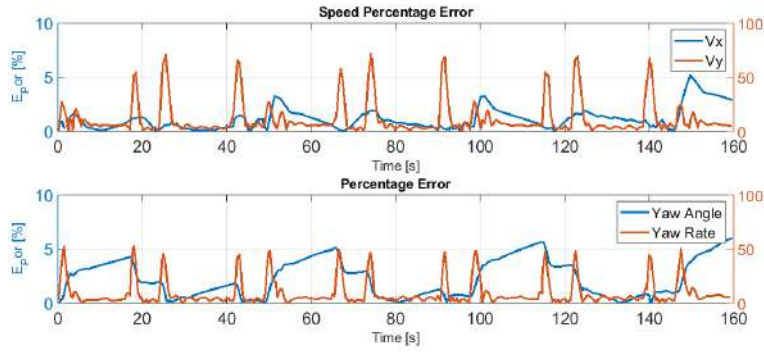
Figure 3.26: Static speed profile results after sensitivity test (error percentage).

The Longitudinal speed and yaw angle percentage error signals in static speed value test are under 5% and even when the mean errors are increasing along the test, their ratio is around 1% per 100 seconds in longitudinal speed and 1% per 40 seconds in the yaw angle. These results are considered enough to continue to the dynamic test.

B. Dynamic speed value: In this case, the utilization of new friction coefficients estimated by the sensitivity test decreases a 71.97% of the mean error percentage in comparison with the yaw mean error percentage reported before. The dynamic speed test Figure 3.28 and 3.27) reports a mean error percentage of 4.47% for longitudinal speed and 23.12% for yaw angle.
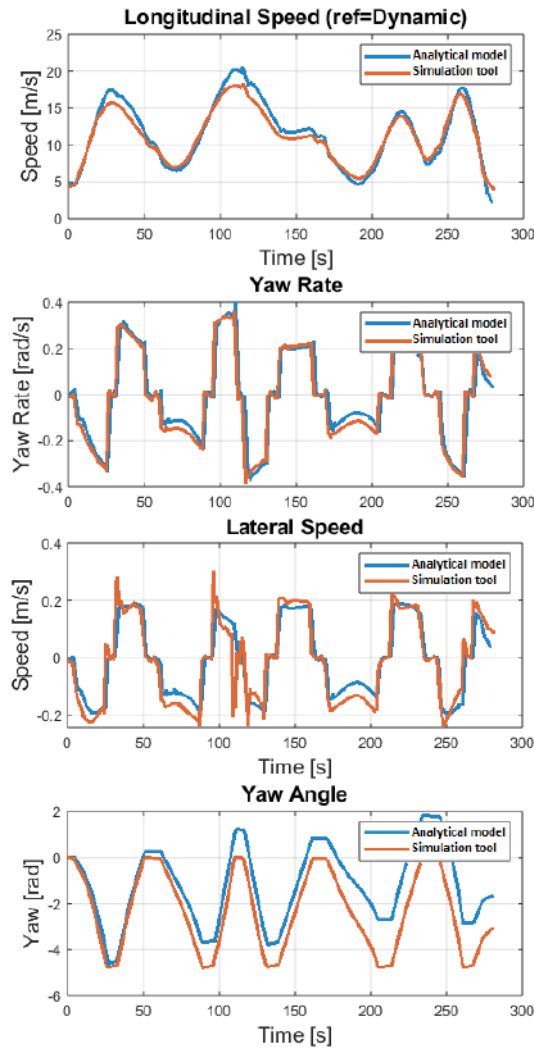
Figure 3.27: Dynamic speed results after sensitivity test.
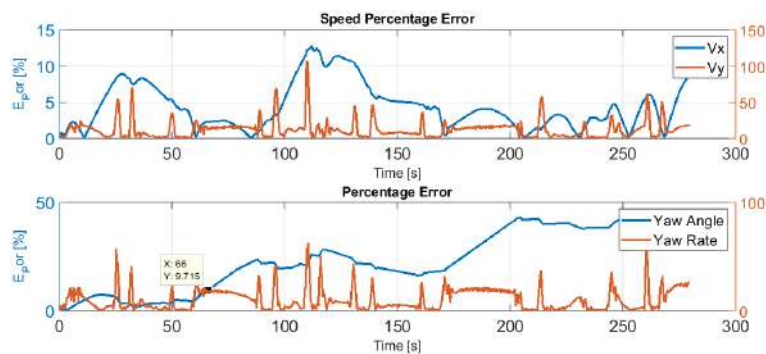
Figure 3.28: Dynamic speed profile results after sensitivity test (error percentage).

Although the yaw angle mean error percentage still being high, the new results let to obtain a prediction horizon of 66 seconds with a consideration of an acceptable yaw error under the 10%, as it can be seen in Figure (3.28).

3.4.2 Speed dynamic model choice

In order to improve the lateral speed dynamic model, additional equations are used to describe the behavior of the friction coefficients for different speed values, but it would increase compilation time too. Also, even with a detailed characterization of the driving profile and road conditions like speed minimum and maximum values or slope angle, the speed estimation results are barely acceptable with linear pneumatic equations. Those results are could be acceptable with the maximum speed value restriction of 60 km/h (An urban speed profile). If a highway speed profile is required, the lateral speed control is not able to make correct speed values predictions.

As a conclusion, even when the presented lateral dynamic model is able to recreate the mechanical behavior of a motorcycle in presence of roll, slope and bank angles with a maximal error of 10% on a period of time around 1 minute; this error represents a nonacceptable energetical representation in the electric model. Therefore, the longitudinal model is chosen to make a fast but enough accurate energy estimation to be implemented in the control steps. However, as the main usage of the lateral dynamic model is to ensure the comfort and the security of the driver along the speed profile proposed, the maximum speed values of the lateral model will be taken into account as constraints into an optimization behavior.

3.5 Conclusion

An electrical vehicle can be represented by different models able to represent different dynamics.

As the dynamic required to the autonomy optimizer is the power losses dynamics along all the traction chain (battery, power electronic converter and electric machine), the losses in the main components of the traction chain were described in three aspects: electrical model, thermal model, and mechanical model.

The electrical losses of the motor are complex to be calculated in real time, for this reason, they had to be represented into a geometrical way; an equivalent simplified model well adapted to an optimization process. On another hand, the battery and inverter losses are directly dependent on the current, for this reason, no additional representation is required.

The thermal dynamic behavior was represented by foster network on each device (motor, battery, and inverter) but the internal amount of components of each device represents a calculus power limitation for this modelization technique. In consequence, only the battery and inverter can be represented by this technique. In order to represent the motor thermal dynamic and creates an optimization profitable model, different efficiency maps have to be used.

Finally, the mechanical model was discussed. The lateral dynamics is not required to represent the energy state of the vehicle. It lets to make the representation of the energetic dynamic with the longitudinal model and then, to reduce the compilation time of the mechanical model.

In the following sections, an optimal controller is proposed. Also, the way how each model will be integrated in the optimization process and the compilation impact over the complete algorithm will be discussed.

Chapter 4

Control and Optimization

4.1 Introduction

This chapter takes the state of art presented in Chapter 2 to highlight the control technique requirements in order to make an energetical optimal control. Based on those controllers and their requirements, the models presented in Chapter 3 are integrated into the proposed optimal control. The specific explored topics are:

- Simplified representation of the efficiency map (Geometric representation): The BLDC motor electric losses are taken into account by a geometrical representation of the surface described by the mathematical expression of copper and iron losses. This representation is introduced in order to avoid the limits of conventional mathematical approaches: complexity, computationally expensive, and time-consuming. It produces very fast results with sufficient accuracy suitable for optimization algorithms under energy-saving constraints.

- Optimization Algorithm: The required dynamic model and their different kind of constraints are presented. Also, various mathematical formulations of the cost function are analyzed to show the impact of different criteria on optimization control under an energetic performance index, allowing to choose the most relevant ones.

- Open Loop Controller: A diagram about how the optimal control technique is integrated into the speed control vehicle is presented. Since the open-loop control technique can not correct the disturbances presented along the trip, only the scope of the closed-loop control technique is discussed.

- Closed Loop Controller: How the states' feedback is integrated into the control technique is exposed. It is contemplated in order to correct the effect of the disturbances presented along the trip based on the analysis of energy disparity (error between reference and measures).

4.2 Simplified Representation of the Efficiency Map (Geometric Representation)

A smart efficiency estimation methodology based on a map representation, allows to save complexity and compilation time. It is proposed to be relevant for the real-time optimization algorithms. The efficiency map is shown in Figure 4.1 and it was obtained from

Parameter	Value
Motor and Battery voltage	72 v
The rated motor output power	3000 w
The rated motor torque	185.6 Nm
The rated motor speed	91.3 RPM
Maximum motor efficiency	96.4 %
Battery capacity	45 Ah
Battery cell	LIR18650
Inverter mosfet	STP75NF75

Table 4.1: Electrical characteristics.

a direct representation made by using a co-simulation composed by logical programming (Python) coupled with magnetic simulation software (ANSYS/Maxwell) [119]. The most relevant parameters of the evaluated electric motor are shown in Table 4.1.

To achieve this, the magnetic simulation software uses dimensional and material characteristics of the motor (Already present in the motor manual) to evaluate eddy current and hysteresis losses. Only in the case of some magnets properties, additional data has to be required to the supplier, this information was shared by motor manufacturer under promise to not be published.
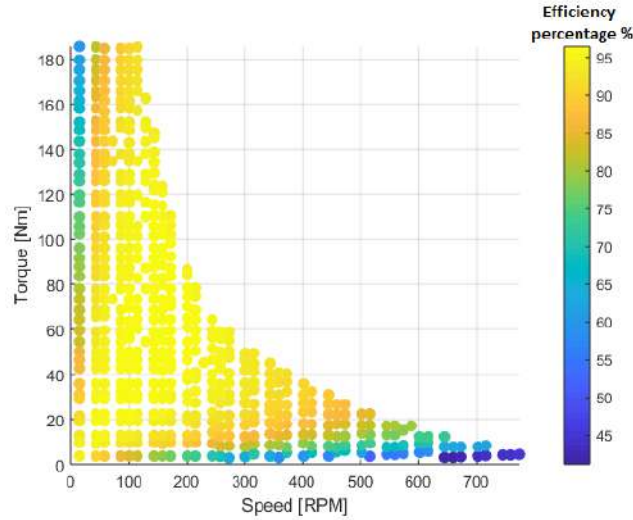
Figure 4.1: Efficiency map obtained by electromagnetic simulation.

The objective is to substitute the mathematical model which describes the efficiency by a convex surface able to be used as an optimization surface. It helps considerably design engineers to set up a simple and relevant solution to make the trade off between complexity formulation, computational time, and performance optimization accuracy. In other words, the resultant surface has to imitate the behavior of the motor efficiency mathematical model in order to orient the speed/torque optimization for operating in the high-efficiency region for energy saving. For this reason, after analyzing the efficiency map data behavior, an elliptic paraboloid is used to describe the efficiency based on trend extrapolation. The general equation is given by:

$$Z = B_0 - \frac{(X - x_c)^2}{a^2} - \frac{(Y - y_c)^2}{b^2} \tag{4.1}$$

Where: Z, X, Y represent the efficiency, the torque and the speed respectively.
Equation 4.1 describes an elliptic paraboloid with center in $(0, 0, B_0)$. Also, the values
"a" and "b" describe the elliptical curves on each Z value and the values "x_c" and "y_c"
describe the elliptical centroid. In order to use a linear regression over the data, the
equation is reorganized like this:

$$Z = B_0 - B_1 X_s - B_2 Y_s \tag{4.2}$$

where:

$$\begin{aligned} B_1 &= \tfrac{1}{a^2} \\ B_2 &= \tfrac{1}{b^2} \end{aligned} \tag{4.3}$$

and:

$$\begin{aligned} X_s &= (X - x_c)^2 \\ Y_s &= (Y - y_c)^2 \end{aligned} \tag{4.4}$$

Once the values "x_c" and "y_c" are obtained from image analisis, the linear regression can
be made over the Equation 4.2. After the linear regression is made, the B_i coefficients
and the centroid of the paraboloid are given in the Table 5.3.

Parameter	Value
B_0	95.79
B_1	1.3149e-4
B_2	0.0013
x_c	157.65
y_c	73.2

Table 4.2: Paraboloid parameters.

Even when the quantification of the error is not required, it lets to quantify the simili-
tude between both representations. For this reason, a comparison between the paraboloid
surface and the efficiency map data is shown in Figure 4.2.
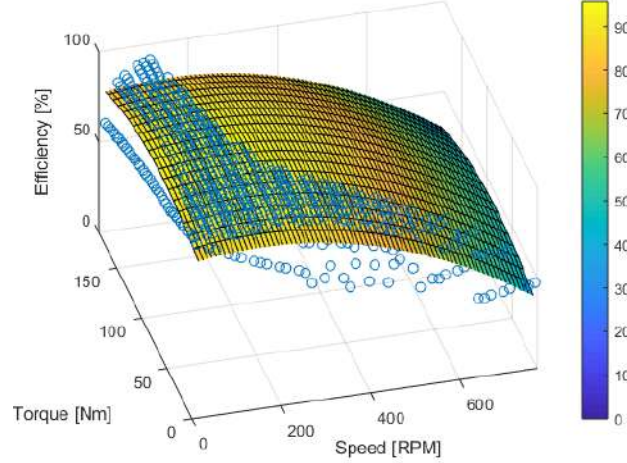
Figure 4.2: Hyperboloid representation of the efficiency map.

The surface resultant offers a range in torque from 0 Nm to 185 Nm and in speed from 0 RPM to 800 RPM. But the efficiency map offers a curve that divides the feasible region from the non-feasible one, it is called the maximum power curve. If the iron and copper motor losses are not taken into account, the maximum power curve can be expressed as a consequence of the relationship between the mechanical and the electrical power by considering constant efficiencies around their average values. This expression is given by Equation 4.6.

$$P_{max} = \frac{T_{Lim} * (N * R_w * \frac{2*\pi}{60})}{\eta_{bat} * \eta_{inv} * \eta_{mot}};$$ (4.5)

Then, the maximum torque is represented by:

$$T_{Lim} = \frac{P_{max} * \eta_{bat} * \eta_{inv} * \eta_{mot}}{(N * R_w * \frac{2*\pi}{60})};$$ (4.6)

Where $T_{Lim}, P_{max}, \eta_{bat}, \eta_{inv}, \eta_{mot}, N, R_w$ are respectively the torque limitation, the maximum power, the average battery efficiency, the mean inverter efficiency, the mean motor efficiency caused by Joule losses, the speed in RPM and the wheel radius. Unfortunately, in Figure 4.3, the effect described in [26], by ignoring core and iron losses can be appreciated. It can be seen that the error of efficiency assessment increases with the speed value. In order to overcome this problem while keeping the model simple, a set of four lines are made to represent the speed limit based on the torque value allowing to cover the optimal geometric representation of the efficiency map.

Now that both surfaces have the same limitations, they can be compared to evaluate the error from the geometrical representation in comparison to the efficiency map data.
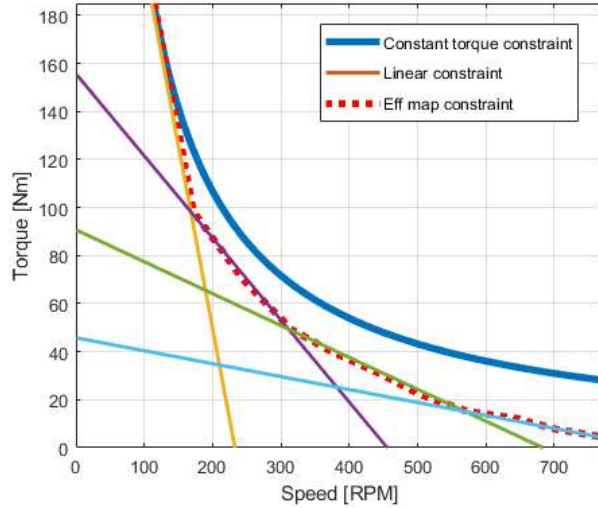
Figure 4.3: Power limitation over geometrical representation.

4.2.1 Error Analysis:

The effect of the error between the efficiency map data and the geometrical representation has to be evaluated under three situations relating to the potential use: Along all the possible values, under an urban driving cycle, and an optimized drive cycle. In order to use the geometrical representation of the efficiency map, the power limitation has to be expressed.

Along all the possible values: The mean error is about 0 (3.03e-15). It means that if the motor would be able to recreate the efficiency data with the same range, the positive and negative error in the measures would be canceled. But in the real drive cycle, there are speed limitations imposed by the traffic zones and also, by the electric devices required to make the motor move. This is why a more complete study is required.

The RMS (Root Mean Square) error is 6.26 W, it means that the estimated efficiency values keep themselves close to the mean error value in comparison with the efficiency signal magnitude (see Figure 4.4). However, there are two regions where the error tends to be higher, those regions are placed close to the origin of the torque and speed axis and they represent the minimum efficiency values.
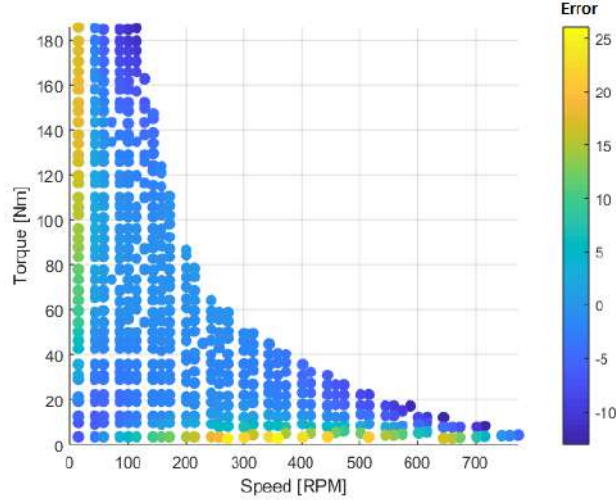
Figure 4.4: Error of geometrical representation.

Along an urban drive cycle: In order to obtain a torque and speed profiles able to be used as reference to this research, the NREL Classe 6 drive cycle developed by Smith Newton from NREL Labs [120] is used. This driving profile is designed for electric vehicles in an urban environment. The speed profile requires a characterization of the electric vehicle and the road characteristics to obtain the torque profile. The electric vehicle characteristics are based on Forest-Litio motorcycle [106] due to it has a motor with a high output nominal power (3000W) able to drain its Lithium battery (45Ah) in less than 100Km. This motor and battery values added to the absence of fast charge capacity, make the Fores-Litio the perfect candidate to experiment with eco-Driving algorithms. Its characteristics are shown in Table 4.3.

Name	Parameter	Value
Mass	M	150.00 [Kg]
Aerodynamic surface	A_f	0.94 [s^2]
Wheel radius	Rwr	0.58 [m]
Air density	ρ	0.96 [$\frac{Kg}{m^3}$]
Drag coefficient	C_d	0.40
Gravity	g	9.81 [$\frac{m}{s^2}$]

Table 4.3: Vehicle characteristics.

Finally, to be close to the real usage, the slope trajectory was taken from a trip from Paris to Brussels. The longitudinal force modeling used to obtain the torque profile is based on Newton's second law of motion along the X-axis.

According to [108], [50] and [17], the most relevant negative forces related to energy losses are:

- Aerodynamic force.

- Rolling resistance force.

- Slope of the road.

Then, the Longitudinal dynamic is described as is shown in Figure 2.13. The mathematical representation is given by:

$$M(\ddot{x}) = \frac{T_f}{R_{wf}} + F_{roll} + F_{aer_x} + F_w sin(\theta_s) sin(\beta) \tag{4.7}$$

Where $T_f, R_{wf}, F_{roll}, F_{aer_x}, F_w, \theta_s, \beta$ are respectively wheel torque, the effective radius of rear wheel, roll resistance, aerodynamic force associated to X-axis, weight, slope angle and bank angle.

As a result of the speed profile made with the presented data, the torque profile shown in Figure 4.5 is obtained.
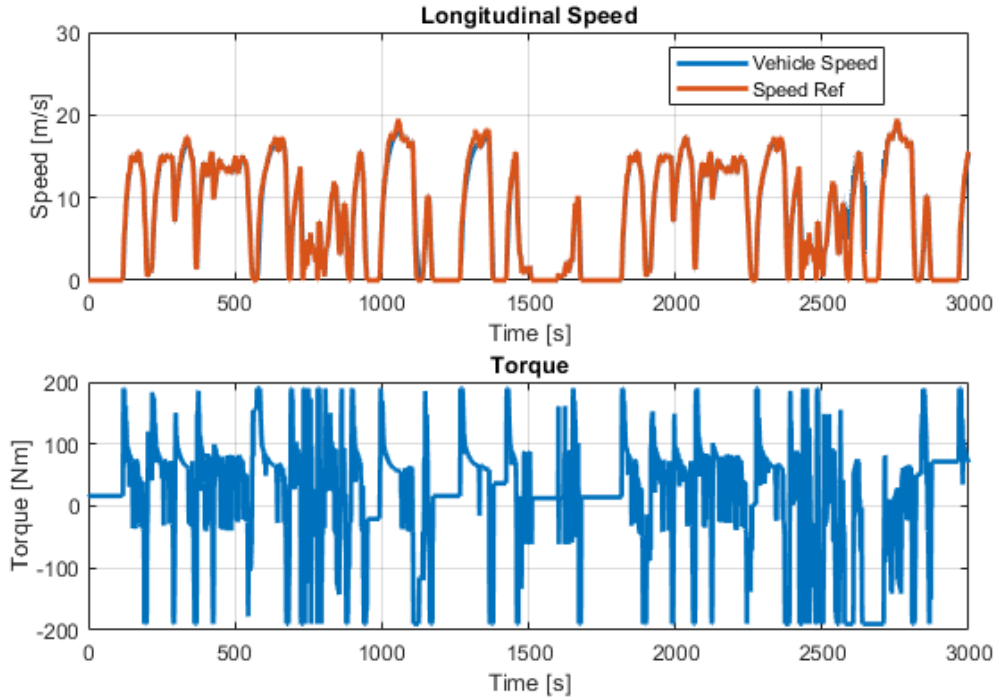
Figure 4.5: Urban profile.

In Figure 4.6.a, the value of efficiency estimated for each torque-speed couple (with a sample time of 1s) is shown as a red circle. The profile is able to cover most of the surface except by the speed limitation of 30 $\frac{m}{s}$ imposed by the inverter to protect the battery and the motor.

The error of each torque-speed couple (30 000 samples) is shown in Figure 4.6.b. The error values presented let to calculate that the mean error is 1.76 along the trajectory but the RMS error increases to 6.84. The minimum error efficiency value is -6.87 and the maximum is 24.19 when the speed is close to zero but the road requires high values of torque to achieve this low speed. In conclusion, the geometrical representation of the efficiency map is able to reproduce the efficiency with an RMS error of 6.54, which is still acceptable accuracy considering the simplicity of the model in comparison with the theoretical model presented in Seccion 2.
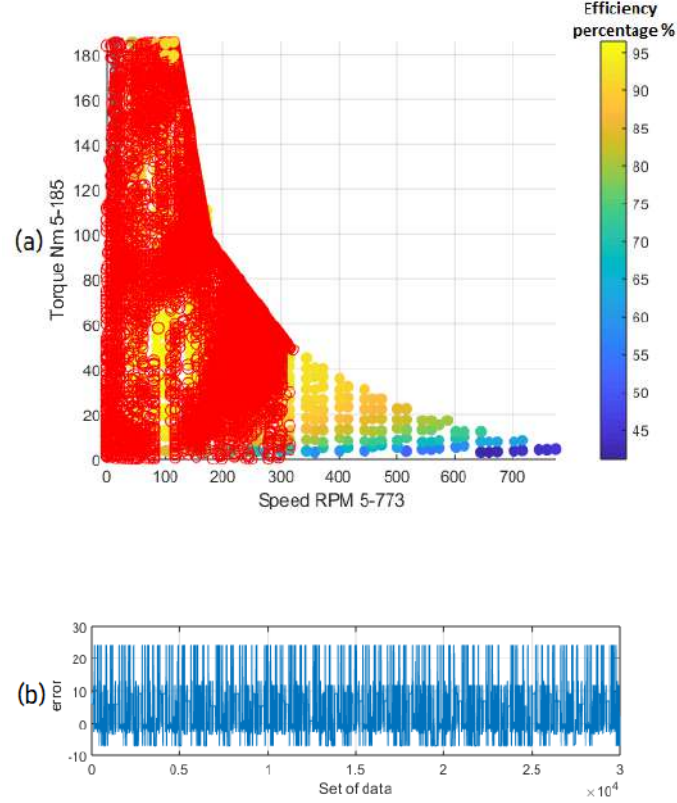
Figure 4.6: Error of efficiency along a urban profile.

Along an optimized drive cycle: In order to determine how the error of the geometric representation of the efficiency map affects an optimized drive cycle, the following optimization process was made:

$$
\begin{aligned}
& min J(x) \\
& J(x) = -Z = -B_0 + B_1 X_s + B_2 Y_s \\
& s.t. \\
& -T_{max} \leq U \leq T_{max} \\
& 0 \leq x_2 \leq V_{max} \\
& \dot{x} = f(x, u)
\end{aligned}
\tag{4.8}
$$

where: B_0, B_1, B_2, X_s and Y_s are represented by the maximal eficiency, the decremental coefficient in speed axis, the decremental coefficient in torque axis and finally, the speed and torque displaced axis. Also, T_{max}, T_{min} and V_{max} are the physical motor limits in torque and speed. Finally, $\dot{x} = f(x, u)$ is represented by (4.7).

The optimization goal is to minimize the energy required to complete a trip. The cost function represents the maximization of the efficiency function without taking into account any traffic constraints, just the speed limitation imposed by the inverter.

State and control constraints: The state constraints are obtained from a QSMOTOR of 3000W suitable for our use case [13]. The applied constraints are presented in the Table 4.5.

Parameter	Value
T_{max}	185 [Nm]
V_{max}	30 [$\frac{m}{s}$]

Table 4.4: State constraints.

As a result of the speed optimization based on the torque demand by the NREL Class 3 Speed profile and the external characteristics presented in Section 2.5, the torque profile shown in Figure 4.7 is obtained. This driving profile does not consider the speed constraints like starting/stopping caused by external obstacles (traffic lights, other vehicles or curves, ...). It lets to calculate the impact of the optimized speed profile on energy saving.

As shown in Figure 4.8, the efficiency value along all the trip is close to the paraboloid centroid. The mean error is -0.37 along the trajectory (30 000 samples). In this case, the RMS error is about 2.38. The minimum error efficiency value is -7.49% and the maximum is 21.65% when the speed is close to zero. In conclusion, the geometrical representation of the efficiency map is able to provide accurate information with an RMS error of 2.38. In the optimized conditions, the results are better and more accurate than those using an urban driving profile. Then, it is possible to conclude that the geometrical representation of the surface is an acceptable approximation of the theoretical efficiency of the high-efficiency region (the interest region).
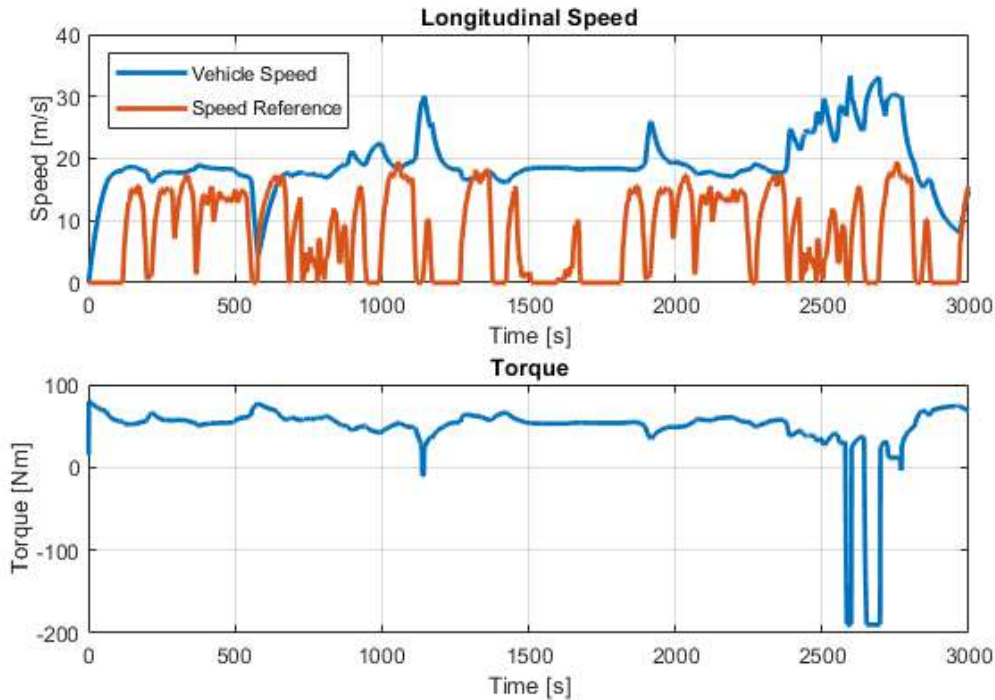
Figure 4.7: Optimizated profile.
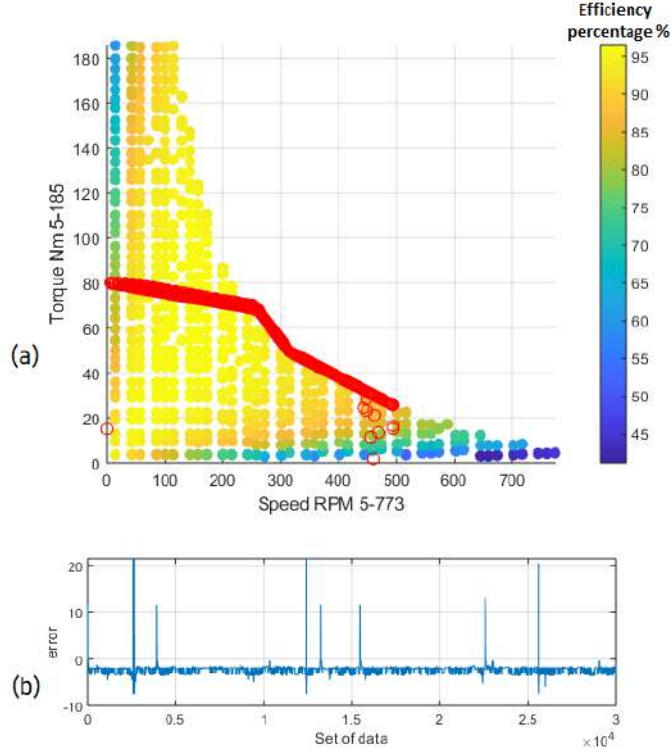
Figure 4.8: Error of efficiency along an optimizated profile.

When the geometrical representation is used, 80.22% of the compilation time required to make a speed profile optimization is reduced. This comparison is made with a cost function that uses the mathematical model of the motor efficiency proposed by [16]. The equation of the used efficiency mathematical model is given by the equation 4.9.

$$\eta = \frac{1}{1 + \frac{R_s}{3/2p\Psi^2}\frac{T}{\Omega} + \frac{L_s^2}{R_s}\frac{T\Omega}{3/2p\Psi^2}}$$ (4.9)

where: $\eta, R_s, p, \Psi, T, \Omega, L_s$ are the efficiency, the stator resistance, the number of pole pairs, the permanent magnet flux, the mechanical torque, the mechanical speed and the stator inductance. This equation is obtained by a relationship between the mechanical power and the electric power then, it underestimates the effect of motor materials or motor dimensional characteristics effect over the friction, iron, and copper losses.

As a conclusion of this electric model part, the effect of the error of the geometrical representation (simplified model) is evaluated under three situations: along all the possible values, under an urban driving cycle, and an optimized drive cycle. In all cases, the geometrical representation provides a good accuracy with an RMS error under 7, this value decreases to 2.38 when an optimized driving profile is applied. Therefore, the geometrical representation of the efficiency map is acceptable considering the simplicity of the model in comparison with the complete theoretical model. It is able to reduce significantly the compilation time (about 80%) in comparison with other proposed models. This allows making a real-time optimization algorithm under energy-saving constraints. However, to increase the relevance of this approach and to be more suited for industrial challenges, the thermal effect has to be integrated in a dynamic way. For this purpose, the resistivity characteristic of each component is varied according to a lookup table which relates the device's temperature with a resistivity value. Also, the thermal dynamic described in

Section 3.3 is integrated to make the thermal estimation.

The following section explores way how the optimization algorithm is able to use the geometrical efficiency representation and the electrical, mechnaical and thermical models presented before in order to increase the energy savings.

4.3 Optimization Algorithm

In order to reduce the effect of the power losses observed in Section 3.2, and enhance the performance, an optimization process is proposed to covering a wide range of parameters affecting the system. This new paradigm allows showing the impact of different criteria on optimization control under an energetic performance index. The most important elements to address the proposed approach can be divided into two categories. First, physical limits and power losses are introduced in the cost function as the input signal minimization and efficiency maximization. Second, the resistive losses on driver and battery which are strongly related to two characteristics of the current signal: Its magnitude and its variation. For this reason, they are also included in the cost function by the input signal variation minimization, the speed limitation, and the speed reference tracking.

A weighted cost function is proposed to explore the effect of the different elements considered to keep a balance between the objective to complete the travel and to keep the system in the most efficient point. The design process of the proposed optimization algorithm requires the following components: the dynamic model, the states and control constraints, boundary conditions and cost function.

4.3.1 Dynamic Model

The EV is modeled as a particle along a one dimensional axis. The motion of the vehicle is the result of the sum of forces applied on the body and just the longitudinal forces were considered (see Sections 3.4, 2.4 and 2.3.2). The model used to describe the system's dynamics is:

$$\dot{x_1} = x_2$$
$$\dot{x_2} = (\frac{T}{R_w}) - F_l)/m$$
$$\dot{x_3} = \frac{T}{R_w * Eff(x_2,T)}) * x_2$$

(4.10)

$$F_l = F_{aereo} + F_{roll} + F_w$$

(4.11)

Where: $x = \begin{bmatrix} d & v & e \end{bmatrix}$; $v(t)$ is the vehicle's longitudinal speed, $d(t)$ is the travel distance and $e(t)$ is the energy. The input is: $u = T$; T describes traction and braking torque. F_l describes the uncontrolled inputs (looses). $Eff(x_2, T))$, represent a simplified abstraction of the motor efficiency.

This longitudinal model can therefore be applied to estimate the EV demand power.

4.3.2 State and control constraints

As explained previously, there are two kinds of constraints to be integrated into the optimization process:

- The physical constraints describe the constraints imposed by the components selected. They include the maximum torque which the system is able to produce, constraint by the expresion guiven by Equation 4.12.

$$T_{min} \leq T \leq T_{max}$$

(4.12)

- The design constrains which describe the feasible region of the model states. If the states are outside this feasible region, the behavior cannot be replicated by the vehicle in a real test. Those are:

$$X_{min} \leq x_1 \leq X_{max} \tag{4.13}$$

$$V_{min} \leq x_2 \leq V_{max}: \tag{4.14}$$

$$\int_{t_0}^{t_f} E_{tot_{seg_i}} \partial t \leq E_{tot} \tag{4.15}$$

Constraint (4.13) limits the feasible region of x_1 and also, it avoids an overdamped behavior. Constraint (4.14) is related to a physical restriction of electric motor described in (4.12). Finally, constraint (4.15) is a physical limitation of the quantity of energy available in the battery. Where $E_{tot_{seg_i}}$ is the energy developed by the system along a single sample time and E_{tot} is the total energy available in the battery.

The minimum and maximum values presented in constraint equations are given by the Table 4.5.

Table 4.5: State and control constraints.

Parameter	Value	Parameter	Value
V_{min}	0 $[\frac{m}{s}]$	T_{min}	-220 [Nm]
V_{max}	30 $[\frac{m}{s}]$	T_{max}	280 [Nm]
X_{min}	0 [m]		
X_{max}	370 000* [m]		
TotEne	72*45*3600 [Ws]		

4.3.3 Boundary Conditions

Boundary conditions describe the behavior desired by the system at the initial and final point of the trajectory. In this case, the main objective is to cover the distance between an initial position (which is the initial condition equal to zero), to the final position (which is represented by x_{1f}) with a constraint amount of energy. Also, the initial value of the vehicle speed is zero and the final value of x_2 is fixed, i.e.:

$$\begin{array}{ll} x_1(t_0) = 0 & x_1(t_f) = x_{1f} \\ x_2(t_0) = 0 & x_2(t_f) = x_{2f} \end{array} \tag{4.16}$$

4.3.4 Cost Function

The cost function has been progressively established by integrating the various elements discussed in Section 2.3.1:

$$J_0 = \int_0^{t_f} (V_{ref} - x_2(t))^2 \; dt \tag{4.17}$$

$$J_1 = \int_0^{t_f} -Eff_m(x_2(t), T(t)) \; dt \tag{4.18}$$

$$J_2 = \int_0^{t_f} -Q_1 Eff_m(x_2(t), T(t)) + Q_3 \delta T(t)^2 \; dt \tag{4.19}$$

$$J_3 = \int_0^{t_f} -Q_1 Eff_m(x_2(t), T(t)) + Q_2(V_{ref} - x_2(t))^2 \ dt \qquad (4.20)$$

$$J_4 = \int_0^{t_f} -Q_1 Eff_m(x_2(t), T(t)) + Q_2(V_{ref} - x_2(t))^2 + Q_3 \delta T(t) \ dt \qquad (4.21)$$

Each cost function has its own purpose. J_0 is the pure speed tracker, it helps to determine the value of final time (t_f) and gives the reference of the power demand along the traject in normal driving profile conditions. J_1 is a pure efficiency cost function-oriented to keep the motor in the maximum efficiency along all the journey. J_2 studies the effect of the input signal variation penalization. J_3 explores the effect over the energy-saving when a weight variation is proposed in order to evaluate the softness of the speed limitation caused by the efficiency maximization, Finally, J_4 keeps the balance optimization between speed tracking and efficiency but adding an input minimization to limit the current without limitations over the torque variation.

"Q_i" values represent the weight of each optimization penalties over the complete cost function. Those values let to activate and deactivate different penalization terms or oriented the cost function to take into account more than one term but giving more weight to someone between them.

4.3.5 Performance Analysis and Cost Function Selection

In this preliminary test, the "Q_i" values are binary (1 or 0) in order to select the correct terms to be included into de cost function. In future steps, "Q_i" values are deeply defined. In order to compare all cost function components, the same trip between Paris and Brussels is done. All the physical and energy constraints, as well as any other vehicle characteristic, are obtained from the Forest-Litio electric motorcycle manual. Even when the traffic conditions are not represented, the same mixed speed profile (Urban/Rural) is used in all cases. The objective of the test is to evaluate the system losses (total and classified by traction chain element) and the time required to complete the trip. Those variables let to analyze the impact of each cost function component over the total energy optimization performance.

As it can be seen in Table 4.6, even when the efficiency function (J_1) is able to increase the autonomy of the vehicle in comparison with the speed tracking cost function (J_0). But this still being negligible because the criteria aims to keep the speed profile in the most efficient operating point but with high level of power demand. As a consequence, autonomy improvement is not so significant but the travel time is reduced significantly. According to the energetic study presented in the last sections, the speed and torque magnitude limitation and the torque variation limitation represent a tool to decrease the power required by the vehicle. J_2 and J_3 are the representation of each approach separately. As was expected, the speed constraint is related to the resistive power losses then, J_3 is able to optimize this kind of losses and as a result, its range is bigger than the range of J_2. However, the optimization of the torque signal variation achieves too a significant autonomy augmentation (in comparison to J_1) and also lets to ensure a suitable driving profile for the motor and driver capabilities. In order to explore the effect of all penalization components presented in J_1, J_2,and J_3, J_4 is proposed. J_4 achieves a significant autonomy improvement and also, reduce the travel time while the power losses are reduced too in comparison with J_3. In conclusion, even when (J_3) is the cost function with the best autonomy, when Q_1 and Q_2 have a binary behavior (0 or 1), (J_4) represents the best option with a good trade-off to increase the autonomy, reduce the travel time and to propose a suitable driving profile. If Q_1 and Q_2 have an entire range (from -inf to

-inf) J_3 is a better option because it can obtain almost the same power losses results with a smaller effect over the mean speed of the vehicle. It means that this value (the mean speed) can be modified completely by the relationship between Q_1 and Q_2.

Table 4.6: Cost functions comparison.

	J0	J1	J2	J3	J4
Autonomy [km]	93.02	94.74	106.25	129.69	122.95
	100%	101.8%	114.2%	139.4%	132.1%
Inverter Losses	4.3%	2.3%	2.1%	2.0%	1.8%
Motor Losses	14.8%	8.5%	6.8%	6.5%	6.4%
Battery Losses	9.5%	6.7%	7.6%	6.7%	6.6%
Travel time [h]	11.8	5.3	5.9	7.6	6.7

In this section, the components required to make an optimization algorithm are evaluated to conclude the best trade-off suitable for on-line optimizations. Now, in the following sections, the proposed optimization problem is implemented in open-loop and closed-loop algorithms to test the compilation time required and its performance when specific disturbances are added.

4.4   Open Loop Controller

As it was presented in Section 2.5, an eco-driving methodology consists in finding the optimal way to reduce the overall energy consumption. Then open-loop and closed-loop control oriented to make energy optimization are going to be referenced as "Eco-Driving Controller" from now. The first design of an Eco-Driving Controller is an open-loop controller. It is a control process without feedback, so the output has no influence or effect on the control action. The control scheme is presented in Figure 4.9. The controller assumes that the state x2 does not present any noise.
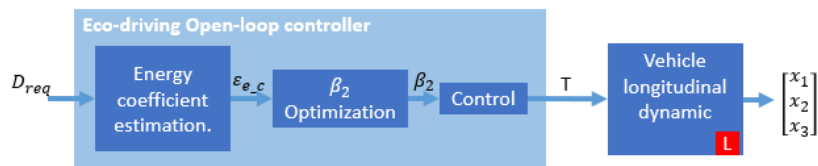
Figure 4.9: Open-loop control diagram.

Where the Eco-Driving Controller can be described by three blocks:

- Energy coefficient estimation: This block takes the distance required by the driver and the energy available in the battery (SOC) to calculate a maximum feasible energy coefficient required to complete the travel. This coefficient (ξ_{e_c}) expresses the amount of energy used per kilometer and it is calculed with the total energy used over the total distance already covered along the trip, as it is shown in Equation 4.22.

$$\xi_{e_c} = \frac{E_{used}}{D_{covered}} \qquad (4.22)$$

92

Also, this block takes historical traffic data to make an initial speed profile estimation. The profile estimation is crucial for real time Eco-Driving Controller and to consider the randomness feature of real driving cycle.

- β_2 Optimization: β_2 expresses the weight of the efficiency penalization (It was called Q_1 in the before sections due to it was constant and imposed without any previous calculation for cost function exploring reasons). The energy coefficient and the speed profile estimation are used to find the β_2 value required to achieve the minimum error between the autonomy expected and the autonomy required. As a result of this process a Figure 4.10 is obtained.

- Control: This block is described in Section 4.3. It uses the optimized value β_2 to solve the optimization problem described in Section 4.4.2. This allows calculating the optimal torque and speed values required by the driver to ensure the energy coefficient desired and to complete satisfactorily the travel.
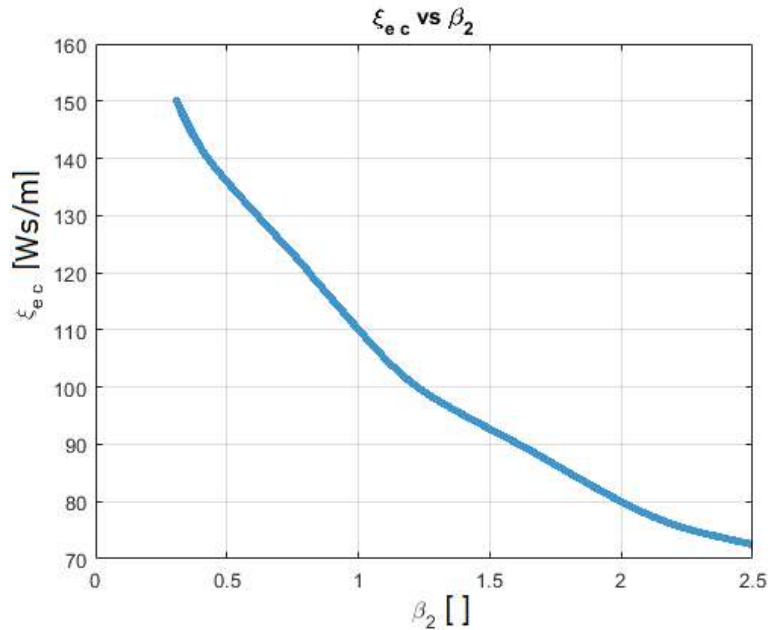
Figure 4.10: Energy coefficient ξ_{e_c} vs β_2 coefficient.

In the following sections the way how the speed profile estimation and the optimal problem control (OPC) are implemented in the block "Energy coefficient estimation" and the block "Control" respectively.

4.4.1 Speed Profile Estimation.

This estimation is essential for a real-time Eco-Driving Controller and depends on driving conditions. The objective of this algorithm is to use past data of a defined time-window to classify the driver behavior in some way and then, to relate that driver behavior with estimated energy consumption.

As it is mentioned in Section 2.5, there exist many speed profiles and each one makes an effort to represent the speed conditions in rural and urban conditions. If the speed profile is added to additional conditions data like the slope profile and the vehicle characteristics, the power demand is obtained. However, the variables involved in a speed profile are more

complex than the rural or urban environment, the speed profile covers a driver style as a result of cultural, educational and emotional causes. After a driver style estimation is made, the speed profiles can be related to the driver style estimation results. The most used classification variables are presented in Table 4.7 [121].

In this research, only the longitudinal dynamic is considered then, variables like the lat-

Parameter	Category	Source
Lat. and long. acceleration	Sporty, normal and relaxed	[122]
Lat. and long. acceleration GPS	Sporty, normal and relaxed	[123]
Jerk	Sporty, normal and relaxed	[124]
Friction coeff. circle, Lat./long. acceleration Lat./long. desacceleration	Sporty, normal and relaxed	[125]
Lat. and long. acceleration, brake pedal, line changes	Sporty, normal and relaxed	[126]
Lat. and long. acceleration, brake pressure, steering angle gradient.	Sporty, normal and relaxed	[127]
Lat. and long. acceleration, Lat. and long. desacceleration mean speed	Sporty, normal and relaxed	[128]

Table 4.7: Variables required to make a driving style estimation.

eral speed, lateral acceleration, steering angle gradient, or pedal position do not represent an option to be considered inside the speed profile estimation algorithm, even when they can increase the accuracy of the classification.

Another important aspect to take into account is the time windows (the amount of past states measures required) used to make the estimation. Even when small-time windows like [124] can be useful to cover complex driving styles, the speed profile estimated by this kind of algorithm is constantly evolving along the trip due to the number of external characteristics considered (like road, traffic or weather). As a consequence, the variation presented in the results is not acceptable to make long energetical estimations. For this reason, in this research, the time window size is a choice based on the size of the different speed profiles considered in the classification process.

In Figure 4.11, the mean and maximum values of speed and acceleration show to make a better representation between driving styles. For this reason, the mean longitudinal speed and the maximum longitudinal acceleration are selected as the measured variables to make the estimation but also, since the traject is known, kind of road covered (urban or rural) is also useful to make the estimation. Using these classification variables, three speed profiles are chosen as a representation of the three driving styles. It lets to make a classification and at the same time, keep an energetical representation of each driving style. This choice lets two define the classification sets: (Relaxed, Normal, and Dynamic), and the estimation algorithm input variable (mean speed, maximum acceleration, and road kind).

Speed profile	Componet	Driving style represented	Mean Speed [m/s]	Max. Accel. [m/s^2]	Max. Jerk [m/s^3]
NREL class 3	Urban	Relaxed	1.8	1.9	1.6
WLTC class 1	Urban	Normal	5.3	0.8	1.2
WLTC class 1	Rural	Dynamic	11.7	0.7	0.4

Table 4.8: Speed profiles chossen to make a driving style representation.

It is important to notice that there are comparable speed profiles like Urban WLTC class 1 and Urban WLTC class 2. In these cases, the WLTC class 2 is used as an equivalent speed profile of WLTC class 1 but the differences between them are used as disturbances. In other words WLTC class 2 can be used to test the algorithm classification. The chosen set of classification with its representative variables are presented in Table 4.8.
Even when exists many algorithms to make the supervised classification of the driver behavior [127], [125], as the neuronal network or clustering, the fuzzy logic is chosen based on the following characteristics:

- The compilation time is low due to the number of sets required.

- By definition, the fuzzy logic avoids making strong changes in the classification output with small input changes. It helps to obtain a consistent estimation along the trip.

- Easy implementation.

- It does not require information about the relationship between input and outputs.

- Historical data can be used to training the algorithm and improve the results.

- The algorithm presents robustness according to the training data used.

The classification algorithm chosen is a Mamdani Fuzzy classification with a centroid de-fuzzification method [128]. It was chosen by its low compilation time (0.23 second) and its accuracy.
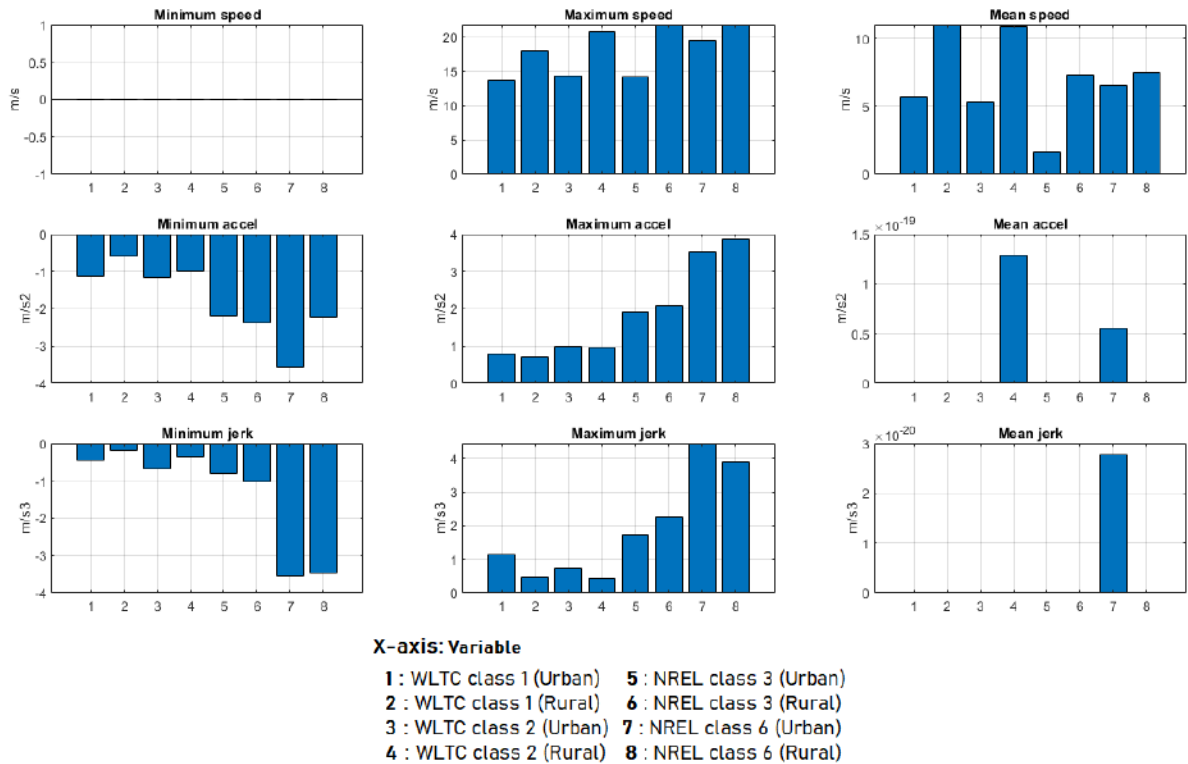
Figure 4.11: Variables suggested to make driving style estimation.

Urban			
Speed range [m/s] / Accel. range [m/s^2]	< 3	3-7	> 7
< 0.8	Relaxed	Relaxed	Normal
0.8 - 1.5	Relaxed	Normal	Dynamic
1.5 - 2.5	Normal	Dynamic	Dynamic
> 2.5	Dynamic	Dynamic	Dynamic
Rural			
Speed range [m/s] / Accel. range [m/s^2]	< 3	3-7	> 7
< 0.8	Relaxed	Relaxed	Normal
0.8 - 1.5	Relaxed	Normal	Normal
1.5 - 2.5	Relaxed	Normal	Dynamic
> 2.5	Normal	Dynamic	Dynamic

Table 4.9: Speed profiles variables classification.

As a result of this classification method, the algorithm can classify the driving style with an accuracy of 72% when the time windows do not overcome the 120 seconds and increase its accuracy to 88% with time windows around 500 seconds. Unfortunately, a bigger time window means a higher compilation time and in case that the estimation is wrong, the mistake persists for a longer period. For those reasons, a time-window of

100 seconds is used and 72% of accuracy is considered enough to make an initial energy required estimation.

This classification method lets to use the vehicle longitudinal dynamic states to estimate the correct driver behavior. Since the driver behaviors are related to a speed profile, this classification lets to make energetical estimations. The driver behavior estimation error has to be considered as a part of the phenomena corrected by the close-loop version of the energetical optimal controller. It will be presented in Section 4.5.

Now that the estimation algorithm implementation inside the block "Energy coefficient estimation" (see diagram in Figure 4.9) was already discussed, the following section will present how the optimal problem control (OPC) is implemented in the block "control" of the same diagram.

4.4.2 The Optimal Problem Control Implementation

To make an appropriate integration for the optimisation problem under energetic performance index, presented in Equation 4.8, there are several different methods in the bibliography, the most representatives were presented in Section 2.5. One of the suitable solutions uses the optimal control theory.

In order to verify the scope of the optimal control, first this problem is solved under an open loop configuration to quantify the autonomy gain and to find the balance coefficient (β_2) limitations.

$$\min_u J_n$$

$$
\begin{aligned}
&s.t. \\
&T_{min} \leq u \leq T_{max} \\
&X_{min} \leq x_1 \leq X_{max} \\
&V_{min} \leq x_2 \leq V_{max} \\
&\dot{x} = f(x, u)
\end{aligned}
\tag{4.23}
$$

Where $\dot{x} = f(x, u)$ is represented by Equation 4.7. The software used to solve the optimization problem is Imperial College London Optimal Control Software "I-CLOCS". This software is used to simplify the interaction with the nonlinear problem solver from Matlab ("fmincon"). It also provides access to new solvers and different discretization methods (Euler method, Trapezoidal method, Hermite-Simpson method.. etc) as well as hessian approximation. The compilation time of the algorithm is around 41 seconds with the following configurations:

- Solver: IPOPT.

- Discretization method: Euler.

- Convergence tolerance of the optimization: 1e-9.

- Maximum number of iterations: 100

- Hessian approximation: Exact.

The algorithm was compiled in an Intel(R) Core(TM) i5-8250U CPU with 8.00Go of RAM. Due to its compilation time, this software is only used to explore with a high sensibility of the cost function along the feasible region but is not properly to closed loop control implementation and in real time usage.

Finally, since all the implementation described in the diagram 4.9 is already covered,

in the following section the performance of the open-loop approach of the Eco-Driving Controller will be tested. The test will analyse the way how the variation of two variables (the different speed profiles and the weight of the efficiency component of the cost function in comparison with the other components) affect the energy optimization performance.

4.4.3 Sensitivity Analysis of Eco Driving Balance.

Since it is described in Section 4.3.5, the cost function of the OPC requires a weight β_2. This parameter will determine the preference of the Eco-Driving algorithm (open-loop and closed-loop) between the multi-objective penalization proposed in Section 4.3.4. This test will help to determine the range of the parameter β_2 and to explore the scope of the effect of his variation. In other words, the sensitivity test will let to explore the scope of the open-loop control technique. Also, the test aims to determine the characteristic of the nonlinear unidimensional optimization required by the close-loop control block called "β_2 optimization". In order to represent the results, the chosen variables are:

- The speed signal: The minimum, maximal and average values of the speed signal will determine the limitation proposed by the Optimal Controller.

- The efficiency of the motor: Since a geometrical representation of the motor efficiency is included inside the cost function, the augmentation of the parameter β_2 must increase or at least keep constant in high values the efficiency.

- The energy signal: This is the variable required to measure the results of the controller. Its reduction will be defined by the β_2 parameter.

- The autonomy expected: In order to represent the final results of the controller, the cost of each kilometer is used to estimate a final autonomy obtained with each β_2 value.

The speed profiles presented in Section 2.5 are used to compare the behavior of the variables efficiency, speed, energy, and autonomy according to the β_2 variation. All speed profiles have been divided into two categories related to the requested power: medium size vehicles (NREL Class 6 and WLTC Class 2) and low size vehicles (NREL Class 3 and WLTC Class 1) in order to analyze the results in each situation. It allows to compare all tests to cover a distance of 10 km. Also, since in the cost function the value β_2 can increase the ponderation of the efficiency components without reducing the ponderation of speed follow, the β_2 has not a range between 0 and 1 necessarily. The range evaluated in this test is from 0 to 5 in order to find where the optimization is stable and justify the final β_2 range.
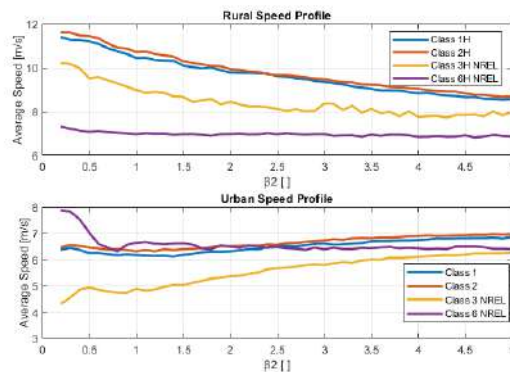
Figure 4.12: Average Speed vs β_2 value.
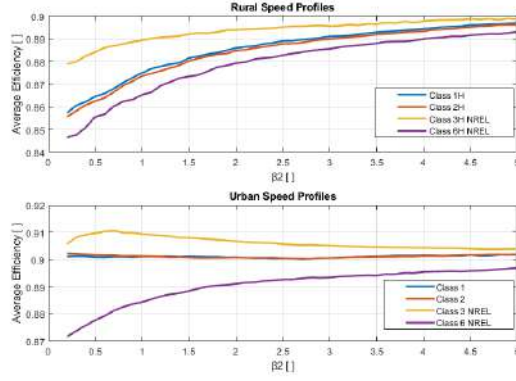
Figure 4.13: Motor efficiency value vs β_2 value.
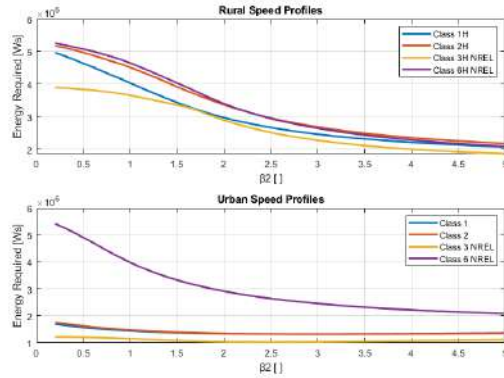
Figure 4.14: Energy required vs β_2 value.

The average speed is shown in Figure 4.12. In this figure, the β_2 is variated (X axis) in order to study its effect over the average speed (Y axis). There are two figures about average speed because each speed profile is divided in its urban traject speed components and rural traject speed components. The increase of β_2 value ensures the controller preference by the optimal speed values in relationship with the amount of torque made on each step. This is the reason why the average speed of all profiles turns around to 7[m/s]. In rural profiles, the high-speed values still being present in the optimized speed profile. This is why even when its optimal mean speed decreases in comparison with the speed values present in rural profiles; It is still being higher than the optimal mean speed proposed when urban profiles are used, due to the higher number of stops and high-speed restrictions. In other words, the maximum values are reduced and minimum speed values are augmented to keep the average speed value close to the optimal value. Also, the feasible speed zone around the optimal value is reduced when β_2 value is augmented.

The obtained motor efficiency value is shown in Figure 4.13. According to the same operating conditions. These figures illustrate in which situations the augmentation of β_2 coefficient is efficient or it is not. As it can be seen, in high-speed values, the β_2 variation causes a strong positive effect related to the suitable impact on over total motor efficiency. By another hand, in the low-speed version of the profiles, (in the most cases) the average speed is close to the optimal speed value and the β_2 variation has not a significant effect.

The energy value required to cover a traject of 10 kilometers with each speed profile is shown in Figure 4.14. Since the average motor efficiency has increased, the amount of
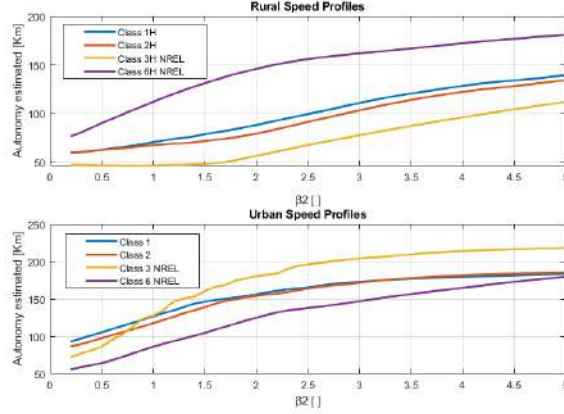
Figure 4.15: Autonomy expected vs β_2 value.

energy required decrease. This analysis is important to determine the two variables required to optimize β_2: The energy coefficient required and the energy behavior expected. In closed loop control, the energy estimation coefficient value is checked in order to ensure the correct energetical cost per kilometer. Then, the initial energy coefficient estimation required is compared to the energy coefficient measured along the travel and a new optimization along the energy behavior expected is made to find the minimum β_2 value required to complete the trip. From this analysis, it can be highlighted the β_2 presents a nonlinear function without local optimal points. This analysis aims to choose a unidimensional optimization methodology as the algorithm required to solve the optimization.

The energy value and the final distance (10 kilometers) let to predict the autonomy under specific conditions (perfect speed profile estimation) shown in Figure 4.15. The efficiency Figure 4.13 shows the biggest potential of the algorithm in high-speed profiles. While the information on autonomy values obtained in low-speed profiles will be used as a limitation due to traffic regulation. In low-speed profiles, the highest autonomy variation is obtained in β_2 values from 0 to 2. Also, if the β_2 value is superior to 2, the speed variation can not be followed in normal traffic conditions. For this reason, in electric vehicles outside of an autonomous environment, the considered β_2 range is from 0 to 2.

In conclusion, the algorithm is able to obtain improvements of more than 50% of the vehicle autonomy with limitations around 30% of maximum and minimum speed values under the hypothesis of a perfect speed profile estimation and the chosen range of β_2. However, those results are highly related to the efficiency function representation and the driver capacity to follow the speed profile proposed by the optimal controller. Also, it is important to highlight that the addition of disturbances caused by the speed profile estimation error can decrease significantly the autonomy expected. This phenomenon added to traffic and driver interaction has to be reduced by the closed loop controller version. Even when the speed profile proposed by the controller can not be used in all traffic situations, a β_2 value from 0 to 2 is able to improve the autonomy in a realistic situation. Also, this algorithm can be extended for autonomous vehicles in order to reduce speed profile limitations. The energy per kilometer is a coefficient able to represent the efficiency required by the driver in order to complete travel. It is used also to find the relevance of the constraints proposed by the Eco-Driving Controller to complete the travel. Finally, due to the nonlinear function which describes the energy per kilometer has not sub-optimal points, an unidimensional algorithm focused on compilation time can be used.

Until this moment, β_2 and speed/torque signal are optimized just one time by the Eco-Driving Controller then the controller is not able to react to the external disturbances. For this reason, the following section presents a closed-loop version of the Eco-Driving Controller.

4.5 Closed Loop Controller

As sensors, actuators, and external disturbances cause errors over the open-loop controller reference tracking, the closed-loop controller is required to reduce their impact and to follow the desired response.

In this case, an NMPC (Nonlinear Model Predictive Controller) is proposed based on the optimal problem requirements and the MPC controller properties exposed in Section 2.5. It has a prediction horizon $N_p = 10$ and a control horizon $N_c = 10$ (equivalent to 10s). Those values are chosen to keep a balance between the compilation time and speed/acceleration dynamics.

The main objective of the cost function is to complete the travel. For this reason two kind of feedback signals are included: Energy control feedback signal and energy estimation feedback signal.

- The energy estimation feedback signal is the data required to verify energy estimation coefficient on each iteration of the NMPC. This information is composed by the energy and distance state data from the system with noise.

- The energy control feedback signal is the data required by the NMPC to estimate the bahavior of the system along the prediction horizon.

The NMPC is a discrete controller. For this reason, it needs a discrete system model eq. Note also, that the torque variation penalization is omited due to the reasons exposed in Section 4.3.5.

$$\min \ J(x, u, k)$$

$$J(x) = \beta_1 * \beta_2 * \phi_1(x_3(N))$$
$$+ \sum_0^N -\beta_2 * \phi_2(x_2(k), T(k)) + (x_2(k) - x_{2_{ref}})^2$$

$$s.t.$$
$$T_{min} \leq T(k) \leq T_{max} \tag{4.24}$$

$$
\begin{aligned}
0 &\leq x_1(k) \leq x_{1_f} \\
x_{2_{min}} &\leq x_2(k) \leq x_{2_{max}} \\
0 &\leq x_3(k) \leq TotEne
\end{aligned}
$$

$$x_{k+1} = f(x, T, k)$$

where $x_{k+1} = f(x, T, k)$ is a discrete version of the model represented by (4.10) and:

$$\phi 1(x_3(1)) = x_3(k) \tag{4.25}$$

$$\phi 2(x_2(k), T(k)) = Eff(x_2, T) \tag{4.26}$$

NMPC is described in Algorithm 2. Also, in Figure 4.16, the flux of data is represented. The EcoDriving controller is composed of two main elements. Firstly, the NMPC required to balance the autonomy and the capability of the driver to follow a speed reference. Secondly, the two blocks required to find the β_2 value: the β_2 optimization and energy estimation coefficient block.

Algorithm 2 NMPC Controller.

---

1. BEGIN
2. Choose the initial states of the vehicle system.
3. Introduce autonomy required (D_{req}).
4. Gathering required information for optimization from three sources: vehicle, rider and digital devices.
5. Calculate energy estimation coefficient required to complete the travel η_{e_c}.
6. Find the β_2 value required to complete the trip.
7. Choose the initial states of the system.
8. Solve optimal problem 4.23.
9. Apply first component of optimal reference for a period of time of Ts.
10. Have the travel ends?.

- 10.1 NO : The time happed is multiple of 1000 seconds?

    − 10.1.1 SI: Use final states as new initial states and go to 5.

    − 10.1.2 NO: Use final states as new initial states and go to 7.

- 10.2 YES: END.
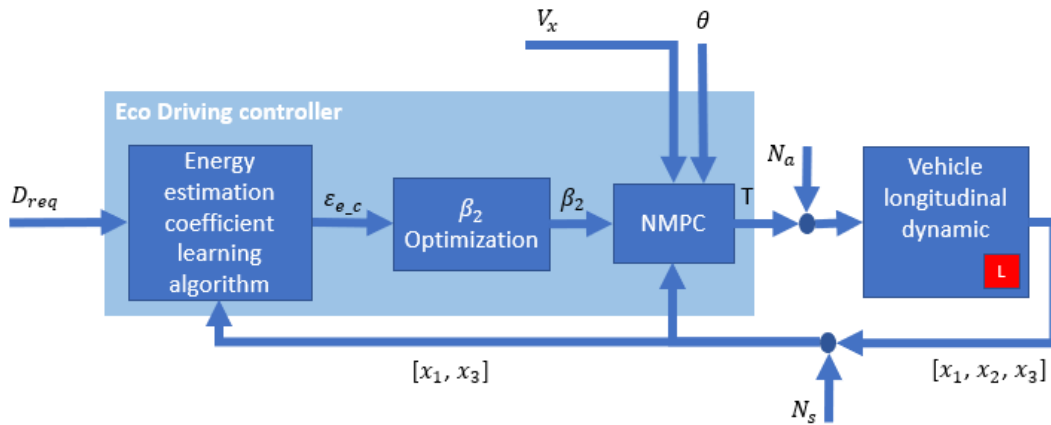
Figure 4.16: Closed-loop control diagram.

The NMPC requires the offline data describe in Table (4.1) and (4.3), the initial states described in Equation 4.10 ($[d, v, e]$), the speed reference and the road slope value to propose the optimal torque value. This value is added to the actuators noise (N_a) and the result is used by the longitudinal vehicle dynamic block to update the states values. When the measurment data is ready, the sensor noise (N_s) is added to the states values and they are feedback to NMPC and energy estimation coefficient block. The energy estimation coefficient block takes into account the distance required by the driver (D_{req}) and the current state (x_1) after a period of time equivalent to the prediction horizon to determine the energy estimation coefficient (ϵ_{e_c}) required to complet the trip. Finally

the β_2 optimization block uses this coefficient to optimize the β_2 value and adjust the energy rate consumtion and the process is replicated until the travel is completed. The mechanical and electrical vehicle characteristics are shown in Table 4.1 and Table 3.8.

Now that all elements of the MPC are defined, the following section presents the closed-loop control simulation results.

4.5.1 Simulation results

To feedback the speed state of the vehicle the closed loop control shown in Figure 4.16 is formulated. The objective of this control loop is to correct the speed error caused by the estimation process, the interaction with the driver and the speed measure.

In the block "NMPC", the Algorithm 2 was implemented using the toolbox MPsee in order to use the fast online Nonlinear Model Predictive Controller implementation. When a numeric optimization is required, many kinds of descending algorithms can be applied but, when the functions are differentiable, the Newton method uses to be an iterative method enough to work. This is why it is highly extended in optimization toolboxes. However, since the method requires solving linear (or nonlinar) system equations and calculate the second derivative, the compilation time can increase according to the system complexity. This is why the Newton method is complemented with other algorithms able to make it faster. The toolbox MPsee offers the algorithm GMRES (generalized minimal residual) to complement the Newton method. It makes approximations of the solution by a vector that belong to a Krylov subspace with minimal residual [129]. For those reasons, the Newton/GMRES real-time optimization method with the single-shooting mode (to save compilation time) is used. The average compilation time obtained with this configuration is 5.7 seconds. This value is not comparable to the minimum time required to make a speed profile estimation with accuracy over 72% (120 seconds) and more importantly, it is not comparable to the timing present in the battery energy dynamic then, it is considered acceptable.

The interaction with the driver refers to its incapacity to follow the speed profile proposed by the optimal controller related to external constraints like traffic or communication limits between the driver and the controller. These disturbances in speed profiles are added to the simulation in order to obtain a more realistic scope of the controller. Considering the expected sensor resolution and actuator noise (see Table 5.1), the disturbances are represented by an integrated uniform random signal with a sample time of 10 seconds and an amplitude of 15% of the maximum motor torque in the case of the current measure and 5% of the maximum speed in the case of the speed sensor. This signal is integrated in order to ensure its continuity, to be coherent with driver behavior and amplitude-frequency components present in the speed profiles signals presented in Section 2.5. On the other hand, the driving style estimation error refers to the difference between the speed profile estimated and the speed profile used by the driver. In this simulation, the traject represented is an urban traject then, the driver style estimated is a "Normal style" which refers to "WLTC class 1/Urban" speed profile. However, the speed profile used is "WLTC class 2/Urban". The urban or rural character of the speed profile is easily classified due to the mean speed variations but the specific speed profile used represents a more difficult classification challenge that is not completely covered by the classification algorithm due to the limited data about the speed profile.

As a result of these disturbances, the autonomy estimation obtained is significatively reduced, in realistic scenarios. The autonomy incrementation from the minimum to the maximum value of β_2 is around 30% except by the "NREL Class 3/Urban" and "NREL

Class 3/Rural" speed profiles. In these cases, the autonomy augmentation is higher than 30% due to the stoped time present in each speed profile. However, even when the close-loop simulation is a better representation of the experiment, the results still being related to the perfect motor efficiency representation. For this reason, the results have to be compared with results obtained with a real platform. Also, the balance coefficient (β_2) is not modified along the travel to face the effect of the disturbances. To add a degree of freedom in β_2 coefficient, an external close-loop is proposed in the next section.
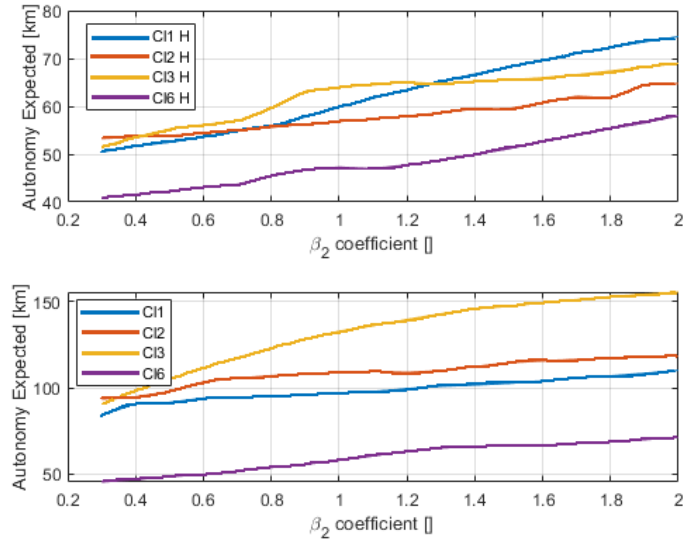
Figure 4.17: Autonomy estimation.

The Eco-Driving Controller in the open-loop version has to control the balance between the speed tracking and the energy savings based on a predefined balance coefficient (β_2). It means that the controller has to handle the sample time of just one dynamic, the speed state dynamic. However, the closed-loop has to handle the sample time of two dynamics strongly differents: the speed state dynamic and the energy state dynamic too. This second dynamic (the energy dynamic) is required to make optimization over the β_2 value along the trip. This way, the feedback information of both variables can be used in the real-time optimization process to adapt the performance of the controller in comparison to the presented disturbances. In order to make the optimizations in a coherent sample time to each variable dynamic, the following section separates the optimization process into two to ensure the lowest computational load.

4.5.2 Double control boucle: Simulation results

In order to understand how the speed disturbances affect the energy estimation and to correct its effect, a second feedback is made. The energy and position states are feedback to calculate the energy coefficient required to complete the travel. Since the energy state has a slow dynamic, the β_2 optimization process is made with a separation of 1000 seconds. In other words, the sample time of the second close-loop is 1000 seconds. As a result of the consideration mentioned before, the controller presented in Figure 4.16 is presented.

The process represented in Figure (4.18) consists of recreating an urban driving mission profile along a trip. The driver is in charge to propose an autonomy required and the

energy per kilometer is calculated. The speed profile chosen is the NREL Classe 3 drive rural cycle developed by Smith Newton from NREL Labs [120] because it was designed for light electric vehicles. The speed profile was repeated until the objective distance is completed by the vehicle.
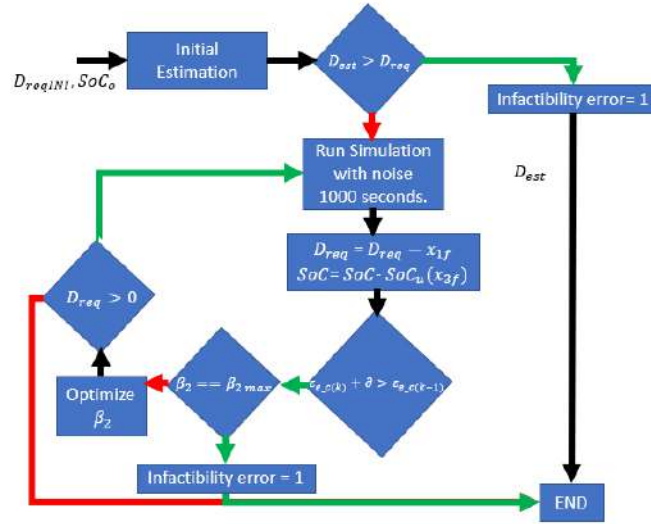
Figure 4.18: Double loop control algorithm.

The controller has into account the battery and driver losses because those losses are proportional to the speed. However, their direct minimization would cause the critical speed reduction of the vehicle. For this reason, an additional proportional controller is made considering the energy coefficient error. The proportional control is not symmetric, the controller gain when the energy coefficient is positive is double than when it is negative, this difference is made to prioritize the trip finalization over the autonomy optimization.

The autonomy values demanded by the driver along the test presented were from 16 [km] to 160 [km] even when the vehicles with similar characteristics are designed for an autonomy between the 80 [km] to 100 [km] according to the user manual [106]. The initial SoC were from 20% to 100%. The controller was able to complete the travel with a maximum error of distance of 1.25% always that the autonomy required ("Reference value" column) is not greater than the 90% of the autonomy estimated with the greatest value of β_2 ("Value expected by estimator" column when $\beta_2 = 5$). The Table 4.10 presents the optimization results of speed profile in three β_2 regions: "maxA", "MaxNA" and "Min". In each β_2 region a couple of distance required and SoC are chosen to force the optimal controller to work with the β_2 values desired to make a comparison between the different regions of β_2. "MaxA" means the initial value of β_2 is the maximum β_2 value admitted by the algorithm ($\beta_2 = 5$) it is a region where a perfect estimation of the environment and the vehicle speed control is required (see Section 4.4.3). "MaxNA" means the initial value of β_2 is the maximum β_2 value admitted by the algorithm after the sensitivity analysis results presented in Section 4.4.3 ($\beta_2 = 2$). This value lets the driver keep the vehicle control but with speed and torque limitations. Finally, "Min" means the initial value of β_2 is the minimum β_2 value admitted by the algorithm ($\beta_2 = 0$), this region shows the utilization of a non-optimized speed profile. As can be seen, The controller was able to complete the travel with a maximum error of distance of 1.25% and it was capable to increase the autonomy over 60% without take away all control from the driver over the

105

SoC [%]	Maximum $\beta_2 \rightarrow \beta_{2_{maxA}}$			
	Value expected by estimator [km]	Reference value [km]	Obtained value [km]	Distance errror [%]
100	177	160	158.7	0.78
50	88	75	74	1.25
20	35	31	30.8	0.64
	Middle $\beta_2 \rightarrow \beta_{2_{maxNA}}$			
	Value expected by estimator [km]	Reference value [km]	Obtained value [km]	Distance errror [%]
100	126	126	125.5	0.33
50	63	63	62.5	0.64
20	25	25	24.8	0.49
	Minimum $\beta_2 \rightarrow \beta_{2_{min}}$			
	Value expected by estimator [km]	Reference value [km]	Obtained value [km]	Distance errror [%]
100	75	75	74.7	0.28
50	38	38	37.9	0.14
20	16	16	18.8	1.02

Table 4.10: Distance error results.

speed profile. Also, in a hypothetic situation where it is not important to keep some control over the vehicle because the external obstacles are perfectly controlled (like an environment of fully autonomous vehicles) the theoretical autonomy optimization increase significantly.

In order to explore a specific case, a trip of 100 [km] ("Reference value" column) with a Class 2 Urban speed profile is proposed. The current SoC of the vehicle is 80% ("SoC" column), it means the vehicle is able to cover around 60 [km] ("value expected by estimator" column) without any optimization and 141 [km] ("value expected by estimator" column) if the vehicle ignores at all the speed profile proposed by the driver and it goes at its optimal speed value ($\beta_2 = \beta_{2_{max}}$). Finally with $\beta_2 = 2$ the controller expected to cover 100 [km] ("value expected by estimator" column) and it was able to cover 99.4 [km] which represent an error of 0.6%.
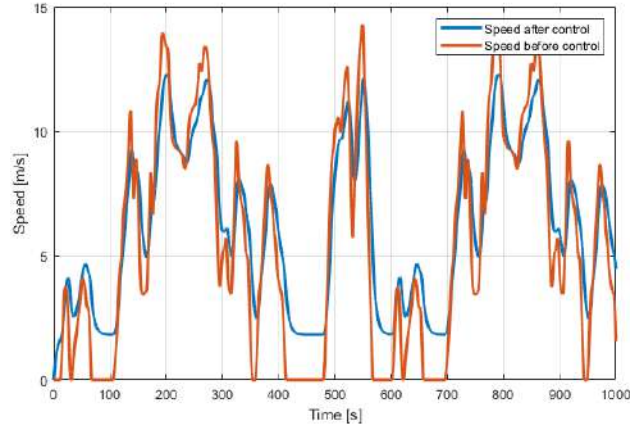
Figure 4.19: Comparison between optimized and unoptimized speed profiles.

With a $\beta_2 = 1.6250$ the internal controller (NMPC) is able to increase the autonomy of the vehicle around a 66% keeping a correlation of 68% between the speed profile proposed by the driver and the one by the controller (Figure 4.19). The speed profile proposed by the controller tends to avoid minimum and maximum speed values of the speed profile proposed by the driver by an acceleration limitation. As a result, the mean value of the vehicle speed and the torque required along the travel are closer to the optimal values according to the electric motor characterization. In a real implementation, some stops could be required by the driver. It would cause an estimation error of the required energy by kilometer, this is why the external controller is required. The proportional gain of the external controller is limited to reduce the noise added to the optimal controller when the magnitude of measurement errors and the unexpected variation between the speed profile described by the driver and the speed profile estimator are considerably bigger than expected.
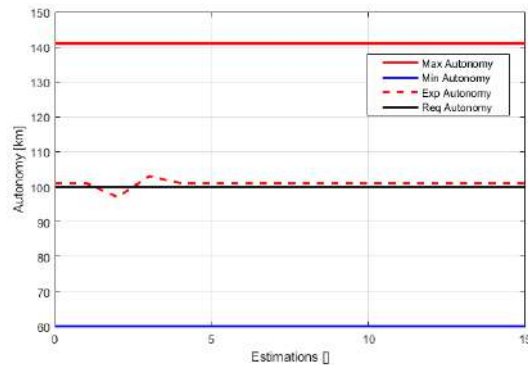
Figure 4.20: Expected autonomy variation along the trip.
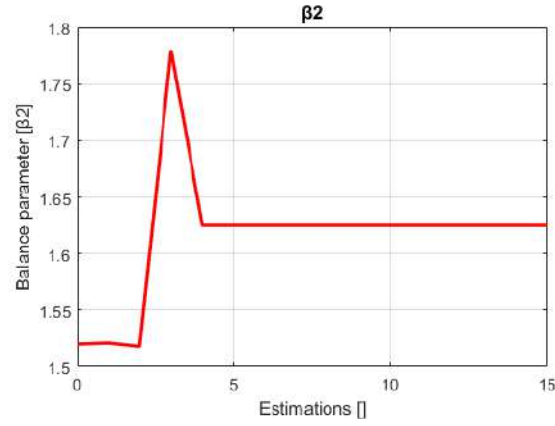
Figure 4.22: β_2 optimization behavior along the simulated trip.
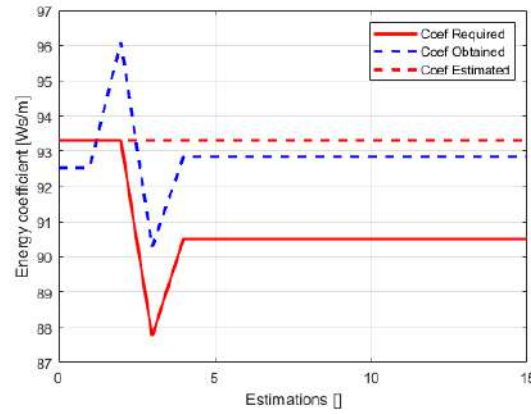
Figure 4.21: Estimation of energy per kilometer variation.

As it can be seen in Figure 4.21, the disturbances caused by wrong measurement or actuator signals noise cause an error in the energy estimation. Since this algorithm helps to determine the β_2 coefficient required to complete the travel, the estimated β_2 ends to be higher or lower than the required one due to the effect of disturbances. As a consequence of a wrong β_2 value, an unbalanced limitation is imposed over the speed profile and the amount of energy demanded by the travel will vary from the battery limitation proposed initially. For this reason, the external controller checks the energy required per kilometer in order to ensure that the estimation is coherent with the last one (calculated in the last sample time). As it can be seen in Figure 4.22, when the energy per kilometer measured is significantly different in comparison with the estimated one, the controller uses the difference between both signals to correct the β_2 value in three steps:

- Calculate the difference between the energy coefficient estimated and measured.

- Use a proportional gain to calculate the new energy coefficient based on the last measured error.

- Recalculate the required optimal β_2 coefficient based on the energy coefficient calculated before.

The resultant β_2 signal describes an overdamped behavior with a peak of 103.5% of the final value. The stabilization time is 4 iteration steps and it is important to note that each iteration corresponds to 1000 seconds. Finally, the vehicle was able to complete the

travel with an SoC error of 0.06% and a final autonomy error of 0.1% (100 meters). The travel time simulated was 3.8 hours and of both control loops the simulation time does not exceed the 35% of the sample time on each case. This β_2 coefficient active correction method ensures the autonomy estimation will be as close as possible to the estimated one initially (Figure 4.20).

4.6   Conclusion

The closed-loop uses the components presented in the open-loop version (see Section 4.4) but also, it lets to take into account the disturbances which affect the speed state. Those disturbances are mainly the speed profile estimation error, the driver capability to follow the speed profile optimized and the speed measuring error. When those disturbances were taken into account the autonomy estimation decreases significantly, but the maximum autonomy augmentation with the maximum balance coefficient $\beta_2 = 2$ still being over the 50%. Those results are possible thanks to the external energy control loop in charge of optimizing the β_2 value in function of the disturbances presented along the trip. Finally, the work made by the different closed-loop version of the Eco-Driving Controller (The MPC block, the energy estimation block and β_2 optimization block) are able to ensure the trip finalization with a 1.25% of maximum autonomy error without matters the initial SoC.

However, the presented results in this chapter still being related to the motor efficiency representation, this characterization has to be carefully made in order to obtain with the real platform, the same results obtained with the simulations. For this reason, in the following chapter, a test bench is proposed to verify the Eco-Driving Controller scope under the real devices behavior.

Chapter 5

Experiment validation

5.1 Introduction:

This chapter aims to make a real implementation of the algorithms presented in Section 4 to present a comparaison between simulation and experimental results. In order to make this comparison, a test bench is built to obtain a replicable and realistic test for optimal controller implementation. Indeed, this section starts with the test bench description, covering the structural analysis required to ensure the functionality of the test bench. The sensors required to measure the desired states and the actuators to represent the opposing forces of the movement. After this, the slight changes made on our algorithm to be implemented according to the test bench software and hardware limitations will be presented. Finally, two comparisons will be carried out to show the relevance and effectiveness of the proposed approach. By one hand the results obtained by simulation and experimentation will be compared to conclude his real scope. This comparison only includes the closed-loop approach of the algorithm, the open-loop one is used to obtain BLDC motor characterization as well as sensor and actuators noise. On another hand, the results obtained by the closed-loop controller in the test bench are compared with the capabilities of other eco-driving algorithms in order to estimate the real value of the optimal control technique proposed in this research study.

5.2 Test bench:

To illustrate the effectiveness of the proposed approach and to verify the simulation results, a reduced scale test bench is proposed with the following requirements:

- A BLDC motor has to be able to develop its highest speed securely.

- A braking system has to be implemented to represent the moving opposition forces.

- The braking system has to be regulable to represent a variation of the moving opposition forces.

- The BLDC motor speed and the energy consumed has to be measurable.

- The platform has to be able to follow a predefined speed profile.

In the next section, the selectrion of the hardware and software used is presented.

5.2.1 Hardware and software specifications.

The first subject to cover in the test bench is the security, which enabled us to select the bicycle training roller "vidaXL". It is build to support a maximal load of 150Kg with a maximum torque of 120 Nm. The structure supports wheels from 26 inches to 28 inches but this limitation is caused principally by the braking system. As the braking system does not let to be dynamically controlled, the training roller brakes are emulated by mechanical load available in our laboratory. It uses an asynchronous motor in generator mode with a maximum power of 300 Watts. Both electrical machines are joined by a chain with two bicycle disk, both with a 32 teeth. Finally, the asynchronous motor current is rectified by an inverter Semikron 08753450/309 in order to interact with a variable electrical load Zenon AL3008BLDC200V10KW_MD21.06. Figure 5.1 shows the experimental test bench.
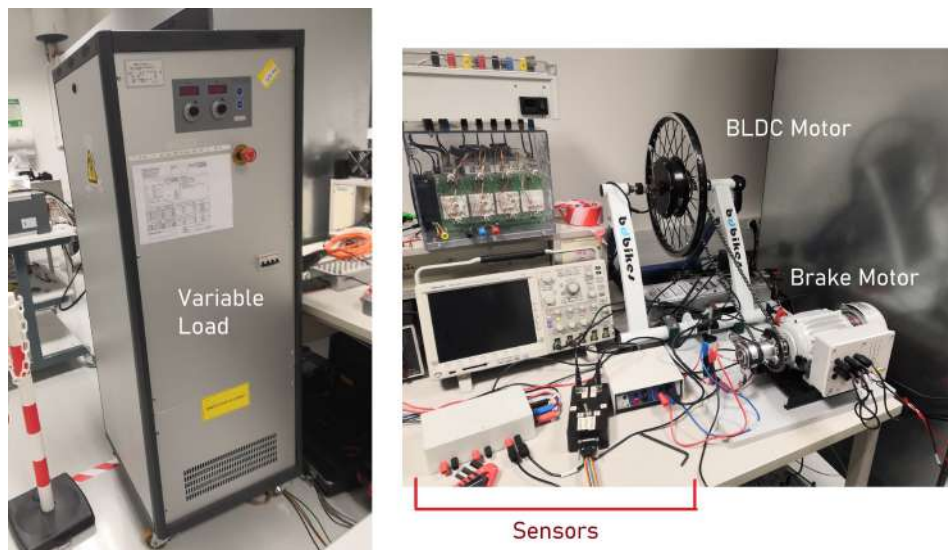
Figure 5.1: Test bench.

The BLDC motor choice is the BLDC1200W included in the OZO kit "Speed Donkey 20" à 24" with a nominal power of 1000W, a peak power of 1200W and limited to 25A" from OZO company. It is used to convert traditional bicycles into electrical bicycles. It has a maximum torque of 98 Nm and a maximal speed of 30 km/h (Limited by inverter) when the motor inverter is feed with 36V. Even when the controller is able to support the 48V in order to increase the mentioned torque and speed values, this option is not used to ensure the structural and electrical safety of the platform. The inverter has a current limitation of 25A and the control technique used is Field-Oriented Control (FOC). Also, the inverter can work without hall sensors. When the hall sensors are not present, the estimation of the stator position is based on the motor EMF and as a result, the output signal is square. It causes an incrementation of the maximal torque and maximal speed but, the acceleration is less fluid and the motor is noisier than the operation with hall sensors.

A real-time dSPACE DS1104 (shown in Figure 5.2) controller board has been used for implementing the control strategy using Matlab/Simulink software. This real-time I/O hardware uses the connector panel to control and make digital or analog measures over any device. The hardware is controlled by the dedicated software (ControlDesk).

Figure 5.2: Controller board connector dSPACE DS1104.

The sensor used to measure the BLDC motor speed is the incremental encoder "XCC1514TSM02Y" with a maximum of revolution speed of 6000 rpm.

The main characteristics of the devices used are presented in Table 5.1.
The global diagram of the proposed test bench is presented in Figure 5.3.
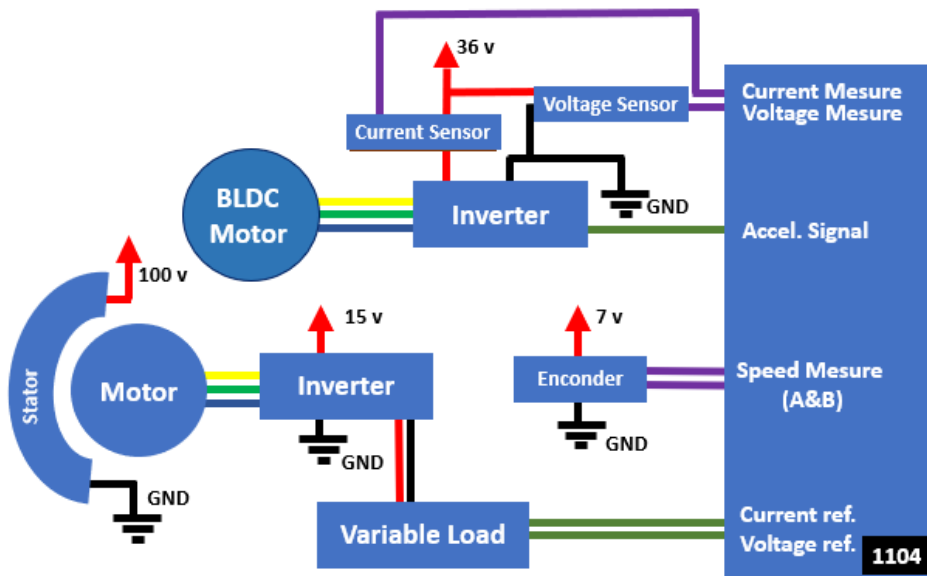
Figure 5.3: Test bench electrical diagram.

In order to explain the driagram connection and the experimental set-up, five steps are followed:

- Develope a GUI (graphical user interface) to interact with hardware in real time.

- Determine how the acceleration signal is related with the speed signal in the traction motor inverter.

- Determine the efficiency function of the BLDC motor (maximum value position and limitation curves).

- Determine what are the test required to verify the controller behavior in a realistic situation.

Device	Parameter	Value
Traction Motor	Motor technology	BLDC
	Nominal power [W]	1200
	Maximal power [W]	1365
	Maximal speed [km/h]	40
	Maximal torque [Nm]	98
	Wheel diameter [cm]	21
Braking Motor	Motor technology	Brushless Motor
	Nominal power [W]	300
	Maximal current [A]	0.95
	Maximal speed [rpm]	1500
BLDC inverter	Control technique	full wave rectifier
	Nominal voltage [V]	15
	Maximal voltage [V]	56
	Maximal output current [A]	25
Brake inverter	Control technique	Full wave rectifier
	Nominal control voltage [V]	15
	Nominal voltage [V]	200
	Maximal output current [A]	25
Encoder	Encoder type	Incremental encoder
	Shaft diameter [mm]	14
	Resolution [points]	256 to 4096
	Maximal speed [rpm]	60006
	Supply voltage [V]	5 to 30 DC
Voltage sensor	Range [V]	500
	Resolution [mV]	100
	Supply voltage [V]	220-240 AC
Current sensor	Range [A]	50
	Resolution [mA]	10
	Supply voltage [V]	220-240 AC
Variable load	Voltage range [V]	10-1000
	Voltage resolution [mV]	100
	Maximal input power [kW]	14
	Current resolution [mA]	100
	Supply voltage [V]	220-240 triphasic AC
Control panel DSpace 1104	Input/Output range [V]	-10 to 10
	Input/Output resolution [mV]	1
	Input/Output maximal current [A]	0.005
	Supply voltage [V]	12

Table 5.1: Test bench specifications.

5.2.2 A. GUI description:

As it was alreary mentioned, the GUI was made in ControlDesk 6.4 software, this version is required in order to be compatible with Matlab 2018a.
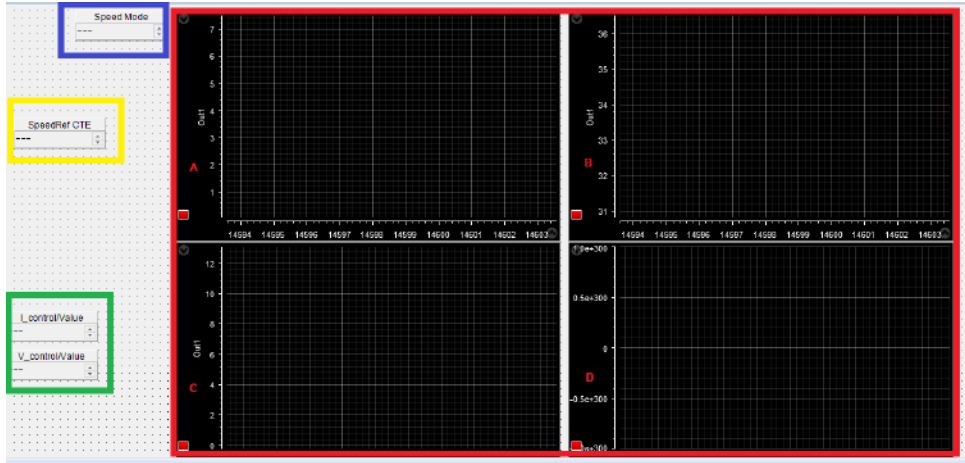
Figure 5.4: GUI Control Desk.

The components of the GUI presented in Figure 5.4 are:

- 1. (Blue) Speed references selector: This value control a multiport switch in Simulink able to choose between the following speed references:

  - Constant speed reference.
  - Sinusoidal speed reference.
  - Non-optimized speed profile.
  - Optimized speed profile.

- 2. (Yellow) Manual Speed reference value: When the constant speed reference is chosen, this numeric input box lets to control the reference value.

- 3. (Green) Variable impedance voltage and current: These numeric input boxes control the impedance reference of the variable impedance when constant values are required.

- 4. (Red) Current(A), Voltage(B), speed(C) and energy coefficient(D) plotter: This plot area lets to show the behavior of relevant variables.

The first important element to understand how the GUI can control the platform is the way how the control signal is built. For this reason, the following section will explain the process to find the equivalence between the voltage proposed by the accelerator and the speed value.

5.2.3 B. Acceleration signal:

The accelerator of the kit "Speed Donkey 20" from OZO company was modified to control the motor from the real-time controller board dSPACE DS1104.

Figure 5.5: Accelerator connection.

In Figure 5.5 the accelerator connection is shown, the modification required is to control the voltage between wires "Signal" and "Mass" to ensure a desired motor speed. In order to establish the relationship between the accelerator signal voltage and the motor speed, two steps are made:

- Meassure the range of the accelerator signal in normal operation (without any modification).

- Meassure the motor speed inside the range find in las step to plot it and to find the relationship.

The voltage range measured in the accelerator signal without any modification was between 1.35 [V] and 2.65 [V] and the data represent a rigth line between the maximum and the minimum valu (see Figure 5.6). The equation which describe the data behavior is:

$$V_{ac} = V_{ref} * \frac{1}{9.23} + \frac{12.4}{9.23} \tag{5.1}$$

Where V_{ac} and V_{ref} are the accelerator signal voltage [V] and speed reference [m/s] respectively.
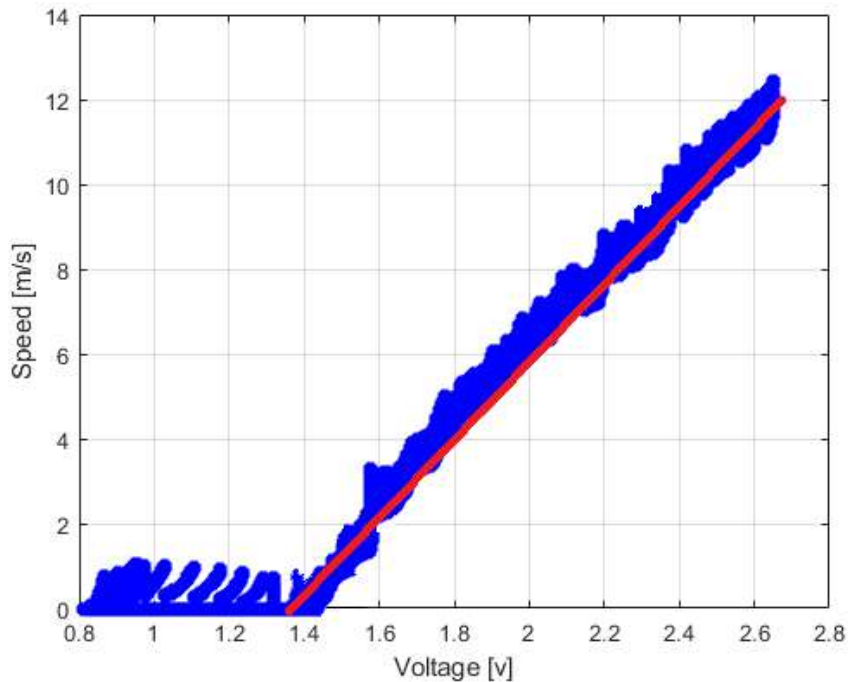
Figure 5.6: Accelerator signal voltage vs motor speed.

Since the motor speed can be controlled from ControlDesk in a range between 0 to 12 [m/s], the next step is to make the BLDC motor working in different regions to explore the efficiency values and to create the geometrical representation described in Section 4.2. The process of how it is achieved will be presented in the following section.

5.2.4   C. Efficiency function:

In order to decrease the computational requirements demanded by the Eco-Driving Controller and make possible an online optimization, a geometrical representation of the BLDC motor efficiency was presented in Section 4.2. In that section, the mechanical limitation and the efficiency values were obtained completely by a virtual process (a co-simulation using logical programming coupled with magnetic simulation software (ANSYS/Maxwell [119])). However, with the motor presented in Section 5.2.1, it is possible to make a scale test. The process followed to obtain the motor efficiency representation is:

- Repeat the co-simulation using logical programming coupled with magnetic simulation software (ANSYS/Maxwell). The parameters of the electric motor evaluated are shown in Table 5.1. This first step lets to obtain a guide of results expected in the following steps.

- Make a rotor blocking test. This test consists in to try to block the rotor with an incremental load. The load has to be higher than the maximal load of the motor at maximal speed along all the tests. As a result, the speed of the rotor has to decrease and the mechanical limitation of the motor will be determined.
It is important to note that the maximal torque achieved by this test has to be lower than 90% of the maximal torque motor constraint in order to avoid motor damage.

- Make a linear representation of the mechanical motor constraints found in step 2.

116

- Verify the maximal efficiency value proposed by the magnetic simulation software (ANSYS/Maxwell). Since an initial efficiency was estimated in step 1, the maximum value has to be verified making working as close as possible to that point and evaluating the efficiency value.
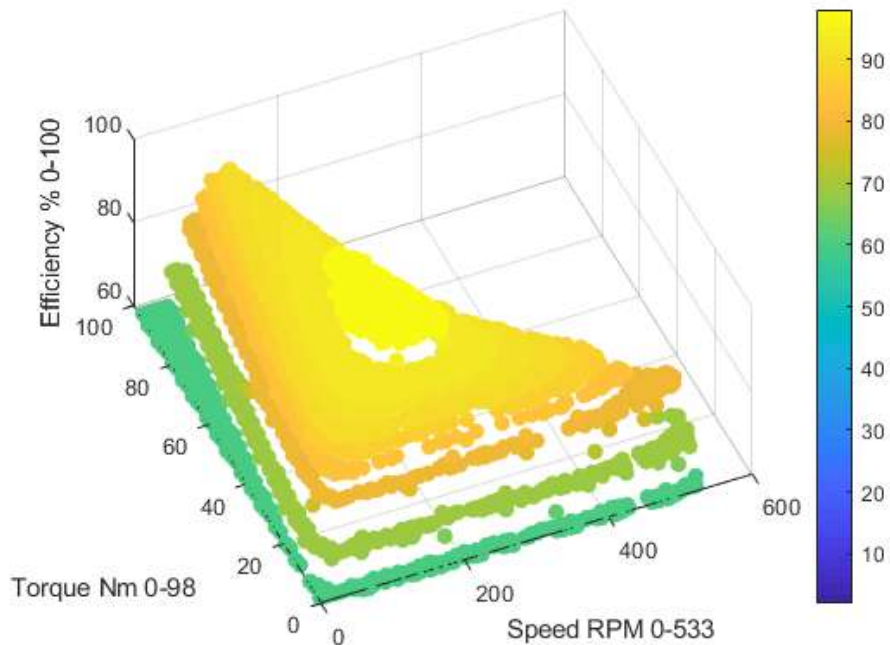
Figure 5.7: Estimated efficiency map from ANSYS.

Having done the co-simulation process (see Figure 5.7), the rotor blocking test consists in trying to block the motor rotor progressively. In order to do that, the brake of the bicycle training roller is used. Also, since the torque can not be measured, the relationship between the speed and torque represented in the simulated efficiency representation is used. To avoid overstepping the 90% of the maximal torque, the speed value can not decrease under 30% of the maximal speed (See Figure 5.7).

As a result of the rotor blocking test, the speed limitation presented in Figure 5.8 is obtained. This curve is reoriented and placed in the speed-torque plane taking into account the following data: Minimal and maximal speed, minimal and maximal torque, (ANSYS/Maxwell) simulation results (See Figure 5.9).
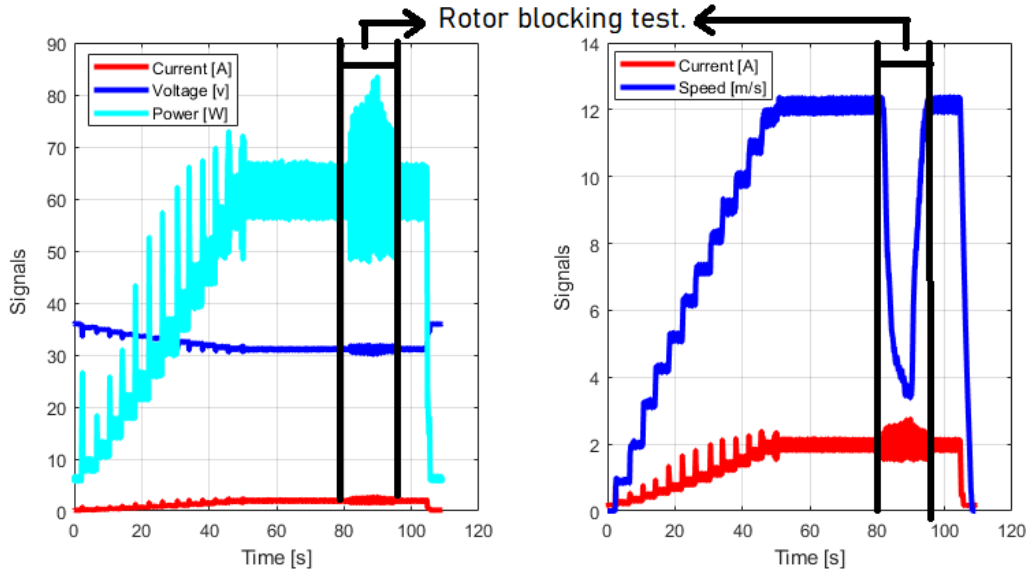
Figure 5.8: Experimental speed curve while rotor blocking test.
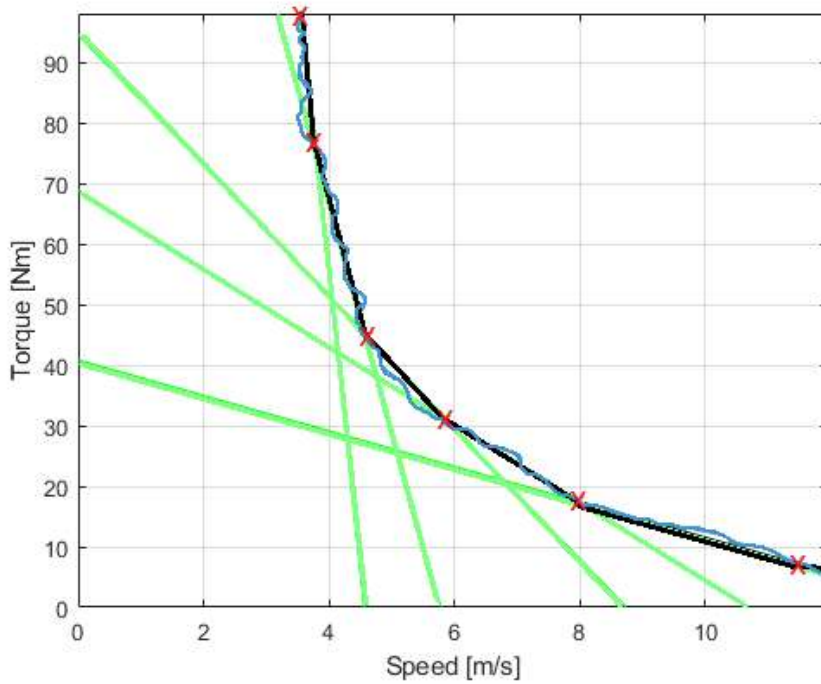
Figure 5.9: Experimental Speed-Torque constraints of BLDC Motor.

Once the constraint speed curve is obtained, the linear representations are introduced to be integrated into the optimization process (see Figure 5.9). The linear representations refer to lines described by the equation: $Y_i = m_i * X_i + b_i$. Where Y_i is the i_{st} torque value, X_i is the i_{st} speed value, and m_i, b_i are the slope and the Y-axis intercept value (when X=0). The linear representation is used by the optimizer to propose realistic speed values according to the torque values estimated along the traject. The slope and Y-axis intercept value resultant of all lines which describe the speed-torque constraint is presented in Table 5.2. Finally, each value of the efficiency function has not to be verified due to the geometrical representation, it only requires the maximal efficiency value to orient

Slope	Value	Intercept	Value
m_1	-2.92	b_1	40.86
m_2	-6.45	b_2	68.96
m_3	-10.81	b_3	94.57
m_4	-37.97	b_4	219.74
m_5	-97.18	b_5	443.03

Table 5.2: Set of lines required to make a linear representation of torque-speed constraints.

the optimization. In order to verify this convergence, the brake of the bicycle training roller is used to place the torque value as close to the maximum efficiency value expected. Also small variances are made with the Zenon variable electrical load. The maximal efficiency point proposed by the geometrical representation has an error of 67 RPM in the speed axis and 7.1 Nm in torque axis. This value is calibrated using the Speed-Torque constraints curve obtained before and the simulated efficiency map obtained from ANSYS as additional information to the calibration process made with the variable electrical load. As a result, the geometrical representation is displaced to agree with this maximal point. As a result simulation and calibration process, the resultant geometrical representation is presented in Figure 5.10.
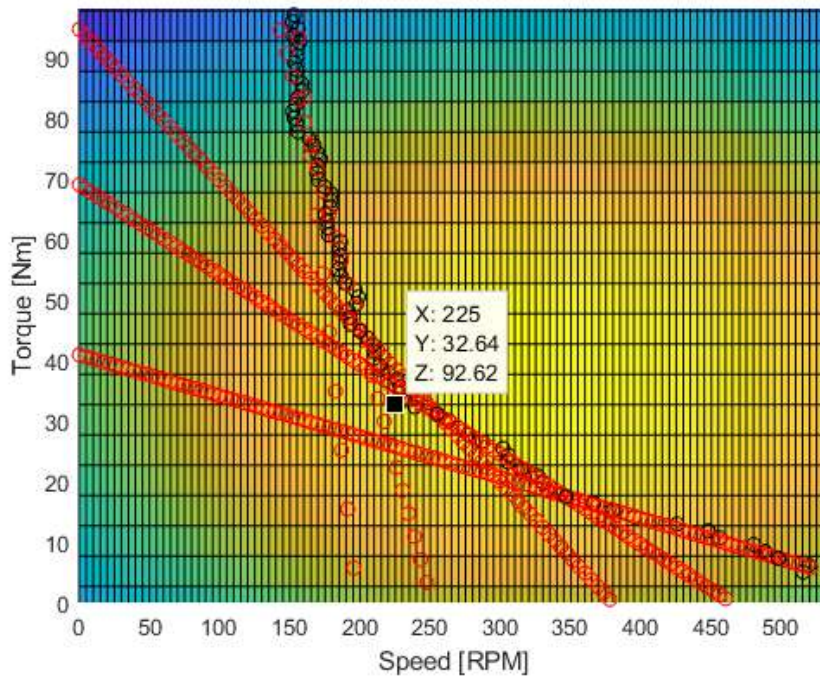
Figure 5.10: Simplified efficiency representation.

Where the hyperboloid coefficients described in Section 4.2 are:

119

Parameter	Value
B_0	92.6
B_1	1.2859e-4
B_2	0.0011
x_c	225
y_c	32.6

Table 5.3: Paraboloid parameters.

Now that all parameters required by the test bench have been explained, the implications of a real implementation are aborded in the next section. This implication refers to the error quantification of processes related to sensors, actuators, and any difference between the electric devices (motor, inverter) and their theoretical representations.

5.2.5 Error quantification

The error quantification covers two aspects. First, the measurement error caused by the resolution of the used sensors and the interaction with the ADC of the DSpace 1104 board. Second, the actuator (the BLDC motor) error caused by the acceleration signal modeling (see Section 5.2.3) and the interaction between the motor inverter and the DSpace 1104 board DAC.

The sensor used in the platform and their resolution are mentioned in Table 5.1. This current and voltage sensors have an RMS error of 0.12 and 0.02 respectively in comparison with the values reported by the variable charge. These error results are reported from the DSpace board, then it includes the ADC resolution effect. Additional to the sensor resolution, the acceleration signal model has an RMS error of 0.4 reported from ControlDesk too, then it includes the DAC resolution effect. All errors mentioned before added to any underestimated characteristic of the model decrease the capability to control the motor in an open-loop approach. The most sensible speed profile to this error effect is the WLTC class 2 with an augmentation 25% of the amount of energy estimated per kilometer. By another way, the less sensible is the NREL class 3 speed profile with an augmentation of 16% of the amount of energy per kilometer estimated. This difference of sensitivity between the different speed profiles is caused by the sensor and actuators error, the differences between the electrical devices and their theoretical models and by the range of speed of each speed profile. In low-speed values, the accelerator error decreases in comparison with medium or high speeds values.

The error presented in this section is one of the most important values to explain the scope of the closed-loop optimal controller results. However, it is required an initial analysis of the effect of those errors over the controller representation capabilities. In order to analyze this effect through a comparison between the theoretical results and the experimental results, the behavior of the energy coefficient variable along open-loop trips is presented in the following section.

5.2.6 Speed and energy coefficient.

The efficiency function was presented in Section 5.2.4. In that section, the simulated efficiency function is verified with two tests: a maximum torque test (rotor blocking) and measurement test along different work points. It is now important to translate this information to the "Energy Coefficient" described in Section 4.4. This coefficient lets to

consider the amount of energy in the battery in comparison with the amount of distance desired to make a more strict or more relaxed optimization.

The first test made in this section is an energy coefficient estimation along a speed signal in stairs shape. This test lets to explore the energy coefficient in different speed values in order to confirm the efficiency function proposed in Section 5.2.4 and also present the minimum energy coefficient that the controller platform is able to obtain in constant speed profiles. As a result of the test, the current, voltage, speed, and power signals shown in Figure 5.11 are obtained.
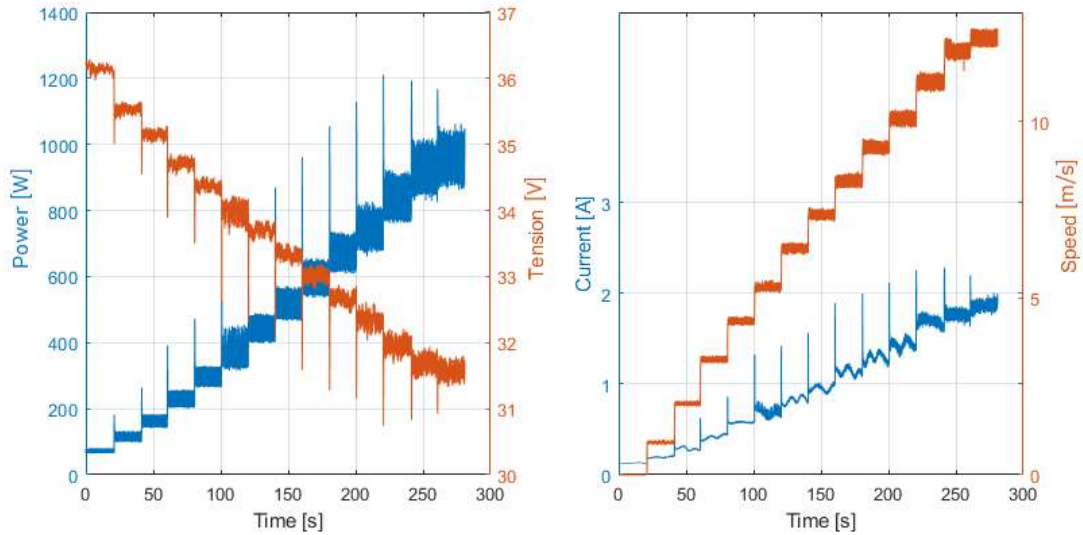
Figure 5.11: Speed vs power.

To analyze the energy used along each step of the speed signal in stairs shape, the power is integrated along the period that corresponds to each step and it is divided by the distance covered. Also, it is important to consider the torque region where the test was made (0-10 Nm), this range of torque was chosen to explore all speed range. As a result, the energy coefficients of Table 5.4 are obtained.

Speed [m/s]	Energy Coef. [Ws/m]
1	124.7
2	80.1
3	70.2
4	68.1
5	68.3
6	69.2
7	70.2
8	71.4
9	73.7
10	74.4
11	76.0
12	77.6

Table 5.4: Energy coefficient along constant speed profile

121

As a conclusion of this test, the most efficient speed in this torque region is around 4.5m/s which can be translated to 204.6 RPM. Then, the efficiency representation has an acceptable error in comparison to the test bench.

Now that complete efficiency function and parameters are determined, an "Open-loop" test can be made. This test consists in making a speed profile optimization along different β_2 values in order to understand the best performance of the controller. This test is made without any additional perturbance (only the sensor and actuator disturbs inherent to the test bench) and the speed profile estimations are ensured to prevent a disturbance that the controller is not able to correct in an open-loop approach.

β_2 []	Rural				Urban			
	Class 6	Class 3	Class 2	Class 1	Class 6	Class 3	Class 2	Class 1
0	79.11	85.28	66.92	70.65	74.68	140.51	74.15	74.69
0.25	68.3	65.59	64.12	66.37	67.26	65.77	65.53	66.34
0.5	66.83	65.35	63.06	64.82	64.1	64.55	64.22	65.31
0.75	65.78	64.45	62.69	62.83	63.36	64.19	64.47	64.91
1	65.3	63.45	61.94	63.15	62.89	63.75	63.48	64.34
1.25	65.14	63.27	62.25	61.81	62.6	63.37	63.6	64.01
1.5	65.22	63.26	61.74	62.09	62.49	63.38	63.15	64.03
1.75	64.69	63.19	61.64	62.1	62.41	63.12	63.21	63.73
2	64.55	62.79	61.74	62.27	62.32	63.03	63.05	63.23

Table 5.5: Energy coefficient along each speed profile

Finally, the result of this test is presented in Table 5.5. As a result, it can be highlighted that in all cases, the augmentation of β_2 ensures the reduction of the energy coefficient. On average, autonomy augmentation is about 20%. This result is lower than the results obtained in simulation but it still being relevant in the electric vehicles field. The reduction of autonomy optimization can be caused by four reasons:

- The motor power is lower in test bench than the motor considered in simulations. It causes the efficiency function to be different.

- The representation of slope profile and aerodynamic force is made with a variable load connected to the inverter of a BLDC motor of 300W. It means the opposite torque is limited by the time delay of variable charge and maximum power of the brake motor.

- The torque estimator does not consider the brake motor model. The torque required along the travel is obtained by a comparison of traction motor friction parameters and traction motor speed obtained in different variable load current values.

- Some elements considered in the simulation that are not considered in test bench as battery losses.

In the following section, the parameters and the range obtained in this section are considered to present a closed-loop approach of the optimal controller.

5.3   Closed-Loop control experimental results

Now that all elements required to make a real implementation have been presented, it is important to explain the test required by the closed-loop controller. In order to be consistent, the test proposed in the following section will be close to the test proposed in simulations presented in sections before, it means that the test aims:

- Exploration of autonomy expected and a comparison with the autonomy obtained with speed and position states feedback.

- Comparison between the autonomy expected with the autonomy obtained into a specific case where the energy state is feedback.

- Analysis of how the speed profile estimator affects the control signal. Since the speed profile estimator has a 28% chance to misunderstand the speed profile, this error causes an initial energy estimation error that has to be corrected by the closed-loop controller. The optimization results have to consider the worst-case to offer a realistic comprehension of the controller capabilities.

5.3.1   Speed and distance states feedback.

As it was shown in Section 4.5.1, each speed profile has its scope to be optimized according to its mean speed, number of stops, and the road characteristics. Since the road characteristics are the same for each test, only the speed profile characteristics are evaluated as a parameter to show the optimization scope.

In order to show the range of distances that can be covered by the same speed profile along different β_2 values, the speed profile estimation is not taken into account. This test lets to observe the optimization scope for different speed profile characteristics. The results of the test are shown in Figure 5.12.
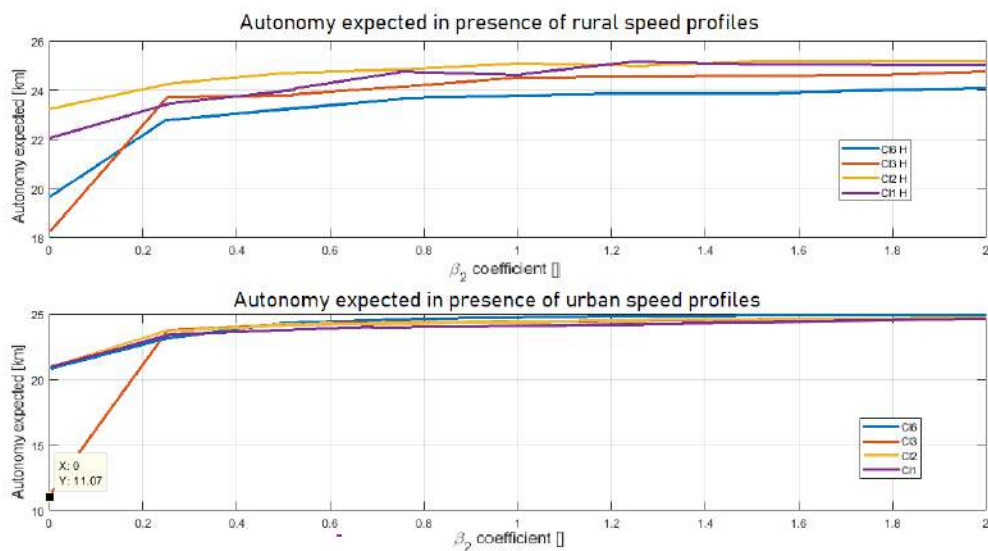
Figure 5.12: Autonomy comparison.

In the test bench results, the autonomy estimation obtained is reduced (from 30% to 20% in average) due to the reasons exposed in Section 5.2.6. In the test bench, the energy

coefficient had a similar behavior that the behavior expected by Figure 4.17, but with remarkable differences on autonomy expected. While all the speed profiles present similar autonomy values in presence of low β_2 values, the speed profile "Class 3" shows to be the most battery consuming speed profile, not the "Class 6" as the simulations show. Also, the most promising speed profiles category to improve the autonomy are the rural ones and not the urban ones. Both differences are caused by the power of the BLDC motor used and the efficiency function estimated. The smaller BLDC motor has a smaller speed range. It causes that even when the speed profiles are normalized to be coherent between both experiments, the efficiency function has a different behavior causing that the number of stops, and the lower speed values are more efficient than in bigger BLDC motor. At the same time, there are remarkable similarities too. autonomy optimization ranges are still being coherent between both experiments. The autonomy incrementation from the minimum to the maximum value of β_2 is around 20% (in the simulation experiment was 30%) except by the "NREL Class 3" speed profile in its urban and rural approach. In both cases (simulation and test bench), the autonomy augmentation reported by the "Class 3" speed profile is higher than 30% due to the stoped time present in each speed profile. Those results confirm the simulation results obtained in Section 4.5.1.

The main propose of the controller is to ensure the distance required by the driver in different initial conditions. For these reasons, the following sections will explore the dynamic of energy estate and how the beta values can correct misestimations made by the speed profile estimator.

5.3.2 Energy state feedback.

In this test, the energy state is feedback to the controller in order to correct the energy coefficient throgh the β_2 parameter. However, as in Section 4.5.2, the SoC and the amount of distance required by the driver are chossen to force the controller to work around a desired β_2 value. Also the distance required in the maximum β_2 value is 90% of the distance expected due to the signal error. It creates a disturb that the controller is not able to correct since it already uses the maximum β_2 value. The results of the test are shown in Table 5.6.

	Maximum $\beta_2 \rightarrow \beta_{2_{maxA}}$			
SoC [%]	Value expected by estimator [km]	Reference value [km]	Obtained value [km]	Distance error [%]
100	79.70	71.73	71.05	0.95
50	39.84	35.86	35.48	1.06
20	15.93	14.34	14.07	1.92
	Middle $\beta_2 \rightarrow \beta_{2_{maxNA}}$			
SoC [%]	Value expected by estimator [km]	Reference value [km]	Obtained value [km]	Distance error [%]
100	70.5	70.5	70.61	0.16
50	35.25	35.25	35.25	0.54
20	14.1	14.1	14.08	0.09
	Minimum $\beta_2 \rightarrow \beta_{2_{min}}$			
SoC [%]	Value expected by estimator [km]	Reference value [km]	Obtained value [km]	Distance error [%]
100	60.7	60.7	64.07	5.49
50	30.36	30.36	32	5.4
20	12.1	12.14	12.24	0.8

Table 5.6: Distance error results in Closed-Loop.

In all cases, the controller was able to complete the travel with a distance error lower than the 5.5%. Also, the minimum and maximum of β_2 values present the biggest error. This result is logical due to the range of β_2 value required to control the energy coefficient signal. When the error overcomes 2% the autonomy achieved was superior to the autonomy required due to the energy coefficient control algorithm behavior (see Section 4.5.2). It means that the control can ensure to the driver 98% of probability to complete the travel when the speed profile was well estimated. The optimization speed profile signal still being similar to the signal presented in Figure 4.19, it means that the optimal controller avoids the highest and the lowest speed values with a priority of lowest values according to the efficiency function represented in Section 5.2.4. Also, the speed signal required by the driver and the speed profile proposed by the controller has a high correlation keeping sensitive to the driver requirements. In order to discuss the specific case presented in Table 5.6, the optimal controller was able to increase 16.1% the autonomy when the initial SoC was 50% and the speed profile used was the "Class 6" urban speed profile. Also, the resultant speed profile had a correlation of 0.87 with the initial speed profile proposed, ensuring to the driver to keep the control feeling over the speed value but also to complete the travel with 0.54% of error. In conclusion, the optimal controller is able to ensure an autonomy optimization, and an energy control able to increase the certainty to finish the trip without decrease dramatically the driver control feeling over the speed variable along the travel.

The results presented are assuming a good speed profile estimation. For this reason, the following section explores the effect of speed profile estimation error and how it affects the probability to complete the travel.

5.3.3 Speed profile estimator error effect.

The speed profile estimator described in Section 4.4.1 lets to obtain an estimation of the speed profile proposed by the driver using only the data available in a longitudinal movement model. However, as it is mentioned in the same section, the error of estimation when the amount of data is less than 120 seconds is about 72%, and if the measurable period is extended to 500 seconds the precision increases to 88%. This estimation is based on speed and acceleration range to detect urban or rural behaviors and tries to estimate the amount of energy required to achieve each kilometer along the travel. The estimation result can be classified as correct if the correct speed profile and its approach (rural or urban) are well estimated. Following this idea, in Figure 5.13 and Figure 5.14, two cases of a correct estimation are shown through the β_2 signal behavior and its effect in the autonomy estimated along the travel. In case A, the speed profile estimated and used are the "Class 3 urban", the initial SoC is 100% and the amount of distance required is 70.5 km. In this case, the estimation is correct but due to the error caused by the magnitude of the disturbance in comparison to the speed signal, the β_2 value has to correct the energy coefficient to demand the correct energy coefficient and reduce the distance error to 0.82%. However, the magnitude of the disturbance in some cases is small enough to avoid requiring a β_2 value correction. An example of this case is shown in Figure 5.14. The speed profile estimated and used is the same but the initial SoC is 20% and the distance required is 14.1 km. In this case, the distance error is about 0.18%.
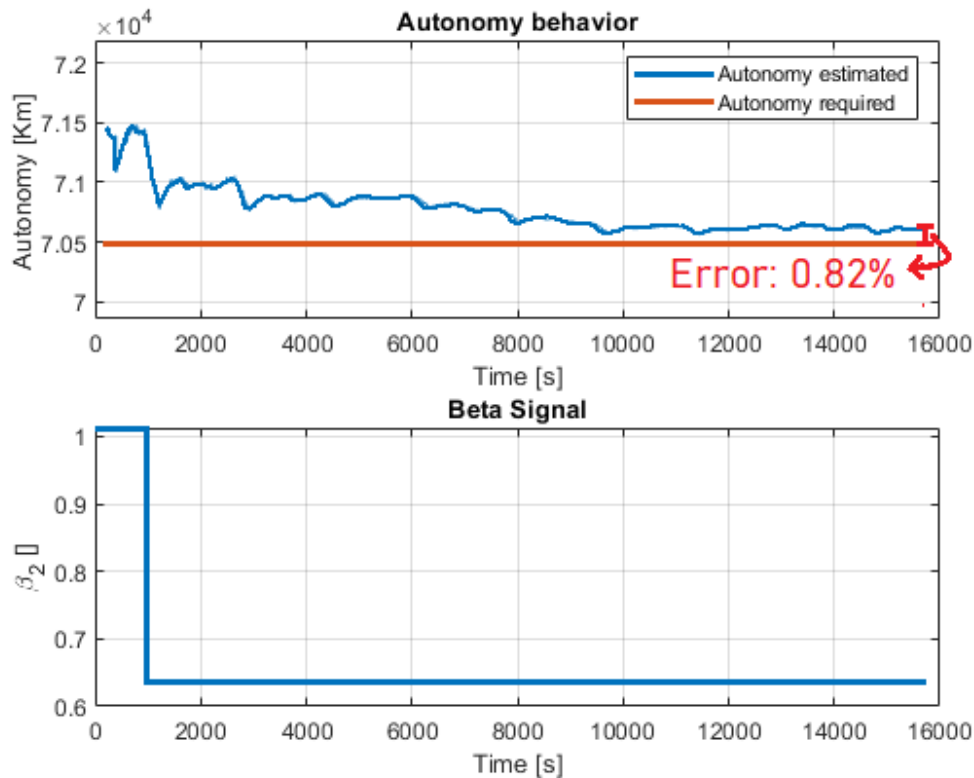
Figure 5.13: Good estimation case A.
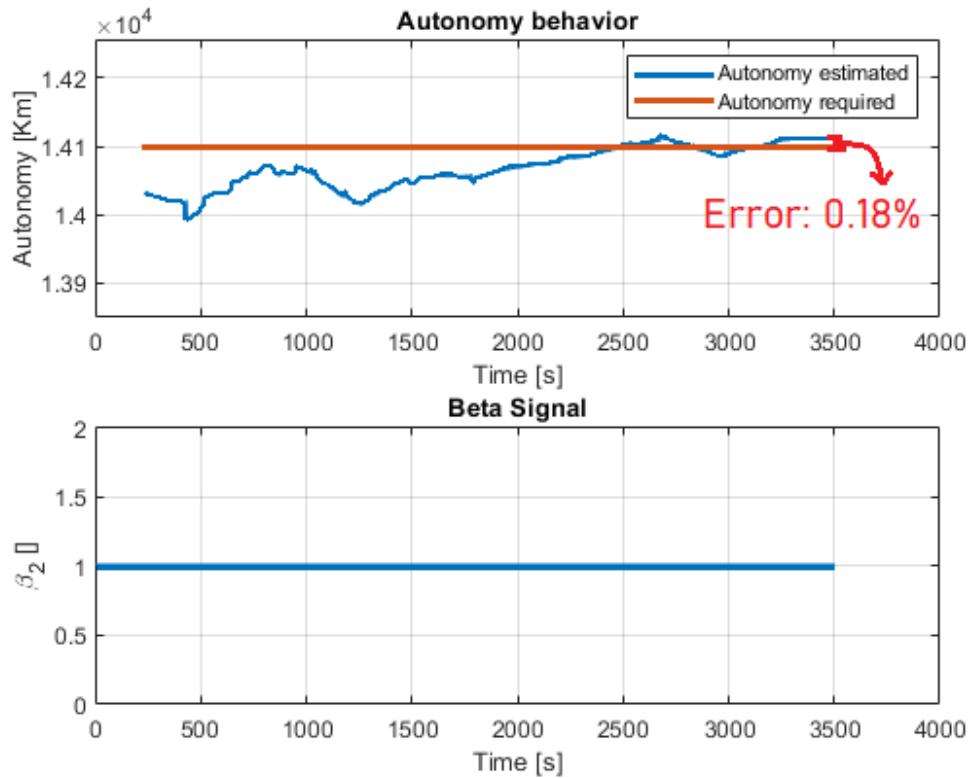
Figure 5.14: Good estimation case B.

As a conclusion of this first case analysis, a correct speed estimation aims to reduce the distance error but there is a strong percentage of the error caused by the random behavior of the disturbances in comparison to the speed values.

Between a correct and an incorrect classification exists a medium category, it will be called (poor estimation). When the speed profile is not well estimated but its approach (rural or urban) is well estimated, the consequence is an energy coefficient error small enough to be managed by the proportional energy controller with some time delays. The results of these cases are shown in Figure 5.15.
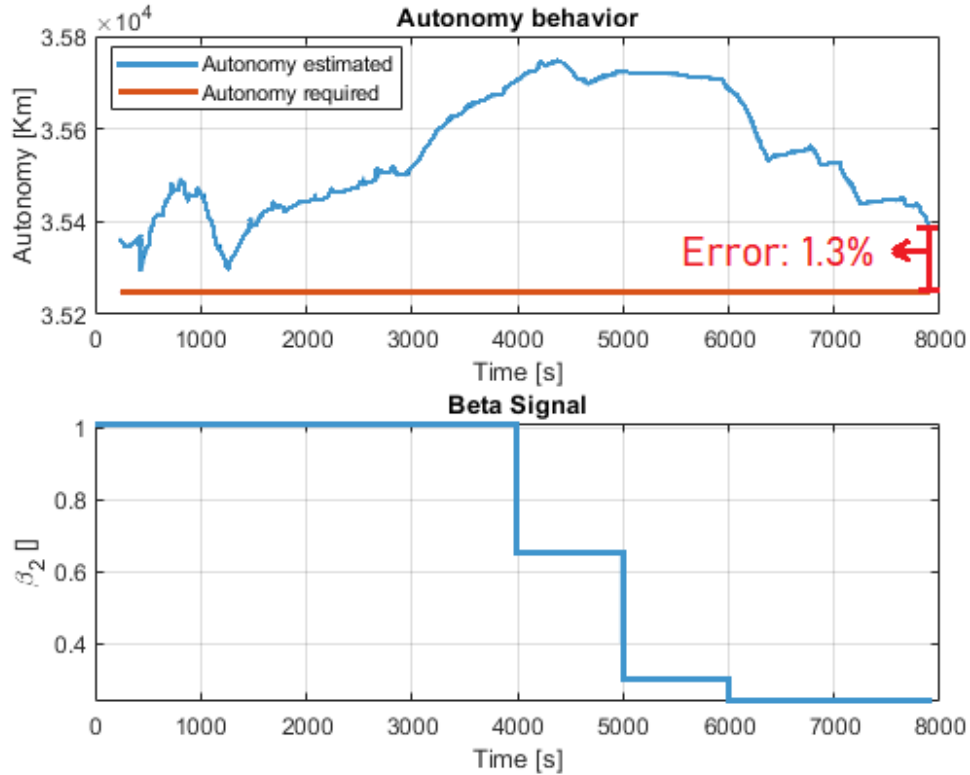
Figure 5.15: Correct urban/rural estimation.

In this case, the initial SoC is 50% and the distance required is 35.25 km. The error caused by the wrong speed profile estimation causes an error that the controller correct but due to the huge difference of sample time, the control signal is slow. However, in those cases, the distance error keeps around 1.3%. This final distance error depends on two factors:

- The amount of distance due to when the distance is bigger, there is more time to make the energy correction with the slow control signal.

- The speed profile misunderstood. Since the rural/urban approach was well estimated, the speed profile estimated has small differences with the speed profile really used in most cases. However, there are specific cases where the difference is big enough to be considered a complete wrong estimation and to be classified as the next case.

When the speed profile and the urban/rural approach are misunderstood or the speed profile estimated has a big enough energy coefficient in comparison with the real one, a "complete wrong estimation" is obtained. This case is presented in Figure 5.16 and as it can be seen, the control signal saturates itself to reduce as possible the energy coefficient error. If the amount of distance required is small, the error can be around 4% but with enough time, the error is reduced even to 2.12% (as in the presented example). In these cases, the control signal increases to the maximum speed variable restrictions, making a trip with a behavior closer to the autonomous experience than a driver-controlled experience. Additionally, the distance error is negative, it means the vehicle is not able to finish the trip.
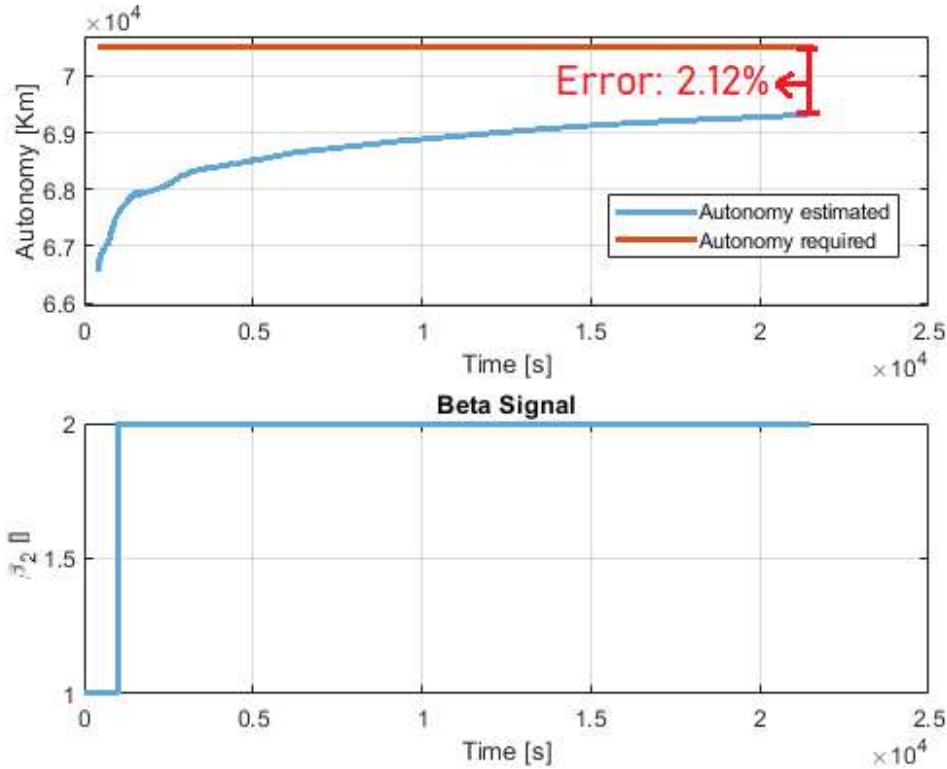
Figure 5.16: Bad speed profile estimation.

The probability to face this scenario with a meassurable period of 120 seconds is about 20%. That means the probability to complete the travel with a distance error lower than 1.5% decrease from 98% to 78.4%. For this reason, an additional estimation tool is implemented. Since the biggest effect over the control signal is caused by the misestimation of the rural/urban approach, when the energy coefficient estimated and measured has an error bigger than 10 [Ws/m], the rural/urban approach estimation is remplaced by the hipotetical rural/urban approach obtained from the road category used (highway, urban road... etc.). This solution brings a "complete wrong estimation" to the classification of "poor estimation" where the distance error is around 1.3% and the error is positive (It means the trip is completed with a remain energy in the battery).

As a conclusion of this section, an additional estimation tool was required to ensure the high probability to complete the travel. However, this tool aims to keep the 100% cases in the classification of "Good estimation" or "poor estimation" where the distance error is positive and its magnitude is around 1.3%. In this reseach, the speed estimation was limited by the longitudinal information of the model but, in a future work implementation those restriction can be overcame by a speed profile estimator based in a lateral and longitudinal model. This approach would improve the effectivity of the optimal controller.

5.4   Conclusions:

The test bench presented in this section lets to make a scale test able to make the representation of the energy consumption process in an electric vehicle when different speed profiles and external conditions are presented. In order to make accurate control, the error sources are presented and quantify to verify its effect over the results expected by

simulations. After the error quantification process, the mathematical model presented in Chapter 3 was adapted to consider the characteristics of a reduced scale electric vehicle. Those considerations cover the limitations of a 1200W BLDC motor with an inverter of 25A.

The implementation presented was able to conclude that in realistic conditions, the online optimal control can be implemented with certain optimal configurations well adapted to real-time operation. The average compilation time of the experimental version optimal control did not increase in comparison with the simulated version due to the real-time orientation of the Simulink algorithm make from the beginning.

Even when the speed profile estimator has a 72% of reliability, the supplemental information about the rural/urban component of the speed profile obtained from the historical data was enough to ensure a 98% of probability to complete the travel with different initial SoC or driver behaviors. The difference between the final distance required and the final distance reported lower than 1.5% of the final distance required. Also, due to the proportional energy control behavior, in the 98% of cases, the distance error is positive, it means that the distance covered is always higher than the distance required by the driver. Finally, the most strict limitation over the speed profile lets to obtain an autonomy gain of about 20%.

In the next chapter, the main conclusions of this research work will be discussed to emphasize the relevant results and to present the best subjects to be considered as future work subject related to of this research work.

Chapter 6

Conclusions and future work

The aim of the research presented is to develop a non-linear optimal controller tested in a test bench specially designed to obtain a longitudinal movement representation of the energy consumption for a desired trip. The optimal controller is able to increase the probability to complete a trip with a limited amount of energy and the most dynamic driving behavior to 98% with a distance error lower than 1.5%. It also ensures that error means remaining energy in the battery and not an additional distance to cover. It is possible, thanks to an energy control made through an online limitation of dynamic driving behavior as much as it is required to ensure an "energy coefficient" small enough to achieve the goal of completing the travel. The variable called "energy coefficient" contains the average amount of energy required to cover one meter along the trip covered. This measurement is used as a reference to build the control signal which is the variable β_2, it represents the grade of strictness required by the balance contemplated in the optimal controller between efficiency and vehicle performance. The optimal controller technique used was an NMPC, it required the incorporation of three main dynamic models which represent the traction chain: The mechanical model, the electrical model, and the thermal model. Those models are required to represent the most representative elements of the power chain: The battery, the inverter, and the motor. Once three models of the three elements have been studied, they have to be adapted for an online optimization approach. The adaptation includes making mathematical simplifications of the most complex models in order to ensure an accurate optimization. The most time-consuming model is the motor efficiency function, then a geometrical representation is proposed as a simplified representation to ensure an accurate optimization. It means to build a function able to guide an optimization as fast as possible (the minimum and maximum of the representation are placed in the same location of the real function).

The comprehension and the implementation of those models require an estimation step where the speed profile used by the driver is estimated based on the information available in the mechanical model already mentioned. The estimation algorithm was a Fuzzy Logic able to obtain a 72% of exact estimation based on a measure with a sample time lower than 120 seconds. The mechanical model used was a longitudinal model. In order to increase the exactitude of the estimator, when the energy coefficient estimated differs from the measured more than 10 [Ws/m], the speed profile approach (rural or urban) is replaced by the estimation made by the historical data of the road that is covered in that exact moment. As a result, the final estimation obtains a 72% of probability to make a correct estimation of the speed profile approach and its urban/rural classification and, a 28% to make a correct estimation of the urban/rural classification even if the speed profile is not the correct one. The energy coefficient error caused by this wrong estimation is

small enough to be corrected by the energy control.

When the speed profile is well estimated, the optimal controller lets not only to increase the probability to complete in a successful way the trip but also to increase the autonomy of the vehicle around a 20%. This incrementation is possible, thanks to the efficiency function implementation in the optimal controller and its interaction with the driver's behavior. In future work, this interaction has to be developed more deeply to give importance to driver awareness over the energy used.

This research opens the possibility of future works on different topics. First of all, the implementation of the optimal control can be explored in two senses: One, the speed profile estimator should be upgraded to do not be limited by the longitudinal mechanical model data. If the longitudinal and lateral mechanical data are used, the speed profile estimator would be able to increase its accuracy without additional estimation cases. Two, the amount of data taken into account by the optimal controller should be increased, because even if the current optimal controller takes into account the weather (for example), a higher trajectory segmentation based on weather conditions, the relationship between the vehicle direction and the wind direction or the slope can increase the resolution of the optimization and as a result, to decrease the amount of energy required. This implementation would require a complete study of the algorithms implementation methodology available in comparison with the computational power available in a vehicle. Also, The new data taken into account could cover a hybrid energy source. In that case, the degrees of freedom would increase and a new horizon in the energy optimization could be explored. The hybridization of the energy source can cover a large list of possibilities, from gas to super-capacitors or hydrogen. For this reason, this subject is a deeper optimization that can include not only energy optimization but also the minimization of the price of the energy used. The energy control is a new subject that starts to call the attention of big vehicle brands, not only for the economical optimization but also because this energy management is able to open two new research subjects: the energy control in autonomous vehicles and their interaction not only between them but also between them and the network. First subject research refers to the affirmation made in Section 4, the beta coefficient that represents the balance between energy efficiency and the speed tracking has limitations due to the driver interaction. In other words, the scope of the results obtained by this research can be increased if an environment with autonomous vehicles can be ensured. The second subject refers to the capacity of the vehicles to be used as energy transportation. The control of energy consumption creates the possibility to ensure interaction between vehicles or between the vehicles and the network to ensure an optimal distribution of the energy as an innovative answer to the increasing energy demand. It would be possible to increase the autonomy of a vehicle taking into account not only the energy level of a particular vehicle but taking into account the energy level of the vehicles around the vehicle.

Finally, it is important to mention that this research is important and relevant not only for electric vehicles but for energy control over any kind of vehicle. If the interaction between the driver and the optimal control can be eliminated (like in an autonomous vehicle environment) the range of β_2 values increases and as a consequence, the distance error, the energy control, and even the autonomy optimization can be extended. I hope this algorithm could be a useful tool to ensure a sustainable grow up of the transport industry in the coming years.

Chapter 7

French summary - Résumé français

7.1   Introduction:

Face aux enjeux environnementaux, l'émergence des véhicules électriques VEs s'est considérablement accentuée ces dernières années. En effet, le progrès et l'intégration de nouvelles technologies ainsi qu'une politique incitatrice ont permis de réduire suffisamment le coût de ce type de véhicule pour en faire un produit rentable et accessible au grand public en considérant le coût global de possession du véhicule. Même si la Chine comptabilise 57% de clients, des pays comme la Colombie affichent actuellement une croissance de 88% en VE par rapport au marché des ventes en 2015. Cet engouement pour le VE lié à la prise de conscience des consommateurs aux problématiques environnementales ainsi que la variation du pétrole et la dépendance qui en découle, a permis d'accroître leur présence sur le marché latino-américain. Cependant, dans des pays comme (EE.UU) ou le comportement du prix du pétrole est relativement plus stable, les VEs n'ont pas encore réussi à percer pour augmenter leur présence, on peut le voir avec la croissance limitée de 2,5% en 2012 à 4,0% en 2017. Les limites des VEs comme le manque d'autonomie, le manque de bornes de recharge ou le prix sont encore des freins suffisants pour que les clients ignorent les avantages de cette technologie mais cela n'est pas tout à fait vrai. De nombreux travaux scientifiques ont déterminé que les VE couvrent déjà les 90% des déplacements effectués par un utilisateur moyen en une journée. Parmi eux des études qui proposent un environnement virtuel assez réaliste, offrant aux utilisateurs la possibilité de déterminer l'énergie réelle nécessaire pour couvrir leurs fonction coûts. Ces limitations de VE ne reflètent pas la totalité des contraintes lié à son intégration, notamment celles de l'usage. En effet, l'utilisateur manifeste souvent une incertitude ou une crainte liée à sa capacité à couvrir un trajet donné. En plus, ce phénomène est d'autant plus contraignant pour les gammes de voitures les moins puissantes. Autrement dit, il est inversement proportionnel à la taille de la batterie du véhicule. Dans ce contexte, les véhicules électriques les plus vendus (moyens et petits) sont les plus touchés par ce phénomène d'incertitude d'autonomie qui impacte et perturbe grandement l'usage et la satisfaction des utilisateurs. Ces travaux de thèse s'inscrivent dans le cadre de cette problématique, dans le but d'apporter une solution originale et pertinente pour les véhicules électriques à deux roues (TWEV) comme les motos ou les vélos, qui restent une des catégories les plus touchées par ce phénomène.

La réduction de l'incertitude d'autonomie constitue un outil puissant pour accompagner l'intégration et l'émergence des TWEV, maillon désormais indispensable de la nouvelle mobilité.

Afin de contribuer à renforcer la confiance des consommateurs dans l'autonomie offerte

par les TWEV, tout en maîtrisant les prix de cette technologie, la principale contribution de ces travaux consiste à développer une méthodologie et un outil capables de déterminer automatiquement les conditions optimales de la trajectoire (couple et vitesse) requises par le véhicule, dans le but de minimiser la consommation d'énergie, en considérant à la fois, les contraintes liées aux conditions externes (météo, trafic, poids du conducteur) et internes (état de charge, efficacité énergétique, limites électriques et thermiques). L'outil nécessitera idéalement (dans sa version la plus performante) des informations et des caractéristiques issues de trois niveaux: le véhicule, le GPS avec accès internet et le conducteur. Les principales informations récupérées du véhicule sont le signal de freinage/accélérateur, des constantes (dimensions, coefficient de traînée, ...) ainsi que les caractéristiques électriques de la chaine de traction (couple, vitesse, puissance, courant, . . .). Le GPS permet de connaitre l'altitude, le trafic, les conditions météorologiques . . . Le conducteur quant à lui, sera en charge d'ajouter des informations variables pour orienter l'optimisation, telles que la masse totale du véhicule, la fonction coût... etc. Il existe de nombreux aspects multi-physiques qui peuvent améliorer l'efficacité énergétique d'une TWEV, allant de l'étape de pré-dimensionnement jusqu'à l'étape d'intégration (aspect système). Nos travaux se positionnent clairement dans l'étape d'intégration, et visent à proposer un outil transverse qui peut s'appliquer facilement sur des chaines de tractions existantes, dont le principe est illustré dans la figure 7.1.
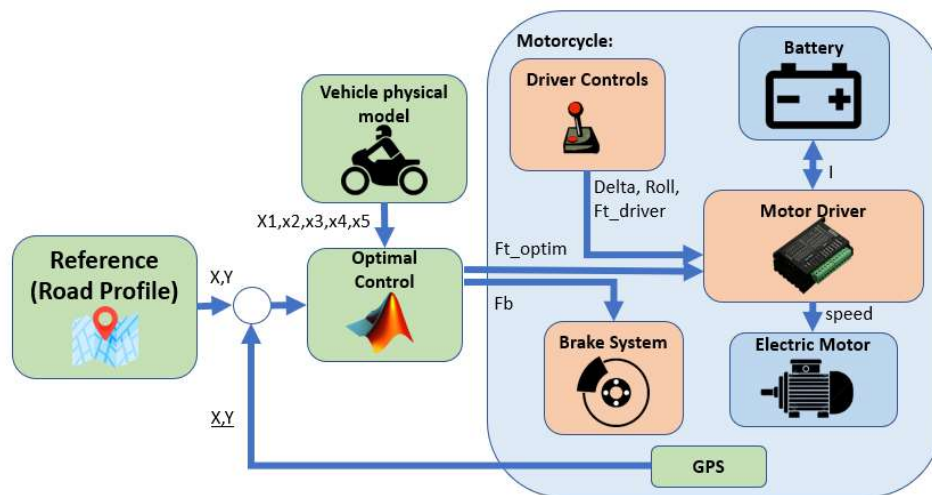
Figure 7.1: Schéma de principe d'une chaine de traction électrique intégrée dans une stratégie de pilotage global.

7.2   État de l'art:

Cette partie expose toutes les connaissances nécessaires à la compréhension de la problématique traitée et explore en même temps les différentes possibilités d'amélioration, en vue du développement de notre outil. Les points explorés sont:

- Modélisation du TWEV: Le VE nécessite souvent une modélisation multi-physique qui nous a permis d'identifier le niveau de finesse requis des modèles et de choisir la technique de commande, compatible avec notre optimisation énergétique temps réel.

- Technique de contrôle-commande de vitesse : cette section analyse les techniques les plus utilisées en contrôle de vitesse /couple appliquées aux chaines de traction VE. L'objectif est de déterminer les exigences à considérer dans le cadre d'une stratégie énergétique.

- Conditions/perturbations externes: cette section étudie les exigences à considérer pour tenir compte dans la modélisation et l'outil à développer, des perturbations externes comme la météo, l'état de la route, les caractéristiques du conteur ... etc.

- Optimiseurs d'autonomie: cette partie analyse les approches existantes en vue de proposer une solution innovante suivant les exigences déjà identifiées.

- Défis des véhicules électriques et verrous scientifiques : en ce basant sur les études précédentes, cette section vise à proposer une démarche innovante et un position-nement au sein de la communauté scientifique.

Les TWEV sont devenus une solution indispensable de la nouvelle mobilité grâce aux pro-grès constatés dans les constituants de la chaine de traction avec une efficacité énergétique qui ne cesse d'augmenter. Mais la gestion globale, en considérant les pertes d'énergie et les couts associés, reste un des principaux défis de cette technologie. Même lorsque des techniques de charge plus rapides ou des sources d'énergie hybrides sont proposées afin de réduire le temps de charge et la variation d'autonomie, la quantité d'énergie embarquée reste toutefois toujours limitée. Par conséquent, la capacité d'un superviseur à gérer la consommation d'énergie, en considérant les contraintes externes et internes permettra aux TWEV de se positionner comme une des solutions écologiques de la nouvelle mobilité, qui associe également le confort et la sécurité. Pour cette raison, le MPC (Model predic-tive control) basé sur le concept de la commande prédictive est choisi dans le cadre de ces travaux, pour les possibilités offertes dans l'optimisation énergétique sous contraintes. Même lorsque le MPC a certaines limites, en particulier la capacité d'implémentation, de nombreuses variantes, liées à l'aspect évolutif, ont été proposées dans la littérature pour surmonter cette limitation. Dans la partie suivante, la modélisation multi-physique (élec-trique, mécanique et thermique) nécessaire à la synthèse de l'algorithme d'optimisation en ligne (temps réel) est présentée.

7.3 Modélisation

Ce chapitre reprend l'état de l'art pour mettre en évidence les exigences du modèle mathé-matique et proposer une représentation énergétique dynamique. Sur la base de ces modèles et de leurs exigences, des adaptations aux exigences du problème traité sont proposées. Le principe de la modélisation multi-physique considérée est présenté dans la figure 7.2. Où le $P_e(\tau, \omega)$ est la puissance estimée basée sur le couple et la vitesse calculés par le modèle longitudinal, le $P_l(\tau, \omega, {}^\circ C)$, $P_r(\tau, \omega, {}^\circ C)$ sont les pertes et la puissance demandée en fonction du couple et de la vitesse calculés par le modèle longitudinal mais aussi de la température, $R_i({}^\circ C)$ est la valeur de l'élément résistif en fonction de la température et $C_b({}^\circ C)$ est la capacité de la batterie en fonction de la température. Les sujets spécifiques explorés sont:

- Modèle électrique: Le modèle électrique des composants est présenté comme la prin-cipale information requise pour obtenir un modèle du véhicule électrique. Comme l'objectif de notre problème de recherche est lié à l'optimisation de l'autonomie, le
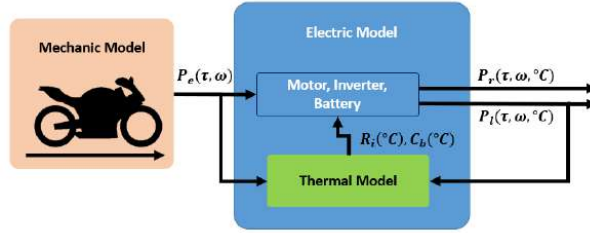
Figure 7.2: Principe de la modélisation multi-physique considérée.

modèle électrique est orienté pour représenter la dynamique des pertes d'énergie de la chaîne de puissance, comment les prévoir et les simuler dans un processus temps réel.

- Modèle thermique: Le modèle électrique nécessite une caractérisation basée sur la température à l'intérieur et à l'extérieur des composants électriques. Pour cette raison, un modèle thermique est nécessaire pour effectuer l'ajustement automatiquement sans diminuer les performances en temps réel du modèle électrique.

- Modèle mécanique: La distribution mécanique des éléments électriques et les considérations mécaniques longitudinales ou latérales du mouvement de la moto déterminent la manière dont le comportement énergétique est calculé. Ensuite, cette section présente les considérations mécaniques liées à l'estimation de l'énergie et comment elles affectent le modèle électrique.

La dynamique requise par l'optimiseur d'autonomie est étroitement liée à celle des pertes de la chaîne de traction (batterie, convertisseur électronique de puissance et machine électrique). Les pertes dans les principaux composants de la chaîne de traction ont été décrites sous trois aspects: modèle électrique, modèle thermique et modèle mécanique. Les pertes électriques du moteur sont complexes à calculer en temps réel, c'est pourquoi un mappage géométrique a été considéré permettant d'introduire un modèle équivalent simplifié bien adapté à un processus d'optimisation. Pour ce qui est des pertes batterie/onduleur, qui dépendent principalement du courant, aucune représentation supplémentaire n'est requise.

Le comportement dynamique thermique a été représenté par un réseau Foster sur chaque constituant (moteur, batterie et onduleur) mais avec différentes finesses de modélisation pour limiter et maîtriser le temps de calcul. Seuls la batterie et l'onduleur ont bénéficié d'un modèle fin. Afin de représenter la dynamique thermique du moteur et de créer un modèle compatible avec l'optimisation temps réel, différentes cartographies d'efficacité énergétique ont été utilisées.

Enfin, le modèle mécanique a été discuté. La dynamique latérale n'est pas requise pour représenter l'état énergétique du véhicule. Seul le modèle longitudinal est considéré pour cette représentation énergétique permettant ainsi de réduire le temps de calcul.

Dans les sections suivantes, un contrôleur optimal est proposé. En outre, la façon dont chaque modèle sera intégré dans le processus d'optimisation et l'impact de la compilation sur l'algorithme complet seront discutés.

7.4 Algorithme d'optimisation

Afin de réduire l'effet des pertes energetiques mentionné dans la section 7.3, et d'améliorer les performances, un processus d'optimisation est proposé pour couvrir une large gamme de paramètres affectant le système. Ce nouveau paradigme permet de montrer l'impact de différents critères sur le contrôle d'optimisation sous un indice de performance énergétique. Les éléments les plus importants pour aborder l'approche peuvent être divisés en deux catégories. Premièrement, des limites physiques et des pertes de puissance sont introduites sur la fonction coût. Deuxièmement, les pertes résistives sur l'onduleur et la batterie qui sont fortement liées à deux caractéristiques du courant (amplitude et ondulations) sont également considérées. Pour cette raison, ils sont également inclus dans la fonction coût par la limitation de la vitesse et le suivi de la référence de vitesse.

Une fonction coût pondéré est proposée pour explorer l'effet des différents éléments considérés afin de maintenir un équilibre entre l'objectif de terminer la fonction coût et de maintenir le système au point le plus efficace. Le processus de conception de l'algorithme d'optimisation proposé nécessite les composants suivants: le modèle dynamique, les états et les contraintes de contrôle, les conditions aux limites et la fonction coût.

7.4.1 Modéle Dynamique

L'EV est modélisé comme un corps massique dans un axe unidimensionnel. Le mouvement du véhicule est le résultat de la somme des forces appliquées sur la carrosserie et seules les forces longitudinales ont été prises en compte. Le modèle utilisé pour décrire la dynamique du système est:

$$\dot{x_1} = x_2$$
$$\dot{x_2} = \left(\frac{T}{R_w}\right) - F_l)/m \tag{7.1}$$
$$\dot{x_3} = \frac{T}{R_w * Eff(x_2,T)}) * x_2$$

$$F_l = F_{aereo} + F_{roll} + F_w \tag{7.2}$$

Où les états sont: $x = \begin{bmatrix} d & v & e \end{bmatrix}$; $v(t)$ est la vitesse longitudinale du véhicule, $d(t)$ est la distance parcourue et $e(t)$ est l'énergie. L'entrée est: $u = T$; T décrit le couple de traction et le couple de freinage. F_l décrit les entrées non contrôlées (perdues). $Eff(x_2,T)$), représente une abstraction simplifiée du rendement du moteur.

7.4.2 Contraintes d'état et de Contrôle

Comme expliqué précédemment, il existe deux types de contraintes à intégrer dans le processus d'optimisation:

- Les contraintes physiques décrivent celles imposées par les composants sélectionnés en incluant le couple maximum que le système est capable de produire, contraint par l'inéquation ci-dessous:

$$T_{min} \leq T \leq T_{max} \tag{7.3}$$

- Les contraintes de conception décrivent la région possible des états du modèle. Si les états sont en dehors de cette région réalisable, le comportement ne peut pas être reproduit par le véhicule dans un test réel. Elles sont:

$$X_{min} \leq x_1 \leq X_{max} \tag{7.4}$$

$$V_{min} \leq x_2 \leq V_{max} \tag{7.5}$$

$$\int_{t_0}^{t_f} E_{tot_{seg_i}} \partial t \leq E_{tot} \tag{7.6}$$

La contrainte (7.4) limite la région réalisable de x_1 et évite également un comportement suramorti. La contrainte (7.5) est liée à la restriction physique du moteur électrique décrite dans (7.3). Enfin, la contrainte (7.6) est une limitation physique de la quantité d'énergie disponible dans la batterie. Où $E_{tot_{seg_i}}$ est l'énergie développée par le système sur une seule période d'échantillonnage et E_{tot} est l'énergie totale disponible dans la batterie.

Les valeurs minimales et maximales présentées dans les équations de contraintes sont:

Table 7.1: Contraintes d'état et de contrôle.

Paramètre	Valeur	Paramètre	Valeur
V_{min}	0 $[\frac{m}{s}]$	T_{min}	-220 [Nm]
V_{max}	30 $[\frac{m}{s}]$	T_{max}	280 [Nm]
X_{min}	0 [m]		
X_{max}	370 000* [m]		
TotEne	72*45*3600 [Ws]		

7.4.3 Fonction Coût

La fonction coût a été progressivement établie à partir des différents éléments évoqués précédemment:

$$J_0 = \int_0^{t_f} (V_{ref} - x_2(t))^2 \ dt \tag{7.7}$$

$$J_1 = \int_0^{t_f} -Eff_m(x_2(t), T(t)) \ dt \tag{7.8}$$

$$J_2 = \int_0^{t_f} -Q_1 Eff_m(x_2(t), T(t)) + Q_3 \delta T(t)^2 \ dt \tag{7.9}$$

$$J_3 = \int_0^{t_f} -Q_1 Eff_m(x_2(t), T(t)) + Q_2(V_{ref} - x_2(t))^2 \ dt \tag{7.10}$$

$$J_4 = \int_0^{t_f} -Q_1 Eff_m(x_2(t), T(t)) + Q_2(V_{ref} - x_2(t))^2 + Q_3 \delta T(t) \ dt \tag{7.11}$$

Chaque étape considérée dans la construction de la fonction coût a son propre objectif. J_0 est le suiveur de vitesse, il aide à déterminer la valeur du temps final (t_f) et donne la référence de la demande de puissance pendant la trajectoire dans des conditions normales de profil de conduite. J_1 est une fonction purement axée sur les coûts d'efficacité qui permet de maintenir le moteur au maximum d'efficacité sur toute la trajectoire. J_2 étudie l'effet de la pénalisation de la variation du signal d'entrée. J_3 explore l'effet de l'optimisation de l'énergie sur de la limitation de vitesse résultante. Finalement, J_4 conserve l'équilibre entre la vitesse suivie et l'efficacité mais en ajoutant une minimisation d'entrée pour limiter le courant sans limiter la variation de couple.

Les valeurs "Q_i" représentent le poids de chaque pénalisation sur la fonction coût finale. Ces valeurs permettent d'activer et de désactiver différents termes de pénalisation ou

d'orienter la fonction coût pour prendre en compte plusieurs termes mais avec des poids différents.

Afin de comparer toutes les composantes de la fonction coût, la même fonction coût entre Paris et Bruxelles est effectuée. Toutes les contraintes physiques et énergétiques, ainsi que les autres caractéristiques du véhicule, sont obtenues à partir du manuel de la moto électrique "Forest-Litio". Même lorsque les conditions de circulation ne sont pas représentées, le même profil de vitesse mixte (Urbain/Rural) est utilisé dans tous les tests. L'objectif du premier test est d'évaluer les pertes globales du système et le temps nécessaire pour terminer la fonction coût. Ces variables permettent d'analyser l'impact de chaque composante de la fonction coût sur les performances d'optimisation énergétique totale.

Comme on peut le voir dans le tableau 7.2, même si la fonction d'efficacité (J_1) est capable d'augmenter l'autonomie du véhicule par rapport à la fonction coût de suivi de vitesse (J_0), celle-ci est encore négligeable car le critère essaie de maintenir le profil de vitesse dans le point de fonctionnement le plus efficace pour le moteur mais avec une sollicitation forte de puissance des autres constituants. En conséquence, l'amélioration de l'autonomie n'est pas si importante mais le temps de fonction coût est considérablement réduit. Selon l'étude énergétique présentée dans les dernières sections, la limitation d'amplitude de vitesse/couple et la limitation de variation de couple représentent un levier important pour diminuer la puissance requise par le véhicule. Comme prévu, la contrainte de vitesse est liée aux pertes de puissance résistives alors, J_3 est capable d'optimiser ce type de pertes et par conséquent, ses résultats sont plus satisfaisants que ceux de J_2. Cependant, l'optimisation de la variation du signal de couple permet également une augmentation significative de l'autonomie (par rapport à J_1) et permet également d'assurer un profil de conduite adapté aux capacités du moteur et du conducteur. Afin d'explorer l'effet de toutes les composantes de pénalisation présentées dans J_1, J_2 et J_3, le critère J_4 est proposé. Ce dernier améliore considérablement l'autonomie et réduit également le temps de fonction coût tandis que les pertes de puissance sont également réduites par rapport à J_3. En conclusion, même lorsque (J_3) est la fonction coût avec la meilleure autonomie, (J_4) représente le meilleur compromis entre autonomie et temps de trajet et propose un profil de conduite adapté. Si Q_1 et Q_2 présentent un comportement non contraint (entre - ∞ et - ∞) J_3 est une meilleure option car il peut obtenir presque la même puissance et les pertes qui en résultent avec un effet limitée sur la vitesse moyenne du véhicule. Cela signifie que cette valeur (la vitesse moyenne) peut être complètement modifiée par la relation entre Q_1 et Q_2.

Table 7.2: Comparaison des résultats des différentes fonctions coût.

	J0	J1	J2	J3	J4
Autonomie [km]	93.02	94.74	106.25	129.69	122.95
	100%	101.8%	114.2%	139.4%	132.1%
Pertes de l'onduleur	4.3%	2.3%	2.1%	2.0%	1.8%
Pertes du moteur	14.8%	8.5%	6.8%	6.5%	6.4%
Pertes de batterie	9.5%	6.7%	7.6%	6.7%	6.6%
Temps de voyage [h]	11.8	5.3	5.9	7.6	6.7

Dans cette section, les composants requis pour créer un algorithme d'optimisation sont évalués pour identifier le meilleur compromis adapté aux optimisations en ligne. Maintenant, dans les sections suivantes, le problème d'optimisation proposé est implémenté
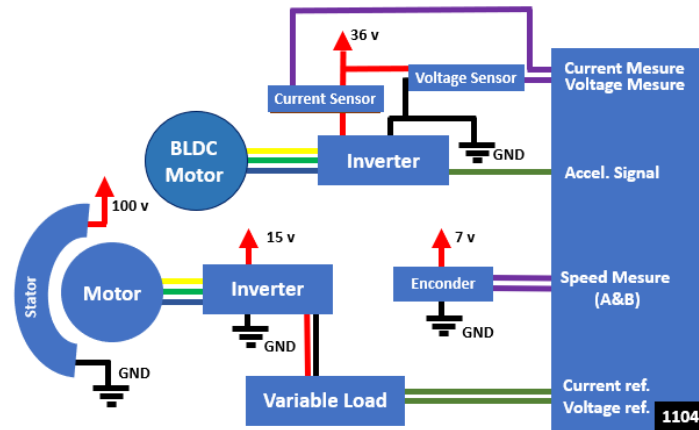
Figure 7.3: Principe du banc de test développé.

dans des algorithmes en boucle ouverte et en boucle fermée pour tester le temps de compilation requis et ses performances dans une plateforme réelle développée à cet effet.

7.5 Validation de l'approche

Ce chapitre présente une comparaison entre les résultats de simulation et ceux obtenus en expérimentation utilisant le banc de test qui a été développé dans le cadre de ces travaux (Figure 7.4). Ce dernier constitue une plateforme à échelle réduite qui utilise, une charge variable et une machine suplementaire pour reproduire un comportement représentatif et évaluer le comportament du contrôleur optimal (Figure 7.3).

En effet, cette section commence par la description du banc d'essai, couvrant l'analyse structurelle requise pour garantir la fonctionnalité du banc, les capteurs nécessaires pour mesurer les états souhaités et les actionneurs pour représenter les forces opposées du mouvement. Après, les modifications apportées à notre algorithme à implémenter selon les limites du logiciel et du matériel du banc d'essai seront présentées. Enfin, deux comparaisons seront effectuées pour montrer la pertinence et l'efficacité de l'approche proposée. D'une part, les résultats obtenus par simulation et expérimentation seront comparés pour conclure de sa véritable portée. Cette comparaison ne comprend que l'approche en boucle fermée de l'algorithme, celle en boucle ouverte est utilisée pour obtenir la caractérisation du moteur BLDC ainsi que la calibration des capteurs et des actionneurs. D'autre part, les résultats obtenus par le contrôleur en boucle fermée dans le banc d'essai sont comparés aux performances d'autres algorithmes d'éco-conduite afin de mettre en avant la valeur réelle de la technique de contrôle optimal proposée dans cette étude.

7.6 Conclusions:

Le but du travail présent est de développer un contrôleur optimal non linéaire évalué dans un banc d'essai spécialement conçu pour obtenir une représentation en mouvement longitudinal de la consommation d'énergie d'une moto électrique. Le contrôleur optimal est capable d'augmenter la probabilité d'achever un trajet à 98 % avec une erreur de distance inférieure à 1,5 %. Cela est rendu possible, grâce à un contrôle de l'énergie réalisé ainsi qu'une limitation en ligne du comportement de conduite dynamique autant qu'il est néces-
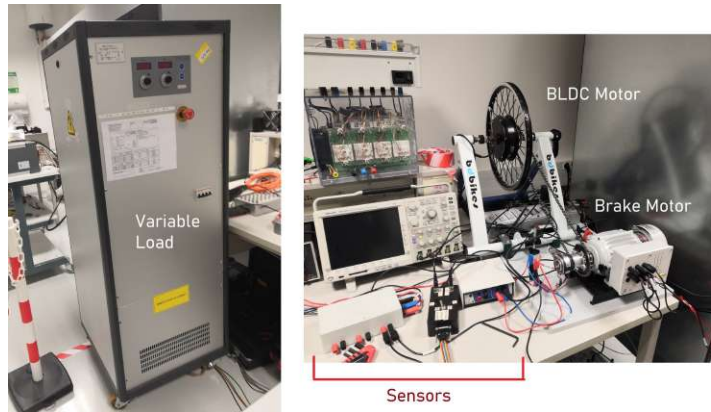
Figure 7.4: Banc expérimental.

saire pour assurer un "coefficient énergétique" suffisamment petit pour terminer le trajet. La variable appelée "coefficient énergétique" contient la quantité moyenne d'énergie nécessaire pour parcourir un mètre. Cette mesure est utilisée comme référence pour construire le signal de commande qui est la variable β_2, elle représente le degré de rigueur requis par l'équilibre envisagé dans le contrôleur optimal entre efficacité et performances du véhicule. La technique de commande optimale utilisée est un NMPC (Nonlinear Model predictive control), elle mobilise trois modèles dynamiques principaux qui représentent la chaîne de traction: le modèle mécanique, le modèle électrique et le modèle thermique. Cette modélisation multi-physique a été adaptée pour une approche d'optimisation temps réel. L'adaptation comprend la réalisation de simplifications mathématiques des modèles les plus complexes afin d'assurer une optimisation précise en un temps compatible avec un fonctionnement en temps réel. Le modèle le plus complexe est la fonction de rendement moteur, ainsi une représentation géométrique simplifiée est proposée.

La compréhension et la mise en place de ces modèles nécessitent une étape d'estimation où le profil de vitesse utilisé par le conducteur est estimé sur la base des informations disponibles dans le modèle mécanique déjà mentionné (modèle longitudinal). L'algorithme d'estimation utilise une logique floue capable d'obtenir une estimation exacte de 72 % avec des informations sur la vitesse et l'accélération prélevées pendant 120s. Afin d'augmenter la précision de l'estimateur, lorsque le coefficient énergétique estimé diffère de la mesure supérieure à 10 [Ws/m], l'approche du profil de vitesse (rural ou urbain) est remplacée par l'estimation faite par les données historiques de la route qui est couverte à ce moment précis. L'erreur de coefficient d'énergie causée est suffisamment petite pour être corrigée par le contrôle d'énergie.

Lorsque le profil de vitesse est bien estimé, le contrôleur optimal permet non seulement d'augmenter la probabilité de terminer avec succès le trajet mais aussi d'augmenter l'autonomie du véhicule autour de 20 %. Cette incrémentation est possible, grâce à l'implémentation de la fonction d'efficacité dans le contrôleur optimal et à son interaction avec le comportement du conducteur. Dans les travaux futurs, cette interaction doit être développée plus en profondeur pour comprendre le facteur humain et sensibiliser au conducteur à l'énergie utilisée. En outre ces travaux peuvent être étendus à l'amélioration de l'estimateur du profil de vitesse en considérant à la fois le modèle longitudinal et le modèle latéral.

Bibliography

[1] B. Fatch, *Commande en position et en vitesse par mode de glissement d'un moteur synchrone triphasé à aimants permanents avec minimisation du chattring.* Masters thesis, Université Mohamed Khider - Biskra., 2016.

[2] T. Instrument, "No Title."

[3] M. Oya, K. Takaba, L. Lin, R. Ishizaki, N. Kawarabayashi, and M. Fukui, "Accurate SoC estimation of lithium-ion batteries based on parameter-dependent state-space model.," in *Communications and Information Technologies (ISCIT)*, 2015.

[4] V. Cossalter, *Motorcycle Dynamics 2nd Edition.* 2006.

[5] E. Mundo, "Las ventas mundiales de coches eléctricos superaron el millón de unidades en 2017," 2018.

[6] Colprensa, "En un 88 % crece la venta de carros eléctricos en Colombia en los primeros meses del año," 2018.

[7] L. C. P. Raffán, "¿Cuánto cuesta andar en un vehículo eléctrico?," 2017.

[8] M. C. CARVAJAL, "Lento crecimiento en la venta y uso de vehículos eléctricos en Estados Unidos," 2018.

[9] M. G. Richard, "Here's How to do a Virtual Electric Car Test-Drive!," 2010.

[10] T.-y. Hong, W.-c. Chen, C.-h. Chiang, and M.-s. Chen, "The Design of Motor Drive with Speed Control for an Electric Bicycle," in *2014 International Symposium on Computer, Consumer and Control*, pp. 864–867, 2014.

[11] V. R. Tannahill, K. M. Muttaqi, and D. Sutanto, "Driver alerting system using range estimation of electric vehicles in real time under dynamically varying environmental conditions," *IET Electrical Systems in Transportation*, vol. 6, no. 2, pp. 107–116, 2016.

[12] A. D and F. R, "Optimization of an Internal Combustion Engine's Efficiency for Fuel Conservation & Green Environment," in *International Conference on Energy Systems and Policies (ICESP)*, 2014.

[13] QSMOTOR, "Torque Test," 2017.

[14] W. Lin, C. Lin, P. Hsu, and M. Wu, "Realization of Anti-Lock Braking Strategy for Electric Scooters," *IEEE Transactions on Industrial Electronics*, vol. 61, no. 6, pp. 2826–2833, 2014.

[15] M. Eshani, Y. Gao, S. Gay, and A. Emadi, *Modern electric, hybrid electric and fuel cell vehicles 2nd. Edition.* 2010.

[16] X. Zhang and C. Mi, *Vehicle Power Mangement, Modeling, Control and Optimization.* Springer, 1st ed., 2011.

[17] J. Reza N., *Vehicle dynamics, Theory and Applications.* Springer, 2nd ed., 2014.

[18] A. Bonci, R. D. Amicis, S. Longhi, E. Lorenzoni, G. A. Scala, and I. Dii, "Motorcycle's lateral stability issues: comparison of methods for dynamic modelling of roll angle," in *2016 20th International Conference on System Theory, Control and Computing (ICSTCC)*, pp. 607–612, 2016.

[19] S. R. Jape and A. Thosar, "COMPARISON OF ELECTRIC MOTORS FOR ELECTRIC VEHICLE APPLICATION," pp. 12–17, 2017.

[20] Duane Hanselman, *Brushless Permanent Magnet Motor Design.* second ed., 2003.

[21] C. Wasko, "Hub-Drive vs. Mid-Drive eBikes: What to Know Before Buying," 2019.

[22] T. Toma, "Rotor Loss in Permanent-Magnet Brushless AC Machines," *Genome Biology*, vol. 2, no. 1, pp. 1612–1618, 2001.

[23] N. Bianchi, S. Bolognani, and P. Frare, "Design criteria of high efficiency SPM synchronous motors," *IEMDC 2003 - IEEE International Electric Machines and Drives Conference*, vol. 2, pp. 1042–1048, 2003.

[24] C. Li, H. Zhu, M. Wu, and Z. Jiang, "Efficiency Map Calculation for Surface-mounted Permanent-magnet In-wheel Motor Based on Design Parameters and Control Strategy," *Jianzhu Cailiao Xuebao/Journal of Building Materials*, vol. 19, no. 6, pp. 1–6, 2016.

[25] M. Fasil, N. Mijatovic, B. B. Jensen, and J. Holboll, "Nonlinear Dynamic Model of PMBLDC Motor Considering Core Losses," *IEEE Transactions on Industrial Electronics*, vol. 64, no. 12, pp. 9282–9290, 2017.

[26] M. Markovic, A. Hodder, and Y. Perriard, "An analytical determination of the torque-speed and efficiency-speed characteristics of a BLDC motor," *2009 IEEE Energy Conversion Congress and Exposition, ECCE 2009*, vol. 6, no. 5, pp. 168–172, 2009.

[27] T. Ishikawa, T. Tsuji, S. Hashimoto, and N. Kurita, "Simple Equivalent Circuit for Efficiency Calculation of Brushless DC Motors," *Journal of international Conference on Electrical Machines and Systems*, vol. 3, no. 1, pp. 54–60, 2014.

[28] Z. Tian, C. Zhang, and S. Zhang, "Analytical calculation of magnetic field distribution and stator iron losses for surface-mounted permanent magnet synchronous machines," *Energies*, vol. 10, no. 3, 2017.

[29] P. Dusane, "Simulation of BLDC Hub Motor in ANSYS - Czech Technical University in Prague Faculty of Electrical Engineering Department of Power Engineering Student : Prathamesh Mukund Dusane," no. June, 2016.

[30] K. Muehlbauer, F. Bachl, and D. Gerling, "Comparison of Measurement and Calculation of Power Losses in AC / DC-Converter for Electric Vehicle Drive," in *2011 International Conference on Electrical Machines and Systems*, pp. 1–4, IEEE, 2011.

[31] K. Muehlbauer, F. Bachl, D. Gerling, and E. L. M. A. Da-pm, "Analysis of Power Losses in AC / DC-Converter for Electric Vehicle Drive," *2011 IEEE Vehicle Power and Propulsion Conference*, pp. 1–4, 2011.

[32] W.-y. Sung, D.-g. Woo, Y.-s. Kim, B.-g. You, and B.-k. Lee, "Advanced Simulation Model for Loss Analysis of Converters in Electric Vehicles," *2012 IEEE Vehicle Power and Propulsion Conference*, no. 1, pp. 1206–1210, 2012.

[33] N. Marina, A. Aziz, and A. Coulson, "Determination of the Power Loss in Inverters which Supplies a BLDC Motor," in *International symposium on fundamentals of electronical engineering.*, pp. 1–43, 2016.

[34] H. H. Bao, W. Zhang, Y. Yang, and Y. Chen, "Calculation and Analysis of IGBT Power Loss in Drive System for EV," *2015 IEEE International Conference on Applied Superconductivity and Electromagnetic Devices (ASEMD)*, pp. 276–277, 2015.

[35] R. Yajun, W. Yang, H. Wang, and H. Qi, "SOC estimation of electric vehicle based on the establishment of battery management system," *IEEE Transportation Electrification Conference and Expo, ITEC Asia-Pacific 2014 - Conference Proceedings*, 2014.

[36] D. Xu, W. Lifang, and Jianyang, "Research on Li-ion battery management system," *Proceedings - International Conference on Electrical and Control Engineering, ICECE 2010*, pp. 4106–4109, 2010.

[37] D. R. Montes, U. Valle, J. Manuel, A. Viveros, U. Valle, and U. Valle, "Design and Construction of an Energy Management System for Electric Vehilce Batteries," in *2015 IEEE Workshop on Power Electronics and Power Quality Applications (PEPQA)*, pp. 1–6, 2015.

[38] J. Wen and J. Jiang, "Battery management system for the charge mode of quickly exchanging battery package," *2008 IEEE Vehicle Power and Propulsion Conference, VPPC 2008*, pp. 3–6, 2008.

[39] A. Enthaler and F. Gauterin, "Significance of internal battery resistance on the remaining range estimation of electric vehicles *," *2013 International Conference on Connected Vehicles and Expo (ICCVE)*, pp. 94–99, 2013.

[40] C. Chen, X. Zhao, Y. Yao, Y. Zhang, J. Rong, and X. Liu, "Driver ' s Eco-Driving Behavior Evaluation Modeling Based on Driving Events," *Hindawi, Journal of Advanced Transportation.*, 2018.

[41] G. Yoshikawa, Y. Taguchi, K. Hatakeda, and T. Kaneko, "Development of a Parameter Identification Method for the Thermal Circuit Model of a Lithium-Ion Battery Installed on a Battery-Powered EMU," pp. 0–4, 2017.

[42] H. Chaoui, S. Member, A. E. Mejdoubi, and H. Gualous, "Online Parameter Identification of Lithium-Ion Batteries With Surface Temperature Variations," *IEEE Transactions on Vehicular Technology*, vol. 66, no. 3, pp. 2000–2009, 2017.

[43] J. Lee, J.-h. Ahn, and B. K. Lee, "A Novel Li-ion Battery Pack Modeling Considerging Single Cell Information and Capacity Variation," in *2017 IEEE Energy Conversion Congress and Exposition (ECCE)*, 2017.

[44] R. Rajamani, *Vehicle Dynamics and Control.* 2012.

[45] A. Bonci, R. De Amicis, S. Longhi, G. A. Scala, and A. Andreucci, "Motorcycle lateral and longitudinal dynamic modeling in presence of tyre slip and rear traction," *2016 21st International Conference on Methods and Models in Automation and Robotics, MMAR 2016*, no. Dii, pp. 391–396, 2016.

[46] C. Sentouh, *Analyse du risque et détection de situations limites: application au développement des systèmes d'alerte au conducteur.* PhD thesis, Evry val d'Essonne, 2007.

[47] T. Kubota and E. Yagi, "Modeling and Stabilization of Motorcycle Shimmy," *ICROS-SICE International Joint Conference 2009*, pp. 4069–4072, 2009.

[48] D. Pomerleau, T. Jochem, P. Batavia, D. Pape, J. Hadden, N. McMillan, and N. Brown, "Run-off-road collision avoidance using IVHS countermeasures," Tech. Rep. December, 1999.

[49] E. Velenis and P. Tsiotras, "Minimum Time vs Maximum Exit Velocity Path Optimization During Cornering," in *Proceedings of the IEEE International Symposium on Industrial Electronics, 2005. ISIE 2005.*, pp. 355–360, 2005.

[50] Z. Younes, L. Boudet, F. Suard, M. Gerard, and R. Rioux, "Analysis of the main factors influencing the energy consumption of electric vehicles," *2013 International Electric Machines & Drives Conference*, pp. 247–253, 2013.

[51] K. Sarrafan, D. Sutanto, K. M. Muttaqi, and G. Town, "Accurate range estimation for an electric vehicle including changing environmental conditions and traction system efficiency," *IET Electrical Systems in Transportation*, vol. 7, no. 2, pp. 117–124, 2017.

[52] S. Mammar, S. Espie, and B. Larnaudie, "Static Hinf Rider for Motorcycle roll stabilization," *2006 American Control Conference*, pp. 5378–5383, 2006.

[53] G. Liu, H. Ren, S. Chen, and W. Wang, "The 3-DoF bicycle model with the simplified piecewise linear tire model," *Proceedings - 2013 International Conference on Mechatronic Sciences, Electric Engineering and Computer, MEC 2013*, no. September 2016, pp. 3530–3534, 2013.

[54] J. L. Mathieu and J. K. Hedrick, "Robust Multivariable Dynamic Surface Control for Position Tracking of a Bicycle," in *Proceedings of the 2010 American Control Conference*, pp. 1159–1165, 2010.

[55] H. N. Shintaroh Murakami and S. Zhu, "Steering Assist Control for Stabilization of a Motorcycle during Braking (Verification of the Control System on Cornering Simulations)," in *2011 IEEE/SICE International Symposium on System Integration (SII)*, pp. 1025–1030, 2011.

[56] A. Saccon, J. Hauser, and A. Beghi, "A Virtual Rider for Motorcycles : Maneuver Regulation of a Multi-Body Vehicle Model," *IEEE Transactions on Control Systems Technology*, vol. 21, no. 2, pp. 332–346, 2013.

[57] Y. Zhang, W. Wang, Y. Kobayashi, and K. Shirai, "Remaining driving range estimation of electric vehicle," *2012 IEEE International Electric Vehicle Conference, IEVC 2012*, pp. 1–7, 2012.

[58] H. Rahimi-Eichi and M. Y. Chow, "Big-data framework for electric vehicle range estimation," *IECON Proceedings (Industrial Electronics Conference)*, pp. 5628–5634, 2014.

[59] R. Yaqub and Y. Cao, "Smartphone-based accurate range and energy efficient route selection for electric vehicle," *2012 IEEE International Electric Vehicle Conference, IEVC 2012*, pp. 1–5, 2012.

[60] S. Kaveh, M. K. M, S. Danny, and T. Graham, "An intelligent driver alerting system for real-time range indicator embedded in electric vehicles Publication Details "An intelligent driver alerting system for real-time range indicator embedded in electric vehicles," in IEEE Industry An intell," vol. 53, no. 3, pp. 1–7, 2016.

[61] G. De Nunzio and L. Thibault, "Energy-optimal driving range prediction for electric vehicles," *IEEE Intelligent Vehicles Symposium, Proceedings*, no. Iv, pp. 1608–1613, 2017.

[62] H. Kato, R. Ando, Y. Kondo, T. Suzuki, K. Matsuhashi, and S. Kobayashi, "Comparative measurements of the eco-driving effect between electric and internal combustion engine vehicles," *2013 World Electric Vehicle Symposium and Exhibition, EVS 2014*, pp. 1–5, 2014.

[63] O. Kraa, M. Becherif, A. Aboubou, M. Y. Ayad, I. Tegani, and A. Haddi, "Modeling and fuzzy logic control of electrical vehicle with an adaptive operation mode," *International Conference on Power Engineering, Energy and Electrical Drives*, no. May, pp. 120–127, 2013.

[64] X. Lin, D. Gorges, and S. Liu, "Eco-driving assistance system for electric vehicles based on speed profile optimization," *2014 IEEE Conference on Control Applications, CCA 2014*, no. 1, pp. 629–634, 2014.

[65] L. Guo, B. Gao, Y. Gao, and H. Chen, "Optimal Energy Management for HEVs in Eco-Driving Applications Using Bi-Level MPC," *IEEE Transactions on Intelligent Transportation Systems*, vol. 18, no. 8, pp. 2153–2162, 2017.

[66] D. Maamria, K. Gillet, G. Colin, and Y. Chamaillard, "On the use of Dynamic Programming in eco-driving cycle computation for electric vehicles," in *2016 IEEE Conference on Control Applications (CCA)*, pp. 1288–1293, 2016.

[67] C. T. Krasopoulos, M. E. Beniakar, and A. G. Kladas, "Velocity and Torque Limit Profile Optimization of Electric Vehicle Including Limited Overload," *IEEE Transactions on Industry Applications*, vol. 53, no. 4, pp. 3907–3916, 2017.

[68] A. Chakrabarty, V. Dinh, M. J. Corless, A. E. Rundell, S. H. Zak, and G. T. Buzzard, "Support Vector Machine Informed Explicit Nonlinear Model Predictive Control Using Low-Discrepancy Sequences," *IEEE Transactions on Automatic Control*, vol. 62, no. 1, pp. 135–148, 2017.

[69] A. Raha, A. Chakrabarty, V. Raghunathan, and G. T. Buzzard, "Ultrafast Embedded Explicit Model Predictive Control for Nonlinear Systems," *2017 American Control Conference (ACC)*, pp. 4398–4403, 2017.

[70] J. Dentler, S. Kannan, M. A. Olivares-Mendez, and H. Voos, "Implementation and validation of an event-based real-time nonlinear model predictive control framework with ROS interface for single and multi-robot systems," *1st Annual IEEE Conference on Control Technology and Applications, CCTA 2017*, vol. 2017-Janua, pp. 1000–1006, 2017.

[71] P. Golchoubian and N. L. Azad, "Real-Time Nonlinear Model Predictive Control of a Battery-Supercapacitor Hybrid Energy Storage System in Electric Vehicles," *IEEE Transactions on Vehicular Technology*, vol. 66, no. 11, pp. 9678–9688, 2017.

[72] X. Qi, P. Wang, G. Wu, K. Boriboonsomsin, and M. J. Barth, "Connected cooperative ecodriving system considering human driver error," *IEEE Transactions on Intelligent Transportation Systems*, vol. 19, no. 8, pp. 2721–2733, 2018.

[73] S. Devaneyan, "Electronic Control Unit for BLDC Motors in Electric Bicycles with 8-bit Microcontroller," in *2010 International Conference on Communication and Computational Intelligence (INCOCCI)*, pp. 201–205, 2010.

[74] M. Kim, J.-g. Choi, J.-i. Lee, H.-s. Yoon, Y.-s. Kim, and I.-s. Cha, "A Study on the DC Motor Speed control for electric bicycle with the load induction unit.," in *ISIE'2000. Proceedings of the 2000 IEEE International Symposium on Industrial Electronics (Cat. No.00TH8543)*, pp. 141–144.

[75] A. Muetze and Y. C. Tan, "Modeling and analysis of the technical performance of DC-motor electric bicycle drives based on bicycle road test data," in *Proceedings of IEEE International Electric Machines and Drives Conference, IEMDC 2007*, vol. 2, pp. 1574–1581, 2007.

[76] E. V. Uot and E. March, "Traction Control of Electric Vehicle : Basic Experimental Results Using the Test," *IEEE Transactions on Industry Applications*, vol. 34, no. 5, pp. 1131–1138, 1998.

[77] W. Cui, H. Zhang, Y. L. Ma, and Y. J. Zhang, "Regenerative braking control method and optimal scheme for electric motorcycle," *International Conference on Power Engineering, Energy and Electrical Drives*, no. May, 2011.

[78] Y. Zhang, J. Li, J. Yi, and D. Song, "Balance Control and Analysis of Stationary Riderless Motorcycles," in *2011 IEEE International Conference on Robotics and Automation*, no. 1, pp. 3018–3023, 2011.

[79] K. Shirahata, "Speed Control Methods of Various Types of Speed Control Motors Kazuya SHIRAHATA," *Oriental Motor*, 2010.

[80] X. Zhang, W. Chen, and Z. Lu, "Key Technologies of Digital-Current-Controlled Bidirectional DC-DC Converter in the Hybrid Electric Vehicle," in *2008 IEEE Power Electronics Specialists Conference*, no. Ccm, pp. 3104–3109, 2008.

[81] N. Kutkut, H. Wiegman, D. Divan, and D. Novotny, "Design Considerations for Charge Equalization of an Electric Vehicle Battery System," *IEEE Transactions on Industry Applications*, vol. 35, no. 1, pp. 28–35, 1999.

[82] S. V. Sterkenburg, E. Rietveld, F. Rieck, B. Veenhuizen, and H. Bosma, "Analysis of regenerative braking efficiency: A case study of two electric vehicles operating in the Rotterdam area," in *Vehicle Power and Propulsion Conference (VPPC)*, 2011.

[83] A. S. Murthy and D. G. Taylor, "Vehicle Braking Strategies Based on Regenerative Braking Boundaries of Electric Machines," *2015 IEEE Transportation Electrification Conference and Expo (ITEC)*, no. 3, 2015.

[84] D. Cao and F. Z. Peng, "A family of zero current switching switched-capacitor dc-dc converters," in *Proc. Twenty-Fifth Annual IEEE Applied Power Electronics Conf. and Exposition (APEC)*, pp. 1365–1372, 2010.

[85] O. Tur, O. Ustun, and R. N. Tuncay, "An Introduction to Regenerative Braking of Electric Vehicles as Anti-Lock Braking System," *2007 IEEE Intelligent Vehicles Symposium*, no. 5, p. 2015, 2007.

[86] J. K. David Magin Flores, Guillermo Marulanda, Ruben Manrrique, Marta Lucia Cano, "Bicicletas electricas: Conceptos basicos y aspectos practicos.," *MUNDO ELECTRICO*, pp. 90–97, 2015.

[87] C. Campus, "Regenerative power control for electric bicycle," in *2006 SICE-ICASE International Joint Conference*, pp. 4362–4365, 2006.

[88] D.-s. Shin, S.-t. Lee, S.-g. Song, H.-j. Kim, and Y.-c. Lim, "Regenerative Energy Control of Electric Vehicles Applied to a Dual Power System," in *2012 IEEE Vehicle Power and Propulsion Conference*, pp. 441–447, 2012.

[89] C. Binggang, C. Binggang, B. Zhifeng, B. Zhifeng, Z. Wei, and Z. Wei, "Research on control for regenerative braking of electric vehicle," *IEEE International Conference on Vehicular Electronics and Safety, 2005.*, pp. 92–97, 2005.

[90] M. Guarisco, F. Gao, and D. Paire, "Autonomy and User experience enhancement control of an electricall assisted bycycle with Dual-Wheel Drive," in *2015 IEEE Industry Applications Society Annual Meeting*, pp. 1–8, 2015.

[91] X. Liu, C. Liu, M. Lu, and D. Liu, "Regenerative Braking Control Strategies of Switched Reluctance Machine for Electric Bicycle," in *2008 International Conference on Electrical Machines and Systems*, pp. 3397–3400, 2008.

[92] B.-R. Liang and W.-S. Lin, "Optimal regenerative torque control to maximize energy recapture of electric vehicles," in *2010 World Automation Congress*, vol. 2, 2010.

[93] L. Bo, "Hinf Robust Controller Design for Regenerative Braking Control of Electric Vehicles," in *2011 6th IEEE Conference on Industrial Electronics and Applications*, pp. 214–219, 2011.

[94] H. Z. Zhou, G. Xu, W. Li, and Meilan, "Fuzzy Logic Control in Regenerative Braking System for Electric Vehicle," in *2012 IEEE International Conference on Information and Automation*, no. June, pp. 588–591, 2017.

[95] D. Wang, W. Zhang, and J. Li, "A PWM Plus Phase Shift Control Strategy for Dual- Active-Bridge DC-DC Converter in Electric Vehicle Charging / Discharging System," *2014 IEEE Conference and Expo Transportation Electrification Asia-Pacific (ITEC Asia-Pacific)*, pp. 1–5, 2014.

[96] Z. Xuhui, X. Wen, Z. Feng, and G. Xinhua, "A New Control Strategy for Bi-Directional DC-DC Converter in Electric Vehicle," in *2011 International Conference on Electrical Machines and Systems*, no. 3, pp. 3–6.

[97] J. W. Dixon and M. E. Ortlizar, "Ultracapacitors + DC-DC Converters in Regenerative Braking System," *IEEE Aerospace and Electronic Systems Magazine*, no. August, pp. 16–21, 2002.

[98] B. S. Kim, H. J. Kim, C. Jin, and D. Y. Huh, "A digital controlled DC-DC converter for electric vehicle applications," *2011 International Conference on Electrical Machines and Systems, ICEMS 2011*, 2011.

[99] W. Li, "Design of Vehicle Control Unit Based on DSP for a Parallel HEV," in *2007 IEEE International Conference on Automation and Logistics*, pp. 1597–1601, 2007.

[100] J. C. Ferreira, V. Monteiro, and J. L. Afonso, "Dynamic range prediction for an electric vehicle," *2013 World Electric Vehicle Symposium and Exhibition, EVS 2014*, pp. 1–11, 2014.

[101] T. Abumi and T. Murakami, "Posture stabilization of two-wheel drive electric motorcycle by slip ratio control considering camber angle," *Proceedings - 2015 IEEE International Conference on Mechatronics, ICM 2015*, pp. 353–358, 2015.

[102] D. M. Giner, J. Kang, and M. Manka, "A corner solver for motorcycles as a tool for the development of a virtual rider," in *2009 IEEE Vehicle Power and Propulsion Conference*, pp. 1110–1117, 2009.

[103] S. Cheng, "Real-time Dynamic Power Management of Electrically Assisted Bicycle," in *2011 IEEE International Conference on Mechatronics and Automation*, pp. 313–318, 2011.

[104] S. Akhegaonkar, L. Nouveliere, S. Glaser, and F. Holzmann, "Smart and Green ACC: Energy and Safety Optimization Strategies for EVs," *IEEE Transactions on Systems, Man, and Cybernetics: Systems*, pp. 1–12, 2016.

[105] EEMB Co., "Lithium-ion Battery Datasheet," tech. rep., 2010.

[106] E. Motion, "Forest Litio User Manual," 2016.

[107] C. Yang, S. Du, L. Li, S. You, Y. Yang, and Y. Zhao, "Adaptive real-time optimal energy management strategy based on equivalent factors optimization for plug-in hybrid electric vehicle," *Applied Energy*, vol. 203, pp. 883–896, 2017.

[108] N. Rizoug, T. Mesbahi, R. Sadoun, P. Bartholomeüs, and P. Le Moigne, "Development of new improved energy management strategies for electric vehicle battery/supercapacitor hybrid energy storage system," *Energy Efficiency*, vol. 11, no. 4, pp. 823–843, 2018.

[109] STripFET, "STB75NF75 STP75NF75 - STP75NF75FP," Tech. Rep. February, 2007.

[110] A. Adib and R. Dhaouadi, "Modeling and analysis of a regenerative braking system with a battery-supercapacitor energy storage," *2017 7th International Conference on Modeling, Simulation, and Applied Optimization, ICMSAO 2017*, 2017.

[111] P. Ragot, S. Member, M. Markovic, Y. Perriard, S. Member, and A. Overall, "Optimization of Electric Motor for a Solar Airplane Application," *IEEE TRANSACTIONS ON INDUSTRY APPLICATIONS*, vol. 42, no. 4, pp. 1053–1061, 2006.

[112] L. Li, X. Li, X. Wang, J. Song, K. He, and C. Li, "Analysis of downshift's improvement to energy efficiency of an electric vehicle during regenerative braking," *Applied Energy*, vol. 176, pp. 125–137, 2016.

[113] N. N. Bespalov and A. E. Lysenkov, "Influence of Fluctuation of MOSFET ' s Elec- trothermal Parameter on Thermal Conditions in Bridge Inverter," *2016 13th International Scientific-Technical Conference on Actual Problems of Electronics Instrument Engineering (APEIE)*, vol. 03, pp. 46–48, 2016.

[114] J. Ye, K. Yang, H. Ye, and A. Emadi, "A Fast Electro-Thermal Model of Traction Inverters for Electrified Vehicles," *IEEE Transactions on Power Electronics*, vol. 32, no. 5, pp. 3920–3934, 2017.

[115] Z. Minghui and L. Weiguo, "Transient coupled electro-magnetic thermal analysis of a permanent magnet brushless DC motor," *2010 International Conference on Computer, Mechatronics, Control and Electronic Engineering*, vol. 4, pp. 221–224, 2010.

[116] D.-m. Miao, Y. Perriard, M. Markovic, P. Germano, and J.-x. Shen, "Thermal Modeling of a BLDC Motor for a Kick Scooter," *2012 IEEE International Symposium on Industrial Electronics*, vol. 100, no. c, pp. 764–769.

[117] A. Ahmed, "Accurate Joule Loss Estimation for Rotating Machines : An Engineering Approach," in *2018 IEEE Energy Conversion Congress and Exposition (ECCE)*, pp. 1569–1573, 2018.

[118] J. L. H. L. Cuiping Li, Shitao Cheng, "Heat dissipation evaluation and optimization of air cooling induction motor used for mini electric vehicle," *2017 20th International Conference on Electrical Machines and Systems (ICEMS), Sydney, NSW*, pp. 1–5, 2017.

[119] Ansys, "ANSYS Maxwell V16," tech. rep., 2013.

[120] R. Prohaska, A. Duran, A. Ragatz, and K. Kelly, "Statistical Characterization of Medium - Duty Electric Vehicle Drive Cycles," *EVS28 International Electric Vehicle Symposium and Exhibition*, no. Md, pp. 1–10, 2015.

[121] M. S. R. Kubaisi, *Adaptive Regenerative Braking in Electric Vehicles*. Doktors der ingenieurwissenschaften, von der KIT -Fakultät für Maschinenbau des Karlsruher Institut für Technologie (KIT) genehmigte, 2018.

[122] D. Ebersbach, *Entwurfstechnische Grundlagen für ein Fahrerassis-tenzsystem zur Unterstützung des Fahrers bei der Wahl seiner Ge-schwindigkeit*. PhD thesis, Technische Universität Dresden, 2005.

[123] B. Deml, J. Freyer and B. Faerber, "Ein Beitrag zur Prädiktion des Fahrstils," *in Fahrer im 21. Jahrhundert. Human Machine Interface*, 2007.

[124] Yi Lu Murphey, Robert Milton and L. Kiliaris, "Driver's style classification using jerk analysis," *Computational Intelligence in Vehicles and Vehicular Systems*, pp. 23–28, 2009.

[125] J. Bossdorf-Zimmer, H. Kollmer, R. Henze and F. Küçükay, "Finger-print des Fahrers zur Adaption von Assistenzsystemen," *ATZ- Automobiltechnische Zeitschrift*, vol. 113, pp. 226–231, 2011.

[126] B. Färber, "Erhöhter Fahrernutzen durch Integration von Fahreras-sistenz- und Fahrerinformationssystemen," *Fahrerassistenzsys-teme mit maschineller Wahrnehmung, M. Maurer and C. Stiller, Eds., Berlin, Heidelberg: Springer Berlin Heidelberg,*, pp. 141–160, 2005.

[127] A. Wilde, J. Schneider and H.-G. Herzog, "Fahrstil-und fahrsitua-tions-abhängige Ladestrategie bei Hybridfahrzeugen," *ATZ- Automobiltechnische Zeitschrift*, vol. 110, no. 5, pp. 412–421, 2008.

[128] M. Schüler, C. Onnen and C. Bielaczek, "IFAC Proceedings Volumes," *A Fuzzy-System for a Classi-fication of the Driver Behavior and the Driving Situation*, vol. 30, no. 8, pp. 693–698, 1997.

[129] H.-b. An and Z.-z. Bai, "A globally convergent Newton-GMRES method for large sparse systems of nonlinear equations [U+2729]," vol. 57, no. 2005, pp. 235–252, 2007.

Chapter 8

Annexes:

8.1   Economical budget.

The Ph.D. research is attached to convocation 727 of 2015. This convocation has 50.000.000.00 COP to be used hardware and software resources. The hardware chose to verify each step of this research is presented in Table 8.1.

Product	Quantity	Cost/unit	Brand	Product reference
Electric Motorcycle 3000KW	1	6.500.000.00	Maker	https://bit.ly/2QDKJ6G
Lithium Battery 72v 60ah	3	5.000.000.00	-	https://bit.ly/2CE4GaJ
Lithium Battery 72v 20ah	4	2.680.000.00	-	https://bit.ly/2OWyWDy
Odroid XU4	2	192.000.00	Odroid	https://bit.ly/2LvNcCb
Odroid Batrery 3000 mAhs	2	51.000.00	Odroid	https://bit.ly/2CDwFHq
Kit Motor4000W/Inverter(Sabvoton)	3	1.923.000.00	QSMOTOR	https://bit.ly/2NAFu63
Sinusoidal controller KLS7275DC	2	1.613.000.00	QSMOTOR	https://bit.ly/2pKWblC
Sabvoton Bluetooth Adapter Module	3	84.000.00	QSMOTOR	https://bit.ly/2PucApO
Fast Charger 72v 20ah	2	630.000.00	-	https://bit.ly/2C95iEc

Table 8.1: Hardware required to test the controller.

The total of economical resources planned in this table is 43.213.000.00COP, the other part of the economic resources are available for tests or shipping duties.